INFORMATION TO USERS

The most advanced technology has been used to photograph and reproduce this manuscript from the microfilm master. UMI films the text directly from the original or copy submitted. Thus, some thesis and dissertation copies are in typewriter face, while others may be from any type of computer printer.

The quality of this reproduction is dependent upon the quality of the copy submitted. Broken or indistinct print, colored or poor quality illustrations and photographs, print bleedthrough, substandard margins, and improper alignment can adversely affect reproduction.

In the unlikely event that the author did not send UMI a complete manuscript and there are missing pages, these will be noted. Also, if unauthorized copyright material had to be removed, a note will indicate the deletion.

Oversize materials (e.g., maps, drawings, charts) are reproduced by sectioning the original, beginning at the upper left-hand corner and continuing from left to right in equal sections with small overlaps. Each original is also photographed in one exposure and is included in reduced form at the back of the book. These are also available as one exposure on a standard 35mm slide or as a 17" x 23" black and white photographic print for an additional charge.

Photographs included in the original manuscript have been reproduced xerographically in this copy. Higher quality 6" x 9" black and white photographic prints are available for any photographs or illustrations appearing in this copy for an additional charge. Contact UMI directly to order.

U·M·I

University Microfilms International
A Bell & Howell Information Company
300 North Zeeb Road, Ann Arbor, MI 48106-1346 USA
313/761-4700 800/521-0600

Order Number 9000740

Heat transfer between a laminar free impinging jet and a heated plate

Wang, Xiaosong, Ph.D.

City University of New York, 1989

U·M·I
300 N. Zeeb Rd.
Ann Arbor, MI 48106

HEAT TRANSFER BETWEEN A LAMINAR FREE IMPINGING JET AND A HEATED PLATE

by

XIAOSONG WANG

A dissertation submitted to the Graduate Faculty in Engineering in partial fulfillment of the requirements for the degree of Doctor of Philosophy
The City University of New York

1989

This manuscript has been read and accepted for the Graduate Faculty in Engineering in satisfaction of the dissertation requirement for the degree of Doctor of Philosophy.

3/7/89

Date

Professor Zeev Dagan

Chair of Examining Committee

3/7/89

Date

Professor Jacques E. Benveniste

Executive Officer

Professor Zeev Dagan - Advisor

Professor L. M. Jiji - Co-Advisor

Professor Yiannis Andreopoulos

Professor Peter Ganatos

Professor Myron Levitsky

Professor Charles Maldarelli

Supervisory Committee

The City University of New York

ABSTRACT

HEAT TRANSFER BETWEEN A LAMINAR FREE IMPINGING JET AND A HEATED PLATE

by

Xiaosong Wang

Advisor: Professor Zeev Dagan

Professor Latif M. Jiji

The analytical solution to the conjugate heat transfer problem associated with laminar liquid jet impingement is presented in this dissertation. The analysis consists of solutions to three problems. The first problem is for the heat transfer in the vicinity of the stagnation point with arbitrary wall temperature or wall heat flux. The second one deals with the heat transfer in the boundary layer region with arbitrary wall temperature or wall heat flux, and the third is the conjugate problem in which the energy equations for the fluid and solid phases are solved simultaneously. Finally, the analytical solution is applied to predict the surface temperature and heat flux of a microelectronic chip cooled by a laminar impinging FC-77 jet or water jet with uniform heat flux specified at the non-impingement surface.

In the stagnation region, both the exact energy equation and the boundary layer energy equation are solved asymptotically. The results show that the non-uniformity of wall temperature or wall heat flux has a considerable effect on the stagnation point Nusselt number. Increasing the wall temperature or wall heat flux with the radial distance r reduces the stagnation point Nusselt number while decreasing

the wall temperature or wall heat flux with r enhances the heat transfer at the stagnation point.

In the boundary layer region, the analysis begins with obtaining the solution to the problem with a step change in wall temperature or wall heat flux. The solution corresponding to the problem with arbitrary wall temperature or wall heat flux is then obtained by the superposition method. The result is matched with that for the stagnation region graphically so that the Nusselt number distribution throughout the stagnation region and the boundary layer region is obtained. For the special case of constant wall temperature, the result is in good agreement with the integral solution of Chaudhury [14].

For the conjugate problem in which an arbitrary temperature or heat flux is prescribed at the non-impingement surface, the general solutions for the fluid and solid phases are matched by requiring the continuity of the temperature and heat flux at the impingement surface. The local Nusselt number is found to depend upon the Prandtl number, Pr, of the fluid, the ratio of the fluid conductivity to the solid conductivity, k, the aspect ratio of the thickness to the radius of the plate, ϵ, and the prescribed temperature or heat flux distribution. For a thick plate, e.g. $\epsilon = 1$, the prescribed temperature or heat flux has little effect on the local heat transfer coefficient. For a thin plate, however, the effect is considerable. Outside the stagnation region, increasing the prescribed temperature or heat flux with the radial distance r enhances the local heat transfer coefficient while decreasing the prescribed temperature or heat flux with r reduces it. The results also indicate that the local heat transfer coefficient becomes higher when k is larger.

ACKNOWLEDGEMENTS

I wish to thank my mentors professor Zeev Dagan and professor Latif M. Jiji for their support and guidance during the course of this research. I also wish to thank all members of the Supervisory Committee for their help and encouragement.

This work was partially supported by Grant No. 775763 from IBM.

Contents

List of Symbols

a	constant defined by equation (2.5)
A	surface area of chip
$a_2, a_5, a_8 \ldots$	constants defined by equation (3.10)
$A_0, \ldots, A_n$	dimensionless functions defined by equation (2.21) in Chapter 2; constant coefficients in equation (4.7) in Chapter 4
b	constant defined by equation (3.18)
$B_0, \ldots, B_n$	coefficients in expansion (3.36) in Chapter 3 constant coefficients in equation (4.7) in Chapter 4
$c_2, c_3, \ldots c_n$	coefficients in prescribed wall temperature, equation (2.18)
d	jet diameter
$d_2, d_3, \ldots d_n$	coefficients in prescribed wall heat flux, equation (2.19)
D_n	dimensionless function defined by equation (2.45)
e	parameter defined by equation (4.9a)
e_1, e_2	constants defined by equation (3.19)
f	dimensionless function defined by equation (3.7)
$F_0, F_1, \ldots F_n$	coefficients in expansion (3.17)
F_q	dimensionless heat flux defined by equation (4.6b)
F_t	dimensionless temperature defined by equation (4.6a)
F_w	dimensionless function defined by equation (2.14c)

G	constant defined by equation (2.41)
g_n	dimensionless function defined by equation (2.38)
h	heat transfer coefficient
H	thickness of solid plate
$\bar{h}$	average heat transfer coefficient
k	fluid conductivity in Chapters 2 and 3; conductivity ratio defined by equation (4.9b) in Chapters 4 and 5
k_f	fluid conductivity
k_s	solid conductivity
Nu	Nusselt number, hd/k in Chapters 2 and 3 and hd/k_f in Chapter 4
P	pressure
Pr	Prandtl number
Q	flow rate, cm^3/s
Q_0	stagnation point heat flux in Chapter 2; prescribed constant heat flux in Chapter 5
q_1	constant wall heat flux after the step change
Q_b	prescribed heat flux on the non-impingement surface
Q_{b0}	prescribed heat flux at $r = 0$ on the non-impingement surface
q_w	wall heat flux
Q_w	prescribed wall heat flux in Chapters 2 and 3; calculated wall heat flux in Chapter 5
r	radial coordinate

R	dimensionless coordinate defined by equation (3.14) in Chapter 3; thermal resistance defined by equation (5.1) in Chapter 5
r_o	jet radius
R_o	radius of solid plate
Re	Reynolds number, $U_o d/\nu$
r_m	radial distance of matching location
T	temperature
T_o	stagnation point temperature
T_1	constant wall temperature after the step change
T_b	prescribed temperature on the non-impingement surface
T_{b0}	prescribed temperature at r = 0 on the non-impingement surface
T_m	temperature distribution at $r = r_m$
T_f	temperature for the fluid phase
T_i	interface temperature
T_j	jet temperature in Chapter 5
T_s	temperature for the solid phase
T_w	prescribed wall temperature
T_∞	jet temperature
u	velocity in radial direction
U(r)	velocity distribution for potential flow
U_o	jet velocity

w velocity in z direction

z coordinate normal to the wall

Greek Symbols

α diffusivity

δ viscous boundary layer thickness

δ' boundary layer thickness defined by equation (3.11)

Δ ratio of thermal boundary layer thickness to viscous boundary layer thickness

δ_s boundary layer thickness in the stagnation region

δ_t thermal boundary layer thickness

δ_{td} dimensionless thermal boundary layer thickness defined by equation (2.64)

ϵ aspect ratio defined by equation (4.3d)

ζ dimensionless coordinate defined by equation (4.3c)

η dimensionless coordinate defined by equation (2.9b) in Chapter 2 and by equation (3.8) in Chapter 3

θ dimensionless temperature defined by equation (2.12)

θ_{cq} dimensionless temperature defined by equation (3.66)

θ_{ct} dimensionless temperature defined by equation (3.61)

θ_m dimensionless temperature defined by equation (2.15a)

θ_s dimensionless temperature defined by equation (2.74) in Chapter 2 and by equation (4.3a) in Chapter 4

θ_{sq} dimensionless temperature for a step change in wall

heat flux, equation (3.33)

θ_{st} dimensionless temperature for a step change in wall temperature, equation (3.13)

θ_w dimensionless wall temperature defined by equation (2.15b)

λ_n eigenvalues defined by $J_0(\lambda_n \xi_m) = 0$

ν kinematic viscosity

ξ dimensionless coordinate defined by equation (2.9a) in Chapter 2 and by equation (3.14) in Chapter 3

ξ_m dimensionless radial distance defined by equation (2.15c)

ρ density in Chapter 2;
dimensionless coordinate defined by (4.3b) in Chapter 4

σ_n eigenvalues defined by $J_1(\sigma_n) = 0$

ϕ dimensionless function defined by equation (2.8)

List of Tables

List of Figures

Chapter 1

Introduction

The conjugate heat transfer between an impinging jet and a solid plate is of interest in many engineering applications, such as the annealing of metal and plastic sheets, the tempering of glass, the drying of textiles, veneer, paper, and the cooling of microelectronic equipment. As was pointed out in [1], the heat transfer coefficients by jet impingement are several times greater than those by other flow patterns. Because of the high heat transfer rate associated with jet impingement, the technique is commonly used in practice.

The rapid development of large scale integrated circuits presents a serious need for more powerful cooling technique since very high heat flux density is generated in the integrated circuit chips. Because of the limitation of the traditional cooling techniques such as air cooling and indirect liquid cooling, it is now recognized that direct liquid cooling such as jet impingement will become a viable cooling technique of microelectronic components with high level heat dissipation. Jet impingement technique can provide technical flexibility and adaptability which are essential for complicated electronic configuration and non-homogeneous thermal conditions. The experiments by Jiji and Dagan [2] show that the single-phase multi-jet impingement cooling is feasible and can be exploited to cool chips with heat flux up to 2×10^{6} W/m^{2}.

The study of the conjugate heat transfer characteristics of a single impinging jet is of significance in engineering applications. When a single jet is used, it is important to examine the heat transfer

characteristics to predict the temperature or heat flux distribution at the impingement surface. In many applications, an array of jets is used to obtain high heat transfer rate and maintain uniform surface temperature. In order to achieve the best arrangement of the jet array, it is essential to understand the heat transfer characteristics of a single impinging jet.

Although considerable experimental work on jet impingement heat transfer has been done, limited analytical studies have been carried out, especially for the case of a free impinging liquid jet and non-uniform wall temperature or wall heat flux. Note that all previous work on jet impingement deals with the fluid phase only. In contrast to a submerged jet, a free liquid jet is discharged into a gaseous rather than liquid environment. It should be mentioned that the heat transfer of free impinging jet is not the same as that of submerged impinging jet since the flow field is different for the two cases. Furthermore, When the wall temperature or wall heat flux is non-uniform, the problem becomes much more complicated and the solution method will be substantially different from those used for uniform wall temperature or wall heat flux.

When a free liquid jet impinges on a flat solid surface, as shown in Figure 1, the entire flow field is conventionally divided into two regions [3]: a potential region and a viscous region (boundary layer). The flow in the potential region may be treated as inviscid and the region may be subdivided into three subregions [4]: the free jet region, the impingement region and the wall jet region. The viscous region before the hydraulic jump may be subdivided into four subregions as follows [5]:

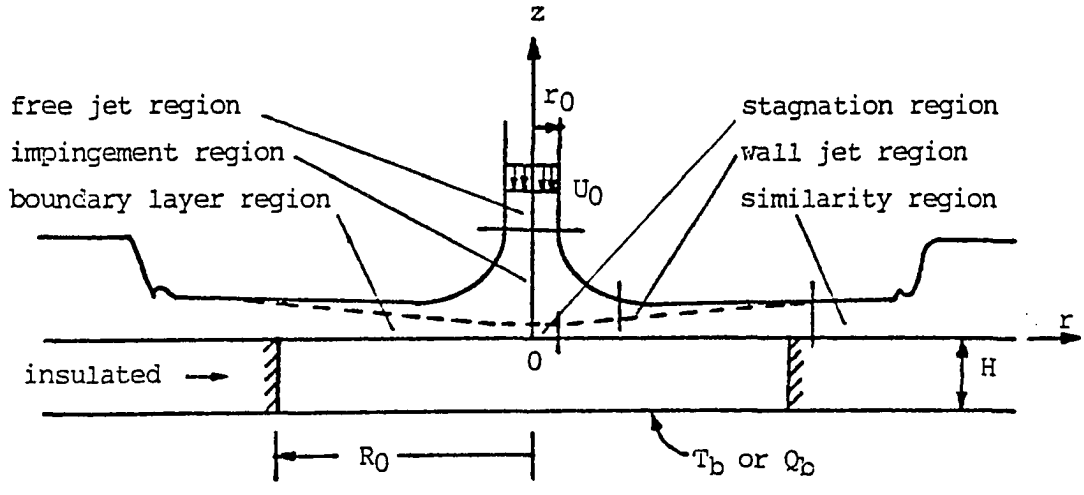

Figure 1 Schematic diagram of a free impinging jet system

1. The stagnation region where the main flow velocity at the edge of the boundary layer grows rapidly from zero at the stagnation point to the jet velocity U_0. The radial dimension of stagnation region is of the order of the jet radius r_0 and the boundary layer thickness is of the order $\sqrt{\nu r_0/U_0}$, where ν is the kinematic viscosity of the fluid.

2. The boundary layer region where the radial distance is greater than r_0. In this region, the velocity outside the boundary layer remains constant and the flow is of the boundary layer type.

3. The transition region where the boundary layer becomes as thick as the whole liquid layer.

4. The similarity region where the whole flow is of boundary layer type and there exists a similarity solution to the velocity field.

In fact, there must be a transition region between the stagnation and the boundary layer regions because at $r \approx r_0$ the flow pattern is different from that in the neighborhood of the stagnation point and in the boundary layer region. In the present work, this region will be considered separately.

An experimental investigation of the hydrodynamic behavior of a single circular free liquid jet impinging on a horizontal surface was carried out by Olsson and Turkdogan [6], who measured the kinetic energy of the liquid film, the thickness of the liquid layer and the surface velocity of radial flow. His measurements show that the surface velocity remains constant up to the hydraulic jump. This is different from the theoretical result of Watson [5] which shows that the surface velocity decreases as r increases in the similarity region.

Heat transfer near a stagnation point has been extensively investigated. Squire [7] and Sibulkin [8] were among the first to study stagnation point heat transfer. Squire obtained the exact solution to the problem of steady, laminar flow heat transfer near a two-dimensional stagnation point with constant wall temperature. Sibulkin extended the problem to the case of axisymmetrical stagnation point. Their solutions show that if the wall temperature is constant, the temperature distribution near the stagnation point is independent of the radial distance from the stagnation point. Transient heat transfer near a stagnation point has been examined by several investigators. Chao and Jeng [9] considered transient laminar forced convection heat transfer for a two-dimensional or axisymmetrical stagnation point due to time dependent uniform wall temperature or wall heat flux. Sano [10] obtained an asymptotic solution for small values of Prandtl number to the problem of unsteady boundary layer in impulsive stagnation flow in which both the flow field and temperature field are unsteady. The effects of blowing and suction on transient heat transfer at a stagnation point due to a step change with time in wall temperature was analyzed by the same author [11]. Kumari and Nath [12] considered the combined effect of forced and free convection on unsteady laminar incompressible boundary layer flow with mass transfer at the stagnation point of a three-dimensional body with time dependent wall temperature. More recently, Smolsky et al. [13] presented experimental and theoretical results of heat transfer in the region near the stagnation point of a sphere and transversely-oriented cylinder immersed in a gas flow under the unsteady conditions resulting from a stepwise change in the flow temperature or the body temperature.

In all previous solutions [7-13], the wall temperature or wall heat flux is either constant or a function of time only. Hence the temperature distribution near the stagnation point is independent of radial location. The boundary layer energy equation used in obtaining these solutions excludes the contribution of radial conduction. However, in many applications, wall temperature or wall heat flux may vary with the radial distance r. In such a case, the temperature distribution near the stagnation point will be a function of the axial distance z as well as r. Furthermore, if the variation of wall temperature or wall heat flux is sufficiently large such that the characteristic length for the temperature field in the r direction is of the same order as the thermal boundary layer thickness, conduction in the radial direction can not be neglected. Consequently, the boundary layer energy equation is not applicable and the exact energy equation should be used. Radial conduction plays a much more important role in the stagnation region than elsewhere since the velocity is so small and thus radial convection is negligible. It is clear that the flow pattern near the stagnation point of a finite jet is similar to that near the stagnation point of a infinite stream and so are the heat transfer characteristics.

The heat transfer between a laminar, circular impinging jet and a flat solid surface has been examined by a number of investigators. Chaudhury [14] investigated the heat transfer in the boundary layer region and similarity region. His solution is based on the velocity distribution obtained by Watson [5]. In his paper, the stagnation region is ignored. An integral solution was obtained in the boundary layer region and a similarity solution to the energy equation was given

in the similarity region. He considered two specific cases. In the first case the wall is thermally insulated for $r \leq r_s$ and is maintained at a constant temperature which is different from that of jet at $r>r_s$, where $r = r_s$ is located in the similarity region. In the second case the wall is maintained at a constant temperature throughout. Brdlik and Savin [1] solved the heat transfer problem of jet impingement with constant wall temperature by the integral method and also obtained experimental results. Their integral solution is based on the assumption that the ratio of thermal boundary layer thickness to viscous boundary layer thickness is $1/Pr^{1/3}$. Only average heat transfer coefficient was obtained in their experimental work. Saad et al. [15] numerically examined heat transfer from a laminar, semi-confined axisymmetric submerged impinging jet. They used an upwind finite-difference representation of the momentum and energy equations to predict the flow and local heat transfer characteristics of a laminar round jet impinging normally on a flat wall. Laminar jet impingement heat transfer including the effects of melting was considered by Lipsett and Gilpin [16]. The solution of the potential flow problem was obtained by finite element method and the boundary layer problem was solved by the Karman-Pohlausen integral method. When there is no effect of melting, the results show that a maximum in heat transfer distribution exists near $r = r_0$, where r_0 is the jet radius.

Heat transfer of submerged wall jets was investigated analytically by Mitachi and Ishiguro [17]. They obtained similarity solutions to the energy equation for the boundary conditions of isothermal wall, uniform

wall heat flux and adiabatic wall. For the case of a step change in the wall temperature, the energy equation is solved numerically.

The heat transfer characteristics of turbulent jet impingement is different from that of laminar jet impingement. It was pointed out by Donaldson et al. in [18] that the stagnation point heat transfer coefficient increases linearly with the turbulence intensity for the relative turbulence intensity less than 10% and for two-dimensional flow. The slope of the linear increase becomes larger when the Reynolds number is increased. The computation of the stagnation point heat transfer in the presence of turbulence can be handled by computing the laminar stagnation point heat transfer and then applying a turbulence correction factor which is a function of the free stream turbulence level and the jet to impingement surface distance. It was reported by Kestin et al. [19] that the correction factor could be as high as 1.8 for turbulence levels as low as 2.7%.

The heat transfer between impinging turbulent jets and solid surfaces has been intensively studied. Watson [5] analytically examined the flow field of the boundary layer region of an impinging turbulent jet by employing Glauert's hypothesis [20] for the eddy viscosity model. Numerical solutions of the turbulent jet impingement heat transfer problem were carried out by Tomich [21], Wolfshtein [22] and Murray et al. [23]. In these solutions, a finite difference technique was used to investigate the flow field and the heat transfer characteristics of turbulent jet impingement. It was concluded that even more recent finite difference codes for turbulent flow calculation would be unlikely to provide acceptable results in the impinging jet system since the turbulent models are not suitable for the heat

transfer problem. Martin [24] summarized the results of many experimental investigations of heat and mass transfer in impinging gas jet system. His summary shows that for single air jet, the local Nusselt number decreases monotonically for large jet to target plate distance. For small jet to plate distance, however, a second maximum value of the Nusselt number which may exceed the stagnation point Nusselt number can be detected. This is due to the transition of the wall boundary layer flow from laminar to turbulent. In [25], Pamadi and Belov pointed out that if the impinging jet is not fully developed, the heat transfer coefficient exhibits two secondary peaks. The inner peak at r = 0.5d, where d is the jet diameter, is due to the non-uniform, mixing-induced turbulence in the developing jet. The outer peak at r = 1.6d-2d is associated with the transition of the flow field from laminar to turbulent. Gardon and Cobonpue [26] measured the local heat transfer coefficient between impinging single or multiple circular turbulent jets and solid surfaces with Reynolds number from $7x10^{3}$ to $1.12x10^{5}$. The results show that the stagnation point heat transfer coefficient varies considerably with the ratio of the distance between the nozzle exit and the impingement surface to the nozzle diameter.

In all previous work on jet impingement heat transfer, only the fluid phase is considered and the boundary conditions are prescribed at the impingement surface. In engineering applications, however, most convective heat transfer problems are conjugate problems in which the conditions at the fluid-solid interface are unknown before the problems are solved. In such a case, the energy equations for the fluid and solid phases should be solved simultaneously.

This thesis investigates the conjugate heat transfer characteristics of a laminar free jet impinging on the top surface of a solid plate with arbitrary temperature or heat flux prescribed on the non-impingement surface. The analysis will consist of solutions to three problems. The first problem is for the heat transfer in the vicinity of the stagnation point with arbitrary wall temperature or wall heat flux. The second one deals with the heat transfer in the boundary layer region with arbitrary wall temperature or wall heat flux, and the third is the conjugate problem in which the energy equations for the fluid and solid phases are solved simultaneously. Finally, the analytical solution will be applied to predict the surface temperature and heat flux of a microelectronic chip cooled by a laminar impinging FC-77 liquid jet or water jet with uniform heat flux specified at the non-impingement surface. In the stagnation region, both the exact energy equation and the boundary layer energy equation will be solved asymptotically. While in the boundary layer region, the energy equation will be solved by the superposition method. The similarity region will be ignored since the heat transfer characteristics in that region are not very different from those in the boundary layer region. The solutions for the fluid phase can be expressed in terms of the prescribed temperature or heat flux. For the solid phase, only a circular part corresponding to the stagnation region and the boundary layer region will be considered. For convenience, the lateral surface of the circular part is assumed to be insulated. As a matter of fact, this is similar to the experimental model for the jet impingement cooling of microelectronic chips in which a chip with high thermal conductivity is press-fitted through a hole in

a plate with very low thermal conductivity. The general solution for the solid phase will be obtained by the method of separation of variables and matched with that for the fluid phase by requiring the continuity of temperature and heat flux at the impingement surface.

Chapter 2

Heat Transfer in the Stagnation Region of a Laminar Impinging Liquid Jet with Arbitrary Wall Temperature or Wall Heat Flux

2.1 Objectives

In the neighborhood of the stagnation point, the radial velocity is very small and the viscous boundary layer thickness is constant. Hence the flow pattern and the heat transfer characteristics in the stagnation region is substantially different from those in the other regions of an impinging jet. This chapter deals with the heat transfer in the stagnation region for the case of arbitrary temperature or heat flux prescribed at the impingement surface. The case of small variation of wall temperature or wall heat flux will be considered first. In such a case, the radial conduction term of the energy equation can be neglected and the resulting equation can be solved by the expansion method for the small values of the radial distance. Then, the solution for the steep variation of wall temperature or wall heat flux will be obtained asymptotically. In this solution, the radial conduction term should be included and the radial convection term can be neglected. When the radial convection term is neglected, the resulting energy equation can be solved by the method of separation of variables. The objectives of this chapter are: (1) to obtain an analytical solution to the energy equation in the vicinity of the stagnation point which can be used to solve the conjugate problem; (2) to investigate the effect of the prescribed wall temperature or wall heat flux on the Nusselt number near the stagnation point.

2.2 Formulation

For steady state, incompressible flow with constant properties and negligible dissipation, the governing equations in the neighborhood of an axisymmetrical stagnation point are

Continuity

$$\frac{\partial u}{\partial r} + \frac{u}{r} + \frac{\partial w}{\partial z} = 0 \tag{2.1}$$

Momentum

$$u\frac{\partial u}{\partial r} + w\frac{\partial u}{\partial z} = -\frac{1}{\rho}\frac{\partial P}{\partial r} + \nu\left(\frac{\partial^2 u}{\partial r^2} + \frac{1}{r}\frac{\partial u}{\partial r} - \frac{u}{r^2} + \frac{\partial^2 u}{\partial z^2} \right) \tag{2.2a}$$

$$u\frac{\partial w}{\partial r} + w\frac{\partial w}{\partial z} = -\frac{1}{\rho}\frac{\partial P}{\partial z} + \nu\left(\frac{\partial^2 w}{\partial r^2} + \frac{1}{r}\frac{\partial w}{\partial r} + \frac{\partial^2 w}{\partial z^2} \right) \tag{2.2b}$$

Energy

$$u\frac{\partial T}{\partial r} + w\frac{\partial T}{\partial z} = \alpha\left(\frac{\partial^2 T}{\partial r^2} + \frac{1}{r}\frac{\partial T}{\partial r} + \frac{\partial^2 T}{\partial z^2}\right) \tag{2.3}$$

where P and T are pressure and temperature, r and z are the radial and axial coordinates measured from the stagnation point, u and w are the velocity components along r and z, and and α are the density, kinematic viscosity and thermal diffusivity of the fluid, respectively. The accompanying hydrodynamic boundary conditions are

$$u = 0 \qquad \text{at} \quad r = 0 \tag{2.4a}$$

$$u = w = 0 \qquad \text{at} \quad z = 0 \tag{2.4b}$$

$$u = U(r) \qquad \text{as} \quad z \to \infty \tag{2.4c}$$

where $U(r) = ar$ is given by the solution to the corresponding potential flow and a is a constant which is the radial velocity gradient of the potential flow at the stagnation point. For the case of a circular impinging jet, [3] gives

$$a = 0.44\frac{U_0}{r_0} \tag{2.5}$$

where U_0 is jet velocity and r_0 is jet radius. The boundary conditions for the temperature field are

$$\frac{\partial T}{\partial r} = 0 \qquad \text{at } r = 0 \tag{2.6a}$$

$$T = T_m(z) \qquad \text{at } r = r_m \tag{2.6b}$$

$$T = T_w(r) \quad \text{or} \quad Q = Q_w(r) \qquad \text{at } z = 0 \tag{2.6c}$$

$$T = T_\infty = \text{constant} \qquad \text{as } z \to \infty \tag{2.6d}$$

where T_∞ is jet temperature, $T_w(r)$ wall temperature, $Q_w(r)$ wall heat flux. $T_m(z)$ is the temperature distribution at $r = r_m$ which is determined by matching the solution in the stagnation region with the solution outside the stagnation region. The matching surface $r = r_m$ is the location where the boundary layer thickness in the stagnation region is matched with that outside the stagnation region.

The solution to the momentum equation (2.2) with the boundary conditions (2.4) is given in [27] and the validity of the solution is restricted to the neighborhood of the stagnation point. The results are

$$u = \sqrt{a\nu}\xi\phi'(\eta) \tag{2.7a}$$

$$w = -2\sqrt{a\nu}\phi(\eta) \tag{2.7b}$$

where $\phi(\eta)$ is a transformation function defined by

$$\phi''' + 2\phi\phi'' - \phi'^2 + 1 = 0 \tag{2.8a}$$

$$\phi(0) = \phi'(0) = 0, \quad \phi'(\infty) = 1 \tag{2.8b}$$

and ξ and η are dimensionless variables defined by

$$\xi = r/\sqrt{\nu/a} \tag{2.9a}$$

$$\eta = z/\sqrt{\nu/a} \tag{2.9b}$$

A series solution to (2.8) was obtained in [28] as follows

$$\phi = b_2\eta^2 + b_3\eta^3 + b_6\eta^6 + b_7\eta^7 + \ldots \tag{2.10a}$$

where

$$b_2 = 0.65597, \qquad b_3 = -0.16667$$

$$b_6 = 0.36443\times10^{-2} \qquad b_7 = -0.39683\times10^{-3} \tag{2.10b}$$

The viscous boundary layer thickness in the vicinity of the stagnation point is constant and given by

$$\delta_s = 1.98\sqrt{\nu/a} \tag{2.11}$$

where ν is the kinematic viscosity. To non-dimensionalize the energy equation (2.3), the following dimensionless temperature is introduced

$$\theta = \begin{cases} (T-T_\infty)/(T_0-T_\infty) & \text{for prescribed wall temperature} \\ k(T-T_\infty)/(Q_0\sqrt{\nu/a}) & \text{for prescribed wall heat flux} \end{cases} \tag{2.12}$$

where k is the thermal conductivity of the fluid, T_0 and Q_0 are the temperature and heat flux at the stagnation point, respectively. The dimensionless forms of the energy equation (2.3) and boundary conditions (2.6), therefore, become

$$\xi\phi'\frac{\partial\theta}{\partial\xi} - 2\phi\frac{\partial\theta}{\partial\eta} = \frac{1}{Pr}\left(\frac{\partial^2\theta}{\partial\xi^2} + \frac{1}{\xi}\frac{\partial\theta}{\partial\xi} + \frac{\partial^2\theta}{\partial\eta^2}\right) \tag{2.13}$$

$$\frac{\partial\theta}{\partial\xi} = 0 \qquad \text{at} \quad \xi = 0 \tag{2.14a}$$

$$\theta = \theta_m(\eta) \qquad \text{at} \quad \xi = \xi_m \tag{2.14b}$$

$$\theta = \theta_w(\xi) \quad \text{or} \quad -\frac{\partial\theta}{\partial\eta} = \frac{Q_w}{Q_0} = F_w(\xi) \qquad \text{at} \quad \eta = 0 \tag{2.14c}$$

$$\theta = 0 \qquad \text{as} \quad \eta \to \infty \tag{2.14d}$$

where Pr is the Prandtl number, $\theta_m(\eta)$ and $\theta_w(\xi)$ are the dimensionless temperatures defined as follows

$$\theta_m = \begin{cases} (T_m-T_\infty)/(T_0-T_\infty) & \text{for prescribed wall temperature} \\ k(T_m-T_\infty)/(Q_0\sqrt{\nu/a}) & \text{for prescribed wall heat flux} \end{cases} \quad (2.15a)$$

$$\theta_w = \begin{cases} (T_w-T_\infty)/(T_0-T_\infty) & \text{for prescribed wall temperature} \\ k(T_w-T_\infty)/(Q_0\sqrt{\nu/a}) & \text{for prescribed wall heat flux} \end{cases} \quad (2.15b)$$

and ξ_m is defined as

$$\xi_m = r_m/\sqrt{\nu/a} \quad (2.15c)$$

2.3 Solutions

2.3.1 Solution for Small Variation of Wall Temperature or Wall Heat Flux

In the case where the variation of wall temperature or wall heat flux is sufficiently small so that the characteristic length of temperature field in the r direction is much larger than the thermal boundary layer thickness, conduction in r direction can be neglected. Hence the energy equation (2.13) and boundary conditions (2.14) reduce to

$$\frac{\partial^2\theta}{\partial\eta^2} + 2\Pr\phi\frac{\partial\theta}{\partial\eta} - \Pr\xi\phi'\frac{\partial\theta}{\partial\xi} = 0 \quad (2.16)$$

and

$$\frac{\partial \theta}{\partial \xi} = 0 \qquad \text{at } \xi = 0 \tag{2.17a}$$

$$\theta = \theta_w(\xi) \quad \text{or} \quad -\frac{\partial \theta}{\partial \eta} = F_w(\xi) \qquad \text{at } \eta = 0 \tag{2.17b}$$

$$\theta = 0 \qquad \text{at } \eta = \infty \tag{2.17c}$$

The prescribed wall temperature $\theta_w(\xi)$ or wall heat flux $Q_w(\xi)$ may be any continuous function of ξ, which satisfies the symmetry condition $\frac{d\theta_w(0)}{d\xi} = 0$ or $\frac{dQ_w(0)}{d\xi} = 0$. Corresponding to the definition in (2.12), $\theta_w(\xi)$ may be expanded in a Taylor series near $\xi = 0$ as follows

$$\theta_w(\xi) = 1 + c_2\xi^2 + c_3\xi^3 + \ldots + c_n\xi^n + \ldots \tag{2.18}$$

where c_n are constants. Similarly, the wall heat flux may be written as

$$-\frac{\partial \theta(\xi,0)}{\partial \eta} = F_w(\xi) = 1 + d_2\xi^2 + d_3\xi^3 + \ldots + d_n\xi^n + \ldots \tag{2.19}$$

where d_n are constants. Since a solution is sought in the vicinity of the stagnation point, the dependent variable θ can be expanded in a Taylor series as follows

$$\theta = A_0(\eta) + A_1(\eta)\xi + A_2(\eta)\xi^2 + \ldots + A_n(\eta)\xi^n + \ldots \tag{2.20}$$

Because of the symmetry, the radial heat flux at r = 0 must be zero, hence $A_1(\eta)$ in (2.20) should vanish. Substituting (2.20) into (2.16), the governing ordinary differential equations for the coefficients A_n are obtained

$$A_n'' + 2Pr\phi A_n' - nPr\phi' A_n = 0 , \quad n = 0, 2, 3, 4 \ldots \tag{2.21}$$

The corresponding boundary conditions for the prescribed wall temperature are

$$A_0(0) = 1, \quad A_n(0) = c_n , \quad n = 2, 3, 4 \ldots \tag{2.22a}$$

$$A_n(\infty) = 0 , \quad n = 0, 2, 3, 4 \ldots \tag{2.22b}$$

For prescribed wall heat flux the boundary conditions are

$$A_0'(0) = -1 , \quad A_n'(0) = -d_n , \quad n = 2, 3, 4 \ldots \tag{2.23a}$$

$$A_n(\infty) = 0 , \quad n = 0, 2, 3, 4 \ldots \tag{2.23b}$$

(1) Solution for Prescribed Wall Temperature

The solution of $A_0(\eta)$ with the boundary conditions (2.22) can be obtained in closed form

$$A_0(\eta) = 1 - \frac{\int_0^\eta e^{-2Pr\int_0^\eta \phi d\eta} d\eta}{\int_0^\infty e^{-2Pr\int_0^\eta \phi d\eta} d\eta} \tag{2.24}$$

while the remaining $A_n(\eta)$ coefficients may be solved numerically. Once $A_n(\eta)$ are obtained, the temperature field is determined by (2.20) and the wall heat flux can be obtained as follows

$$q_w = -k\frac{\partial T(r,0)}{\partial z} = -k(T_0 - T_\infty)\sqrt{a/\nu}[A_0'(0) + A_2'(0)\xi^2 + \ldots] \tag{2.25}$$

Thus the heat transfer coefficient is

$$h = -\frac{k\sqrt{a/\nu}}{\theta_w}[A_0'(0) + A_2'(0)\xi^2 + \ldots + A_n'(0)\xi^n + \ldots] \tag{2.26}$$

and the local Nusselt number is given by

$$Nu = \frac{2r_0h}{k} = -0.9381Re^{1/2}\frac{A_0'(0) + A_2'(0)\xi^2 + A_3'(0)\xi^3 + \ldots + A_n'(0)\xi^n + \ldots}{1 + c_2\xi^2 + c_3\xi^3 + \ldots + c_n\xi^n + \ldots} \tag{2.27}$$

where Re is the Reynolds number defined as $2U_0r_0/\nu$.

(2) Solution for Prescribed Wall Heat Flux

The solution of $A_0(\eta)$ with the boundary conditions (2.23) is

$$A_0(\eta) = \int_0^\infty e^{-2Pr\int_0^\eta \phi d\eta} d\eta - \int_0^\eta e^{-2Pr\int_0^\eta \phi d\eta} d\eta \qquad (2.28)$$

The solutions to $A_n(\eta)$, n = 2, 3, 4 ... with the boundary conditions (2.23) may be obtained numerically. Once $A_n(\eta)$ are determined, the wall temperature is given by

$$T_w = T_\infty + \frac{Q_0\sqrt{\nu/a}}{k}[A_0(0) + A_2(0)\xi^2 + \ldots + A_n(0)\xi^n + \ldots] \qquad (2.29)$$

The local heat transfer coefficient is obtained in the following form

$$h = \frac{k\sqrt{a/\nu}\, F_w(\xi)}{A_0(0) + A_2(0)\xi^2 + A_3(0)\xi^3 + \ldots + A_n(0)\xi^n + \ldots} \qquad (2.30)$$

and the Nusselt number distribution is

$$Nu = 0.9381\, Re^{1/2} \frac{1 + d_2\xi^2 + d_3\xi^3 + \ldots + d_n\xi^n + \ldots}{A_0(0) + A_2(0)\xi^2 + A_3(0)\xi^3 + \ldots + A_n(0)\xi^n + \ldots} \qquad (2.31)$$

For the special case of constant wall temperature or wall heat flux, i.e. $c_2 = c_3 = \ldots = c_n = 0$ or $d_2 = d_3 = \ldots = d_n = 0$, (2.27) and (2.31) reduce to

$$Nu = \frac{0.9381 Re^{1/2}}{\int_0^\infty e^{-2Pr\int_0^\eta \phi d\eta} d\eta} \tag{2.32}$$

which is identical to the result of Sibulkin [8].

The Nusselt number profiles for both cases are shown graphically in Figures 2 and 3 respectively. It is clear from equations (2.24), (2.27), (2.28) and (2.31) that the wall temperature or wall heat flux distribution does not affect the stagnation point Nusselt number. The reason for this is that the boundary layer energy equation is used in obtaining the solution in which radial conduction is neglected. As we will see in the following sections, the stagnation point Nusselt number can be considerably affected by the distribution of wall temperature or wall heat flux when radial conduction is taken into consideration.

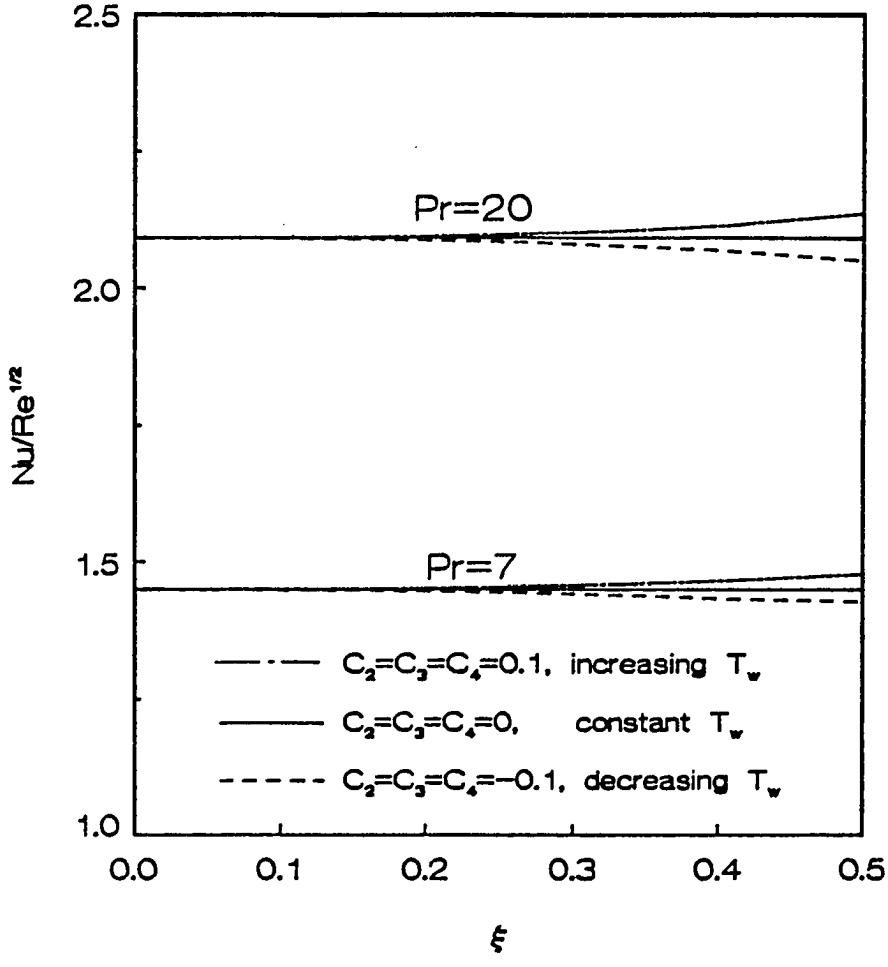

Fig. 2 Nusselt number profile for non-uniform wall temperature with radial conduction neglected

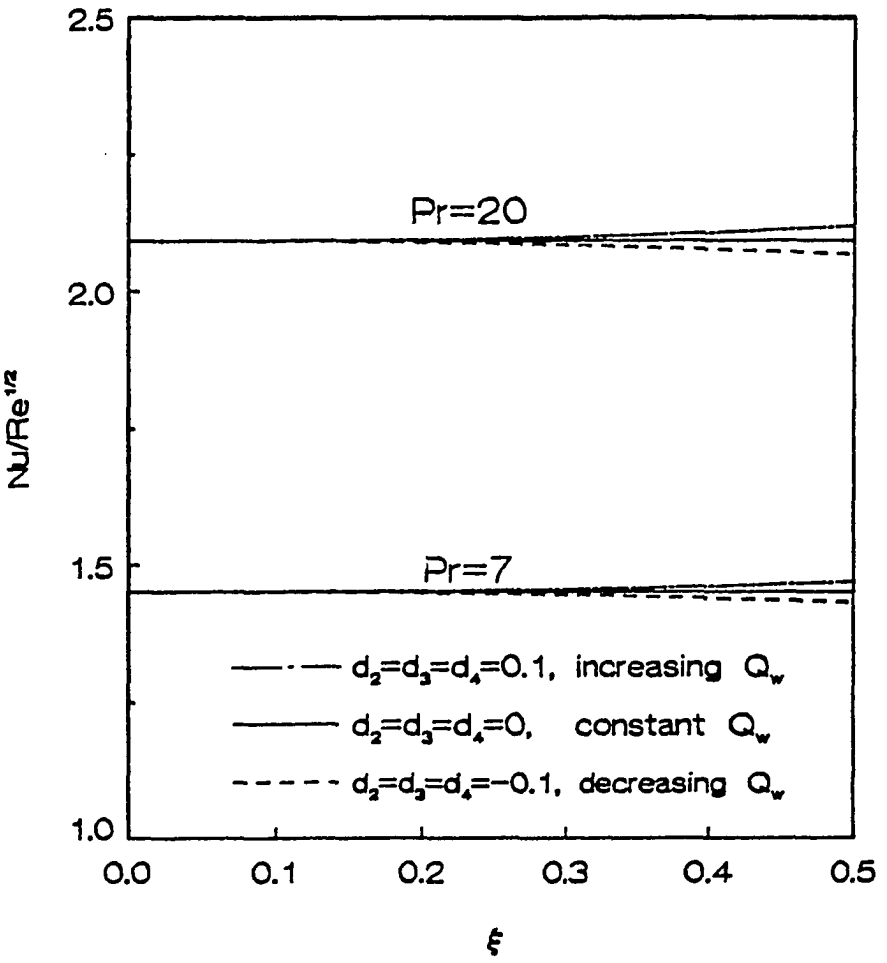

Fig. 3 Nusselt number profile for non-uniform wall heat flux with radial conduction neglected

2.3.2 Solution for Steep Variation of Wall Temperature or Wall Heat Flux

The solution in the previous section is valid for the case where the variation of wall temperature or wall heat flux is small so that the boundary layer energy equation is applicable. If, however, the wall temperature or wall heat flux varies steeply with r, conduction in radial direction must be included. Hence the complete energy equation should be solved. Nevertheless, one can show that the first term in equation (2.13) which represents radial convection can be neglected in the vicinity of the stagnation point. Substitution of (2.20) into (2.13) shows that the first term in equation (2.13) is of order ξ^2 and all other terms are of order one. Hence, in the vicinity of the stagnation point, i.e. for small ξ, equation (2.13) simplifies to

$$\frac{\partial^2\theta}{\partial\xi^2} + \frac{1}{\xi}\frac{\partial\theta}{\partial\xi} + \frac{\partial^2\theta}{\partial\eta^2} + 2\Pr\phi\frac{\partial\theta}{\partial\eta} = 0 \tag{2.33}$$

Since ϕ is independent of ξ, equation (2.33) can be solved by the method of separation of variables. For convenience, we introduce the following equation

$$\theta = \theta_1 + \theta_2 + \frac{\xi^2}{\xi_m^2}\theta_m(\eta) \tag{2.34}$$

and then, equation (2.33) and the boundary conditions (2.14) can be written as

$$\frac{\partial^2\theta_1}{\partial\xi^2} + \frac{1}{\xi}\frac{\partial\theta_1}{\partial\xi} + \frac{\partial^2\theta_1}{\partial\eta^2} + 2\Pr\phi\frac{\partial\theta_1}{\partial\eta} = 0 \qquad (2.35a)$$

$$\frac{\partial\theta_1}{\partial\xi} = 0 \qquad \text{at } \xi = 0 \qquad (2.35b)$$

$$\theta_1 = 0 \qquad \text{at } \xi = \xi_m \qquad (2.35c)$$

$$\theta_1 - \theta_w(\xi) = -\frac{\xi^2}{\xi_m^2}\theta_m(0) \quad \text{or} \quad -\frac{\partial\theta_1}{\partial\eta} = F_w(\xi) + \frac{\xi^2}{\xi_m^2}\theta_m'(0) \qquad \text{at } \eta = 0 \qquad (2.35d)$$

$$\theta_1 = 0 \qquad \text{at } \eta = \infty \qquad (2.35e)$$

and

$$\frac{\partial^2\theta_2}{\partial\xi^2} + \frac{1}{\xi}\frac{\partial\theta_2}{\partial\xi} + \frac{\partial^2\theta_2}{\partial\eta^2} + 2\Pr\phi\frac{\partial\theta_2}{\partial\eta} = -\frac{4}{\xi_m^2}\theta_m(\eta) - \frac{\xi^2}{\xi_m^2}(\theta_m'' + 2\Pr\phi\theta_m') \qquad (2.36a)$$

$$\frac{\partial\theta_2}{\partial\xi} = 0 \qquad \text{at } \xi = 0 \qquad (2.36b)$$

$$\theta_2 = 0 \qquad \text{at } \xi = \xi_m \qquad (2.36c)$$

$$\theta_2 = 0 \quad \text{or} \quad \frac{\partial\theta_2}{\partial\eta} = 0 \qquad \text{at } \eta = 0 \qquad (2.36d)$$

$$\theta_2 = 0 \qquad \text{at } \eta = \infty \qquad (2.36e)$$

By the method of separation of variables, the solution to (2.35) can be obtained as follows

$$\theta_1 = \sum_{n=1}^{\infty} g_n(\eta)J_0(\lambda_n\xi) \qquad (2.37)$$

where λ_n is given by $J_0(\lambda_n\xi_m) = 0$ and $g_n(\eta)$ is governed by the following ordinary differential equation

$$g_n'' + 2Pr\phi g_n' - \lambda_n^2 g_n = 0 \tag{2.38}$$

The boundary conditions corresponding to equation (2.38) are

$$g_n(0) = \frac{2}{G}\int_0^{\xi_m} [\ \theta_w(\xi) - \frac{\xi^2}{\xi_m^2}\theta_m(0)\ ] J_0(\lambda_n\xi)\xi d\xi \tag{2.39a}$$

$$g_n(\infty) = 0 \tag{2.39b}$$

for prescribed wall temperature, and

$$g_n'(0) = -\frac{2}{G}\int_0^{\xi_m} [\ F_w(\xi) + \frac{\xi^2}{\xi_m^2}\theta_m'(0)\ ] J_0(\lambda_n\xi)\xi d\xi \tag{2.40a}$$

$$g_n(\infty) = 0 \tag{2.40b}$$

for prescribed wall heat flux. G in (2.39) and (2.40) is given by

$$G = \xi_m^2\ [J_1(\lambda_n\xi_m)]^2 \tag{2.41}$$

To solve (2.36), we assume that the solution can be written in the following form

$$\theta_2 = \sum_{n=1}^{\infty} D_n(\eta) J_0(\lambda_n\xi) \tag{2.42}$$

Then, D_n can be expressed in terms of θ_2 as follows

$$D_n = \frac{2}{G}\int_0^{\xi_m} \theta_2 J_0(\lambda_n\xi)\xi d\xi \tag{2.43}$$

It follows that

$$D_n'' + 2Pr\phi D_n' = \frac{2}{G}\int_0^{\xi_m}\left[\frac{\partial^2\theta_2}{\partial\eta^2} + 2Pr\phi\frac{\partial\theta_2}{\partial\eta}\right]J_0(\lambda_n\xi)\xi d\xi \qquad (2.44)$$

Introduction of (2.36) into (2.44) leads to

$$D_n'' + 2Pr\phi D_n' - \lambda_n^2 D_n = L(\eta) \qquad (2.45)$$

where

$$L(\eta) = -\frac{8\theta_m}{G\lambda_n\xi_m}J_1(\lambda_n\xi_m) - \frac{2}{G\lambda_n^2}[\lambda_n\xi_m J_1(\lambda_n\xi_m) - 2J_2(\lambda_n\xi_m)](\theta_m'' + 2Pr\phi\theta_m') \qquad (2.46)$$

The boundary conditions for D_n are

$$D_n(0) = 0, \qquad D_n(\infty) = 0 \qquad (2.47)$$

for prescribed wall temperature, and

$$D_n'(0) = 0, \qquad D_n(\infty) = 0 \qquad (2.48)$$

for prescribed wall heat flux.

Equation (2.38) can be solved numerically for any prescribed $\theta_w(\xi)$ or $F_w(\xi)$ since $\theta_m(0) = \theta_w(\xi_m)$ in (2.39) and $\theta_m'(0) = -F_w(\xi_m)$ in (2.40), and thus θ_1 can be determined by (2.37). In order to solve (2.45), it

is necessary to know $\theta_m(\eta)$ which should be determined by matching this solution with the solution outside the stagnation region. Once $\theta_m(\eta)$ is known, θ_2 is determined completely and the temperature distribution near the stagnation point becomes

$$\theta = \frac{\xi^2}{\xi_m^2}\theta_m(\eta) + \sum_{n=1}^{\infty}[g_n(\eta) + D_n(\eta)]J_0(\lambda_n\xi) \tag{2.49}$$

Before proceeding further, the solution in the transition region between the stagnation region and the boundary region will be obtained and $\theta_m(\eta)$ will be determined.

2.3.3 Integral Solution in the Transition Region

The transition region through which the flow field changes with r from stagnation type to the boundary layer type is located at $r \approx r_0$ where the radial velocity is well developed and radial convection is much more important than radial conduction. Hence the latter can be neglected and the temperature field is of boundary layer type. The integral form of momentum and energy equations for radial flow is

$$\frac{d}{dr}\left[\int_0^{\delta} ru(U_0 - u)dz\right] = \nu r\frac{\partial u(r,0)}{\partial z} \tag{2.50}$$

and

$$\frac{d}{dr}[\int_0^{\delta_t} ru(T - T_\infty)dz] = - \frac{\nu r}{Pr} \frac{\partial T(r,0)}{\partial z} \tag{2.51}$$

The velocity and temperature distributions may be assumed to have the forms

$$u = U_0(\frac{2z}{\delta} - \frac{2z^3}{\delta^3} + \frac{z^4}{\delta^4}) \tag{2.52}$$

and

$$T - T_\infty = [T_w(r) - T_\infty](1 - \frac{2z}{\delta_t} + \frac{2z^3}{\delta_t^3} - \frac{z^4}{\delta_t^4}) \tag{2.53}$$

for prescribed wall temperature or

$$T - T_\infty = \frac{Q_w(r)\delta_t}{k}(\frac{1}{2} - \frac{z}{\delta_t} + \frac{z^3}{\delta_t^3} - \frac{z^4}{2\delta_t^4}) \tag{2.54}$$

for prescribed wall heat flux. δ and δ_t are the viscous and thermal boundary layer thicknesses, respectively. Introduction of (2.52) into (2.50) yields

$$\delta(r) = \sqrt{\frac{420}{37} \frac{\nu}{U_0} r + \frac{c}{r^2}} \tag{2.55}$$

where c is a constant to be determined by matching (2.55) with (2.11) at $r = r_m$. The matching conditions are

$$\delta_s(r_m) = \delta(r_m), \qquad \frac{d}{dr}\delta_s(r_m) = \frac{d}{dr}\delta(r_m) \tag{2.56}$$

which give

$$r_m = 0.52 r_0 , \qquad c = 0.81 \frac{\nu}{U_0} r_0^3 \tag{2.57}$$

Substituting (2.52) and (2.53) into (2.51), one obtains an ordinary differential equation which determines Δ, the ratio of thermal boundary layer thickness to the viscous boundary layer thickness for the case of prescribed wall temperature

$$\frac{d}{dr}\{r\delta(r)[T_w(r) - T_\infty]H(\Delta)\} = \frac{2\nu r}{U_0 Pr} \frac{T_w(r) - T_\infty}{\delta(r)\Delta} \tag{2.58}$$

where

$$H(\Delta) = \begin{cases} \frac{2}{15}\Delta^2 - \frac{3}{140}\Delta^4 + \frac{1}{180}\Delta^5 & Pr \geq 1 \\ \frac{3}{10}\Delta - \frac{3}{10} + \frac{2}{15\Delta} - \frac{3}{140\Delta^3} + \frac{1}{180\Delta^4} & Pr < 1 \end{cases} \tag{2.59}$$

and

$$\Delta = \delta_t/\delta \tag{2.60}$$

For the special case of constant wall temperature, equation (2.58) becomes identical to that obtained by Chaudhury [14]. For the case of prescribed wall heat flux, substitution of (2.52) and (2.54) into (2.51) leads to

$$\frac{d}{dr}[rQ_w(r)\delta^2(r)\Delta H(\Delta)] = \frac{2\nu}{PrU_0}rQ_w(r) \tag{2.61}$$

The boundary condition $\Delta(\xi_m) = \Delta_m$ needed to solve (2.58) and (2.61) is determined in such a way that the curve of Nusselt number profile is smooth at $\xi = \xi_m$. Computations show that the Nusselt number near the stagnation point is not sensitive to Δ_m. For $\Delta_m = 0.5/Pr^{1/3}$ and $\Delta_m = 3/Pr^{1/3}$, for instance, the difference in the stagnation point Nusselt number is less than 1%. Once Δ is known, the temperature field in the transition region is determined by (2.53) and (2.54) which may be written in dimensionless form as

$$\theta(\xi,\eta) = \theta_w(\xi)[1 - \frac{2\eta}{\delta_{td}(\xi)} + \frac{2\eta^3}{\delta^3_{td}(\xi)} - \frac{\eta^4}{\delta^4_{td}(\xi)}] \tag{2.62}$$

for prescribed wall temperature, and

$$\theta(\xi,\eta) = F_w(\xi)\delta_{td}[\frac{1}{2} - \frac{\eta}{\delta_{td}(\xi)} + \frac{\eta^3}{\delta^3_{td}(\xi)} - \frac{\eta^4}{2\delta^4_{td}(\xi)}] \tag{2.63}$$

for prescribed wall heat flux. δ_{td} in (2.62) and (2.63) is the dimensionless form of the thermal boundary layer thickness and is given by

$$\delta_{td} = \delta_t/\sqrt{\nu/a} \tag{2.64}$$

Therefore, $\theta_m(\eta)$ is given by

$$\theta_m(\eta) = \theta(\xi_m,\eta) \tag{2.65}$$

2.4 Results and Discussion

Once equations (2.38) and (2.45) are solved, the temperature distribution in the neighborhood of the stagnation point is given by (2.49), hence the heat transfer coefficient can be determined.

(1) Results for Prescribed Wall Temperature

The heat flux on the wall is

$$q_w = -k\frac{T_0 - T_\infty}{\sqrt{\nu/a}}\left\{\frac{\xi^2}{\xi_m^2}\theta_m'(0) + \sum_{n=1}^{\infty}[g_n'(0) + D_n'(0)]J_0(\lambda_n\xi)\right\} \tag{2.66}$$

Consequently, the heat transfer coefficient in the vicinity of the stagnation point is

$$h = -\frac{k}{\theta_w\sqrt{\nu/a}}\left\{\frac{\xi^2}{\xi_m^2}\theta_m'(0) + \sum_{n=1}^{\infty}[g_n'(0) + D_n'(0)]J_0(\lambda_n\xi)\right\} \tag{2.67}$$

and the Nusselt number is given by

$$Nu = -0.9381\frac{Re^{1/2}}{\theta_w}\left\{\frac{\xi^2}{\xi_m^2}\theta_m'(0) + \sum_{n=1}^{\infty}[g_n'(0) + D_n'(0)]J_0(\lambda_n\xi)\right\} \qquad (2.68)$$

(2) Result for Prescribed Wall Heat Flux

For prescribed wall heat flux, the wall temperature is

$$T_w - T_\infty = \frac{Q_0\sqrt{\nu/a}}{k}\left\{\frac{\xi^2}{\xi_m^2}\theta_m(0) + \sum_{n=1}^{\infty}[g_n(0) + D_n(0)]J_0(\lambda_n\xi)\right\} \qquad (2.69)$$

Thus the local heat transfer coefficient is

$$h = \frac{kF_w(\xi)}{\sqrt{\nu/a}\left(\frac{\xi^2}{\xi_m^2}\theta_m(0) + \sum_{n=1}^{\infty}[\,g_n(0) + D_n(0)\,]J_0(\lambda_n\xi)\right)} \qquad (2.70)$$

and the Nusselt number is

$$Nu = \frac{0.9381Re^{1/2}F_w(\xi)}{\frac{\xi^2}{\xi_m^2}\theta_m(0) + \sum_{n=1}^{\infty}[\,g_n(0) + D_n(0)\,]J_0(\lambda_n\xi)} \qquad (2.71)$$

In order to examine the effect of wall temperature or wall heat flux on the heat transfer near the stagnation point, the Nusselt number has been calculated for different profiles of prescribed wall temperature and wall heat flux as well as different values of Prandtl

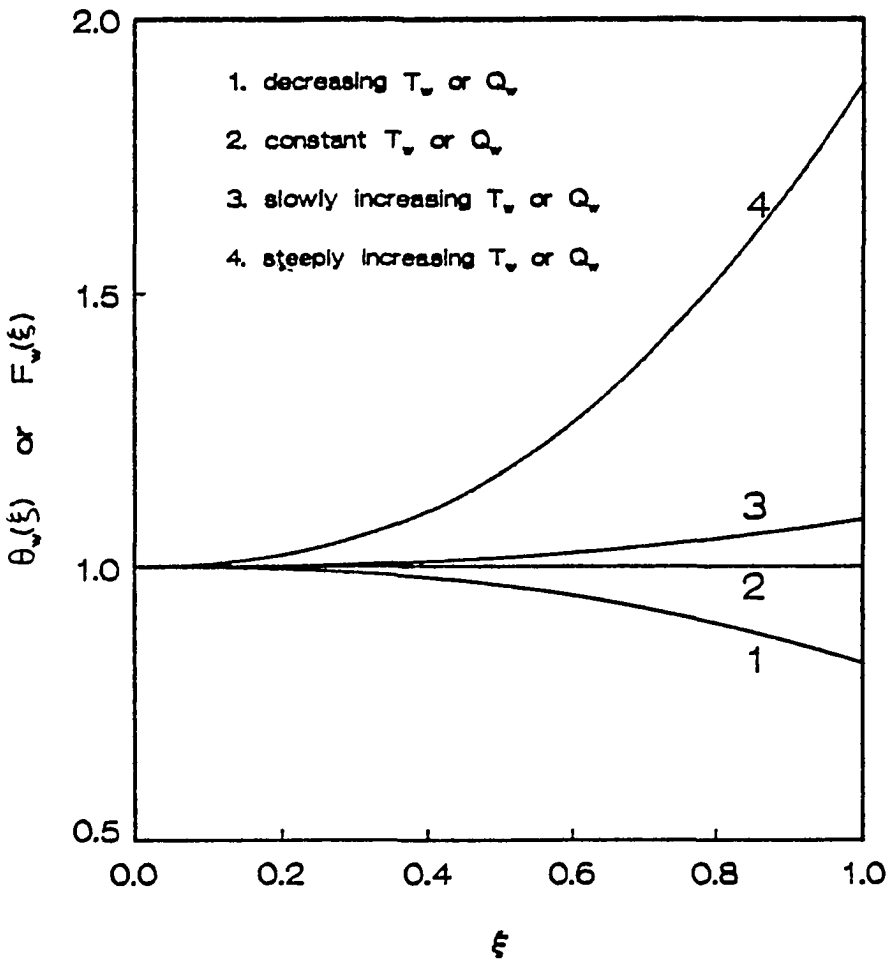

Fig. 4 Prescribed wall temperature or wall heat flux

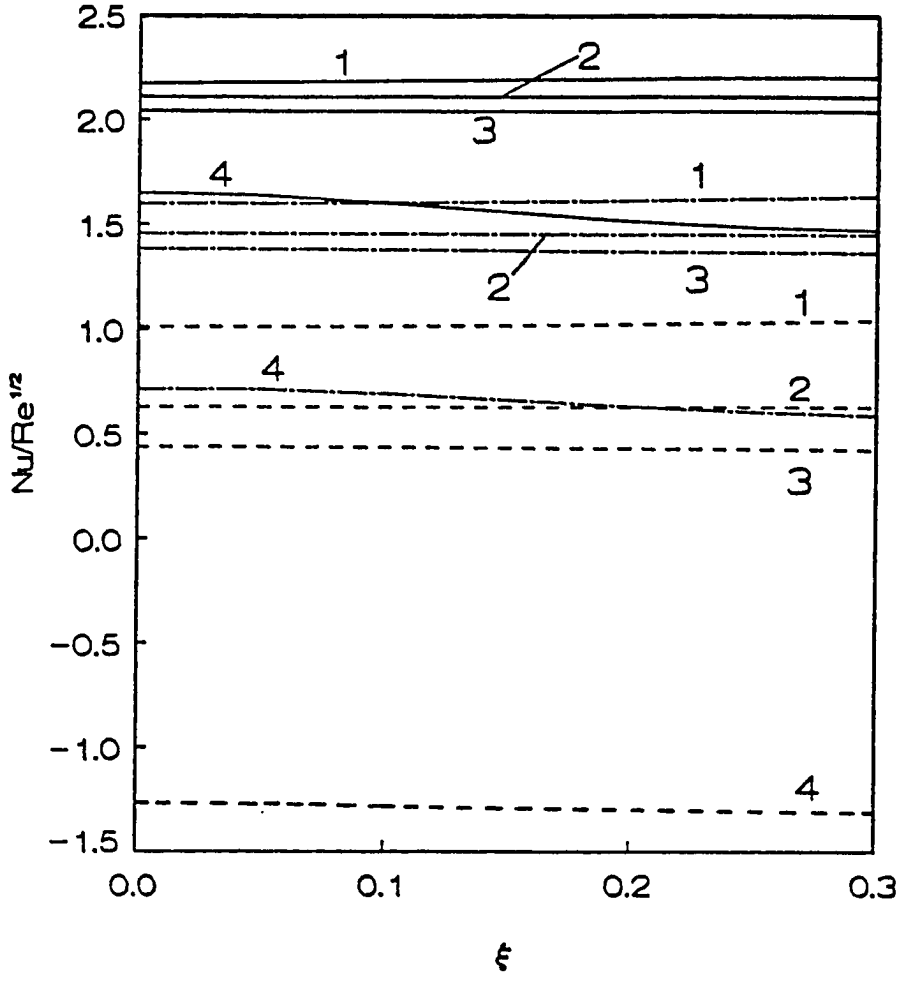

Fig. 5 Nusselt number profile for non-uniform wall temperature shown in Fig. 4

1. for decreasing wall temperature
2. for constant wall temperature
3. for slowly increasing wall temperature
4. for steeply increasing wall temperature

——— Pr = 20 —·— Pr = 7 - - - - Pr = 0.7

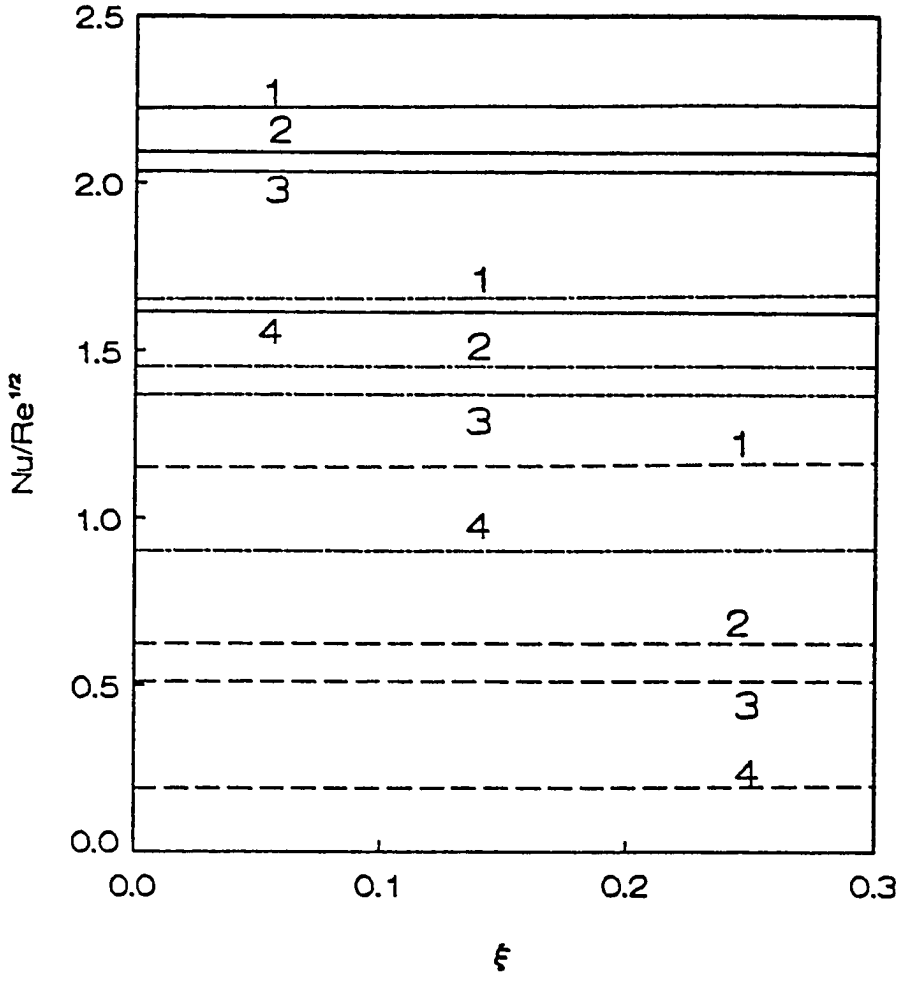

Fig. 6 Nusselt number profile for non-uniform wall heat flux shown in Fig. 4

1. for decreasing wall heat flux
2. for constant wall heat flux
3. for slowly increasing wall heat flux
4. for steeply increasing wall heat flux

——— Pr = 20 —·— Pr = 7 - - - - Pr = 0.7

number. Figure 4 shows these wall temperature and wall heat flux profiles graphically. Curve 1 represents decreasing wall temperature or wall heat flux with r and curve 2 is for constant wall temperature or wall heat flux. While curves 3 and 4 represent slowly and steeply increasing wall temperature or wall heat flux, respectively. Computations show that for the special case of constant wall temperature or wall heat flux, the Nusselt number is essentially the same as that of Sibulkin [8], the difference being less than 0.3% for $Pr \geq 0.7$. Radial variation of Nusselt number is shown in Figures 5 and 6 for $Pr = 0.7$, 7, and 20 corresponding to air, water and Fluorocarbon liquids, respectively.

It can be seen from Figures 5 and 6 that the stagnation point heat transfer can be influenced considerably by the wall temperature or wall heat flux distribution. The reason for this is that when the wall temperature or wall heat flux varies appreciably with r, the characteristic length of temperature field in the r direction may be of the same order as that in the z direction. In such a case, conductions in the r direction and in the z direction are comparable. Furthermore, near the stagnation point the velocity is small so that radial convection is negligible as shown in section 2.3.2. Hence, conduction dominates in the r direction near the stagnation point. The fact that the the velocity is small in the vicinity of the stagnation point can be seen in equations (2.7) and (2.10) which show that u is of order $\xi\eta$ and w is of order η^2.

As shown in Figures 5 and 6, increasing the wall temperature or wall heat flux with r reduces the stagnation point Nusselt number. For slowly increasing wall temperature or wall heat flux, the reduction is

small. For steeply increasing wall temperature or wall heat flux, however, the stagnation point Nusselt number is considerably reduced. When the wall temperature or wall heat flux decreases as r increases, stagnation point Nusselt number is higher than that for constant wall temperature or wall heat flux. This is due to the fact that heat is conducted radially from the stagnation point when the wall temperature or wall heat flux decreases with r. Consequently, the heat flux from the wall to the fluid at the stagnation point is increased. On the other hand, when the wall temperature or wall heat flux increases with r, heat is conducted towards the stagnation point and consequently, stagnation point Nusselt number is reduced. The Figures also indicate that the effect of wall temperature or wall heat flux on the stagnation point Nusselt number becomes more pronounced as the Prandtl number is decreased. This is due to the fact that the radial conduction plays a more important role when the Prandtl number is smaller. It is worth noting that stagnation point Nusselt number can be negative when the wall temperature increases with r very steeply. In such a case, the effect of radial conduction is so sever that the fluid becomes hotter than the wall near the stagnation point and, hence, heat flows from the fluid to the wall although the wall is hotter than the jet.

In Figure 7, the Nusselt number is compared with the result obtained in section 2.3.1 in which the radial conduction is neglected for the case of non-uniform wall temperature. The comparison is given for two different wall temperature profiles. The first one is for the case where the characteristic length of temperature field in the r direction is much smaller than that in the z direction, while the

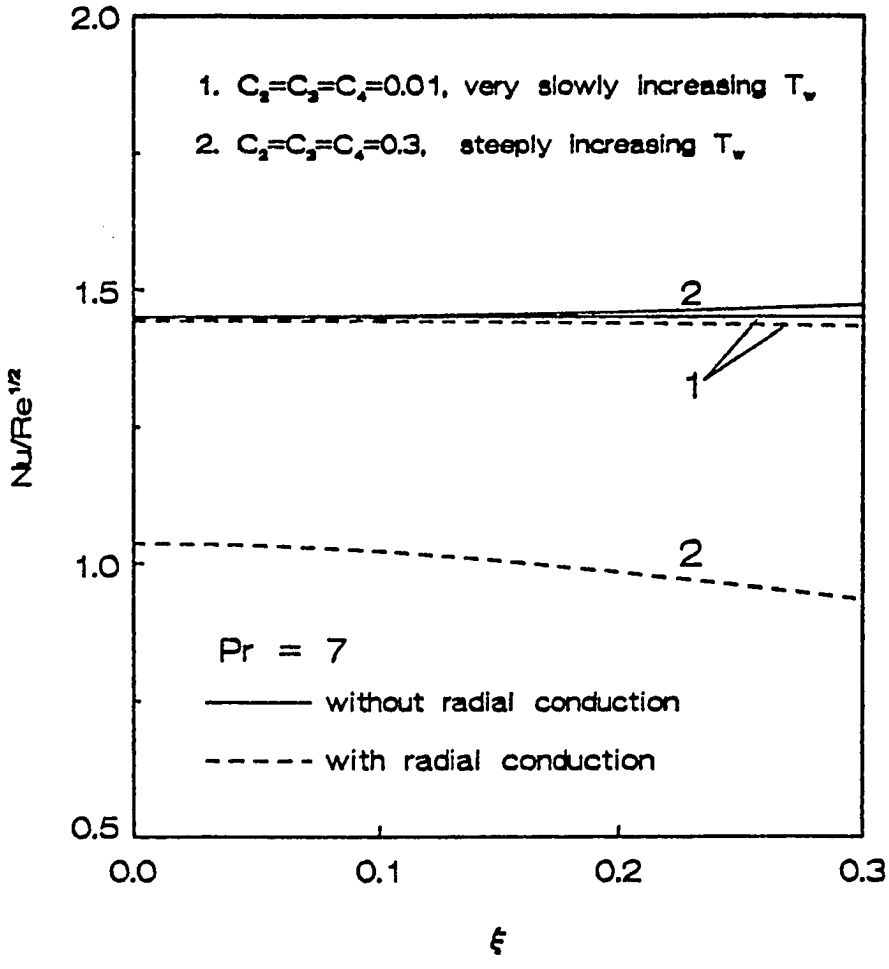

Fig. 7 Comparison between the results with and without radial conduction

second one is for the case where the two characteristic lengths are comparable. It is clear that for the first case the two curves are essentially the same. It follows that radial conduction can be neglected in such a case. For the second case, however, the difference is considerable and hence radial conduction can not be ignored.

The sensitivity of the solution to the value of r_m, the radial distance from the stagnation point to the matching location, is investigated by calculating the Nusselt number for $\xi_m = 15$ and $\xi_m = 25$ for a typical case of moderately increasing wall temperature and $Pr = 7$. The result shows that the Nusselt number near the stagnation point is essentially the same for $\xi_m = 15$ and $\xi_m = 25$. Hence the solution is not sensitive to the value of r_m.

In order to examine the error of the solution resulting from neglecting the radial convection term near the stagnation point, we consider a simplified case where radial conduction is neglected. In such a case, the solution to the energy equation can be obtained analytically for the cases with the radial convection term and without that term. The difference between the two solutions can be taken as an upper bound of the error resulting from neglecting the radial convection term in our solution since the radial convection plays a less important role when radial conduction is included than when it is neglected. For the first case where the radial convection is included, the solution was obtained in section 2.3.1. For the second case where both radial convection and conduction are neglected, the energy equation (2.3) becomes

$$\alpha\frac{\partial^2 T}{\partial z^2} - w\frac{\partial T}{\partial z} = 0 \tag{2.72}$$

and the boundary conditions are

$$\frac{\partial T}{\partial r} = 0 \qquad \text{at } r = 0 \tag{2.73a}$$

$$T = T_w(r) \qquad \text{at } z = 0 \tag{2.73b}$$

$$T = T_\infty \qquad \text{at } z = \infty \tag{2.73c}$$

The dimensionless temperature is introduced as follows

$$\theta_s = \frac{T - T_\infty}{T_w - T_\infty} \tag{2.74}$$

Note that T_w may be non-uniform. Introduction of (2.7) and (2.74) into (2.72) and (2.73) leads to the following ordinary differential equation and boundary conditions

$$\frac{d^2\theta_s}{d\eta^2} + 2Pr\phi\frac{d\theta_s}{d\eta} = 0 \tag{2.75a}$$

$$\theta_s(0) = 1, \quad \theta_s(\infty) = 0 \tag{2.75b}$$

where ϕ is given in (2.8). Note that the first condition in (2.73) is satisfied automatically since T_w must satisfy $\frac{dT_w(0)}{dr} = 0$. The solution to (2.75) is

$$\theta_s = 1 - \frac{\int_0^{\eta} e^{-2Pr\int_0^{\eta}\phi d\eta}\, d\eta}{\int_0^{\infty} e^{-2Pr\int_0^{\eta}\phi d\eta}\, d\eta} \tag{2.76}$$

The wall heat flux can be obtained as

$$q_w = \frac{k(T_w - T_\infty)}{\sqrt{\nu/a}\int_0^{\infty} e^{-2Pr\int_0^{\eta}\phi d\eta}\, d\eta} \tag{2.77}$$

Thus the heat transfer coefficient is

$$h = \frac{k}{\sqrt{\nu/a}\int_0^{\infty} e^{-2Pr\int_0^{\eta}\phi d\eta}\, d\eta} \tag{2.78}$$

and the Nusselt number is

$$Nu = \frac{0.9381 Re^{1/2}}{\int_0^{\infty} e^{-2Pr\int_0^{\eta}\phi d\eta}\, d\eta} \tag{2.79}$$

which is independent of wall temperature profile and is the same as (2.32). This result is plotted in Figure 8 and compared with the result including radial convection. The Figure shows that the two results are exactly the same at $\xi = 0$. This is because the velocity is zero at $\xi = 0$ and hence the effect of radial convection vanishes. For $\xi > 0$, however, the two results are slightly different and the difference increases

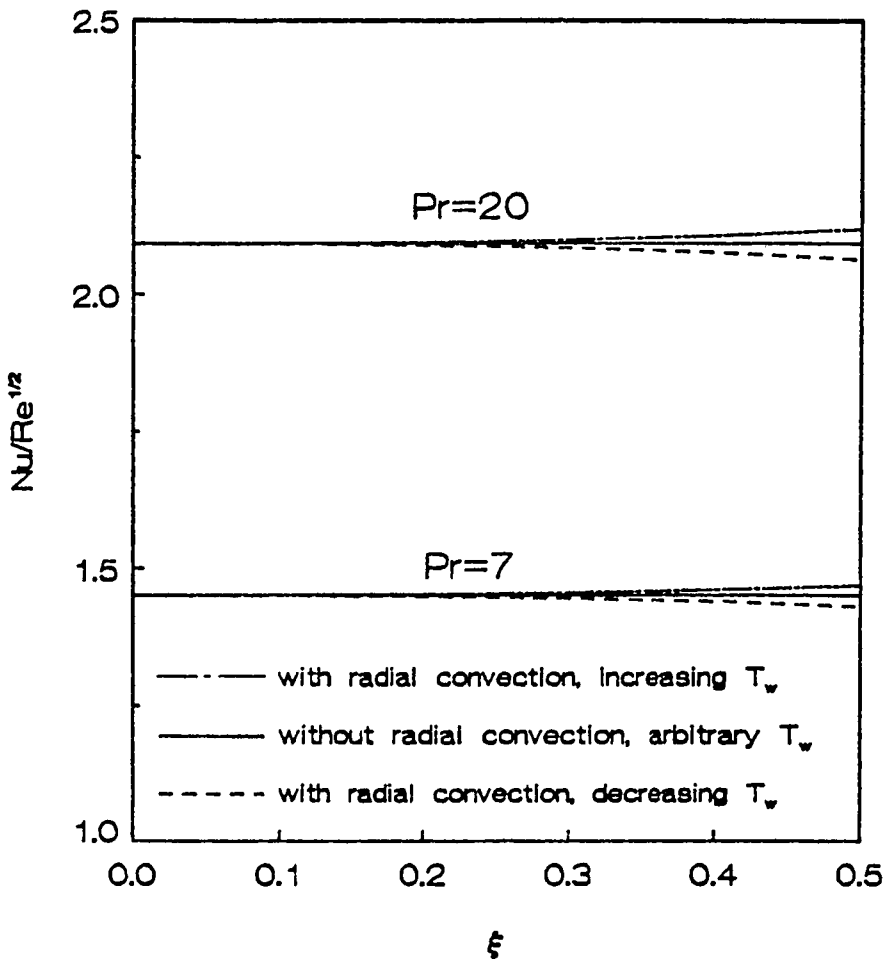

Fig. 8 Comparison between the results with and without radial convection

with r. When the wall temperature or wall heat flux increases with r, the Nusselt number with the effect of radial convection is slightly higher than that without the effect of radial convection. The reason is that the radial convection enhances the wall heat flux when the wall temperature increases with r and reduces the wall temperature when the wall heat flux increases with r. On the other hand, the Nusselt number including the radial convection is slightly lower than that excluding the radial convection if the wall temperature or wall heat flux decreases as r increases. This is due to the fact that the radial convection reduces the wall heat flux if the wall temperature decreases with r and increases the wall temperature if the wall heat flux decreases with r. For $\xi \ll 1$, the difference is negligibly small hence neglecting the radial convection is a reasonable simplification near the stagnation point.

2.5 Concluding Remarks

The heat transfer near the stagnation point of a circular free impinging jet with non-uniform wall temperature or wall heat flux has been investigated analytically. The solution shows considerable effect of wall temperature or wall heat flux distribution on the stagnation point Nusselt number when the variation of wall temperature or wall heat flux is not small. The reason is that the radial velocity is so small that the radial convection is negligible in the vicinity of the stagnation point. Hence the radial conduction plays a much more important role near the stagnation point than it does in other regions. Consequently, considerable error would result from using boundary layer energy equation in the presence of appreciable variation of wall temperature or wall heat flux.

Chapter 3

Heat Transfer in the Boundary Layer Region of a Laminar Impinging Liquid Jet with Arbitrary Wall Temperature or Wall Heat Flux

3.1 Objectives

In the boundary layer region, the radial velocity is well developed and the temperature field is of boundary layer type. This chapter will deal with the heat transfer in the boundary layer region for arbitrary wall temperature or wall heat flux. Because of the linearity of the energy equation, the superposition method can be used to obtain the solution. The analysis will begin with obtaining the solution to the problem with a step change in wall temperature or wall heat flux. The solution to the corresponding problem with arbitrary wall temperature or wall heat flux is then obtained by superposition. The result will be matched with that for the stagnation region obtained in chapter 2 so that the Nusselt number distribution throughout the stagnation region and the boundary layer region can be obtained. The objectives of this chapter are: (1) to investigate the heat transfer characteristics in the boundary layer region of an impinging liquid jet for arbitrary wall temperature or wall heat flux; (2) to obtain an analytical solution which can be used to solve the corresponding conjugate problem.

3.2 Formulation

In the boundary layer region, radial convection is much more important than the radial conduction and hence the temperature field is of boundary layer type. For such a flow, the governing equations are

Continuity

$$\frac{\partial u}{\partial r} + \frac{u}{r} + \frac{\partial w}{\partial z} = 0 \tag{3.1}$$

Momentum

$$u\frac{\partial u}{\partial r} + w\frac{\partial u}{\partial z} = \nu\frac{\partial^2 u}{\partial z^2} \tag{3.2}$$

Energy

$$u\frac{\partial T}{\partial r} + w\frac{\partial T}{\partial z} = \alpha\frac{\partial^2 T}{\partial z^2} \tag{3.3}$$

The accompanying velocity boundary conditions are

$$u = w = 0 \qquad \text{at} \quad z = 0 \tag{3.4a}$$

$$u = U_0 \qquad \text{as} \quad z \to \infty \tag{3.4b}$$

where U_0 is the jet velocity. The boundary conditions for the temperature field are

$$T = T_w(r) \quad \text{or} \quad Q = Q_w(r) \qquad \text{at } z = 0 \tag{3.5a}$$

$$T = T_\infty \qquad \text{as } z \to \infty \tag{3.5b}$$

where T_∞ is jet temperature, $T_w(r)$ wall temperature and $Q_w(r)$ wall heat flux. The solution to the momentum equation (3.2) which satisfies the boundary conditions (3.4) is given in [5]. The result is

$$u = U_0 f'(\eta) \tag{3.6a}$$

$$w = \frac{\nu}{z}\left(-\eta f + \frac{\eta^2}{3} f' \right) \tag{3.6b}$$

where f is given by

$$f''' + ff'' = 0 \tag{3.7a}$$

$$f(0) = f'(0) = 0, \quad f'(\infty) = 1 \tag{3.7b}$$

and η is defined as

$$\eta = \sqrt{\frac{3U_0}{2\nu r}}\, z \tag{3.8}$$

The primes in (3.6) and (3.7) denote differentiation with respect to η. A series solution to (3.7) can be obtained as follows

$$f = a_2\eta^2 + a_5\eta^5 + a_8\eta^8 + a_{11}\eta^{11} + \ldots \tag{3.9}$$

where

$$a_2 = 0.23480\ , \qquad a_5 = -0.18377\times10^{-2} \tag{3.10a}$$

$$a_8 = 0.28252\times10^{-4}, \qquad a_{11} = -0.45686\times10^{-6} \tag{3.10b}$$

As was pointed out in [5], the above solution is based on the assumption of $r \gg r_0$ so that the conditions in the stagnation region do not affect the flow in the boundary layer region. To investigate the spatial range in which the above solution is applicable, we use the integral solution to examine the effect of the conditions in the stagnation region on the flow in the boundary layer region. Obviously, the integral solution obtained in chapter 2 is also valid in the boundary layer region. The term c/r^2 in (2.55) represents the influence of the stagnation region on the boundary layer thickness in the boundary layer region. If this effect is neglected, the boundary layer thickness given in (2.55) becomes

$$\delta' = \sqrt{\frac{420}{37}\frac{\nu}{U_0}r} \tag{3.11}$$

Comparison between (3.11) and (2.55) shows that for $r \geq 2r_0$, the stagnation region influence on the boundary layer thickness in the boundary layer region is smaller than 0.5%. It follows that solution (3.6) is valid for $r \geq 2r_0$ with negligible error.

3.3 Solutions

Because of the linearity of the energy equation (3.3), it is possible to obtain the solution by the superposition method. We seek a solution for the general case of arbitrary wall temperature or arbitrary wall heat flux. As shown in Figure 9, an arbitrary wall temperature distribution $T_w(r)$ or wall heat flux distribution $Q_w(r)$ may be divided into two parts. In the first part, the wall temperature or wall heat flux is $T_{w_1} = T_w(r) - T_w(r_1)$ or $Q_{w_1} = Q_w(r) - Q_w(r_1)$ for $r > r_1$ and is zero for $r \leq r_1$. In the second part, the wall temperature or wall heat flux is $T_{w_2} = T_w(r)$ or $Q_{w_2} = Q_w(r)$ for $r \leq r_1$ and is $T_{w_2} = T_w(r_1)$ or $Q_{w_2} = Q_w(r_1)$ for $r > r_1$. It follows that the temperature distribution in the boundary layer region for $r > r_1$ can also be divided into two parts. We will proceed by first obtaining the solution to the problem with a step change in wall temperature or wall heat flux. Then we obtain the solutions to the problem with $T_w = T_{w_1}$ or $Q_w = Q_{w_1}$ and $T_w = T_{w_2}$ or $Q_w = Q_{w_2}$ as shown in the Figure. Finally, the solution to the problem with arbitrary wall temperature or wall heat flux is obtained by superposition.

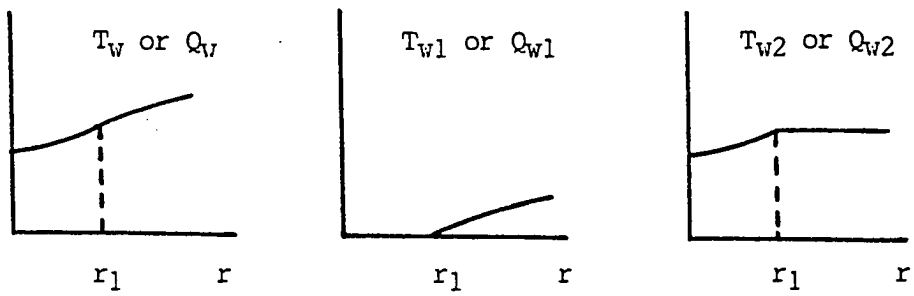

Fig. 9 Division of arbitrary wall temperature or wall heat flux

3.3.1 Solution for a Step Change in Wall Temperature

In the present section, we consider the case where part of the wall, $r \leq r^*$, is assumed to be thermally insulated and the rest maintained at a constant temperature T_1. The end point, $r = r^*$, of the thermally insulated part is located in the boundary layer region. Therefore, for $r \leq r^*$ the wall temperature is uniform and equal to the fluid temperature which is assumed to be zero for convenience. Consequently, the boundary conditions are

$$T(r^*, z) = 0, \quad T(r,\infty) = 0, \quad T(r>r^*,0) = T_1 \tag{3.12}$$

To write the energy equation and the boundary conditions in dimensionless form, we introduce the following dimensionless temperature and coordinates

$$\theta_{st} = \frac{T}{T_1} \tag{3.13}$$

and

$$R = 1 - \frac{r^*}{r}, \qquad \xi = b\frac{\eta}{R^{1/3}} \tag{3.14}$$

where η is defined in (3.8) and b is a constant to be determined later. The dimensionless forms of energy equation (3.3) and boundary conditions (3.12), therefore, become

$$\frac{\partial^2\theta_{st}}{\partial\xi^2} + \left[\frac{2Pr}{9b^2}\frac{1 - R}{R^{1/3}}\xi f' + \frac{Pr}{b}R^{1/3}f\right]\frac{\partial\theta_{st}}{\partial\xi} - \frac{2Pr}{3b^2}R^{2/3}(1 - R)f'\frac{\partial\theta_{st}}{\partial R} = 0 \tag{3.15}$$

and

$$\theta_{st}(R,0) = 1 , \qquad \theta_{st}(R,\infty) = 0 \tag{3.16}$$

The transformation (3.14) has two advantages: (1) R is always less than unity. This is very important for obtaining a series solution in powers of R. (2) The boundary conditions at $r = r^*$ and at $z = \infty$ are merged into one, therefore the number of boundary conditions is reduced to two. Since R is bounded between 0 and 1, the dependent variable θ_{st} can be expanded in a Taylor series as follows

$$\theta_{st} = F_0(\xi) + F_1(\xi)R + F_2(\xi)R^2 + F_3(\xi)R^3 + \ldots \tag{3.17}$$

Upon substituting (3.9), (3.14) and (3.17) into (3.15), comparing the coefficients of like power of R and introducing the following definitions

$$b = \frac{(4a_2)^{1/3}}{3}Pr^{1/3} = 0.32644Pr^{1/3} \tag{3.18}$$

$$e_1 = \frac{10Pr\ a_5}{9b^6} = -1.6875Pr^{-1} \tag{3.19a}$$

$$e_2 = \frac{16Pr\ a_8}{9b^9} = 1.1933Pr^{-2} \tag{3.19b}$$

$$F_1 = F_{11} + e_1F_{12} \tag{3.20a}$$

$$F_2 = e_1F_{21} + e_2F_{22} + F_{23} \tag{3.20b}$$

the governing ordinary differential equations and the boundary conditions for the universal functions $F_0(\xi)$, $F_{11}(\xi)$, $F_{12}(\xi)$, $F_{21}(\xi)$, $F_{22}(\xi)$ and $F_{23}(\xi)$, are obtained as follows

$$F_0'' + 3\xi^2 F_0' = 0 \tag{3.21a}$$

$$F_0(0) = 1, \quad F_0(\infty) = 0 \tag{3.21b}$$

$$F_{11}'' + 3\xi^2 F_{11}' - 9\xi F_{11} = -\frac{15}{4}\xi^2 F_0' \tag{3.22a}$$

$$F_{11}(0) = F_{11}(\infty) = 0 \tag{3.22b}$$

$$F_{12}'' + 3\xi^2 F_{12}' - 9\xi F_{12} = -\xi^5 F_0' \tag{3.23a}$$

$$F_{12}(0) = F_{12}(\infty) = 0 \tag{3.23b}$$

$$F_{21}'' + 3\xi^2 F_{21}' - 18\xi F_{21} = 3\xi^4 F_{11} - \xi^5 F_{11}' - 9\xi F_{12} - \frac{15}{4}\xi^2 F_{12}' + \frac{1}{10}\xi^5 F_0' \tag{3.24a}$$

$$F_{21}(0) = F_{21}(\infty) = 0 \tag{3.24b}$$

$$F_{22}'' + 3\xi^2 F_{22}' - 18\xi F_{22} = 2.3864(3\xi^4 F_{12} - \xi^5 F_{12}') - \xi^8 F_0' \tag{3.25a}$$

$$F_{22}(0) = F_{22}(\infty) = 0 \tag{3.25b}$$

$$F_{23}'' + 3\xi^2 F_{23}' - 18\xi F_{23} = -9\xi F_{11} - \frac{15}{4}\xi^2 F_{11}' \tag{3.26a}$$

$$F_{23}(0) = F_{23}(\infty) = 0 \tag{3.26b}$$

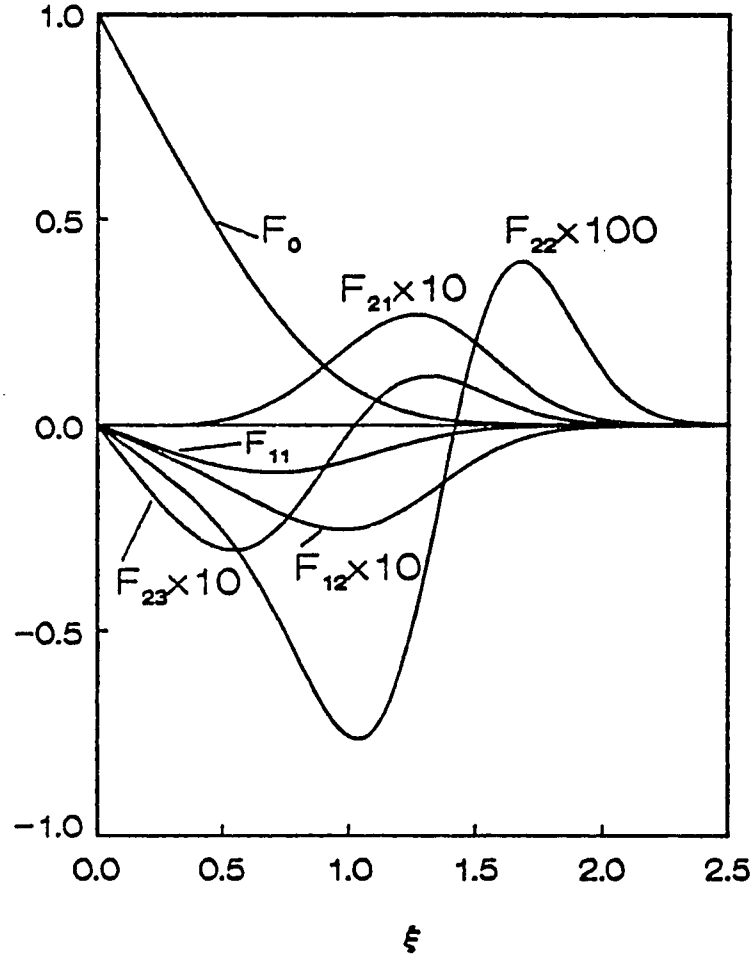

Fig. 10 F_{ij} functions for a step change in T_w

Table 1. Wall Derivatives

$F_0'(0)$	$F_{11}'(0)$	$F_{12}'(0)$	$F_{21}'(0)$	$F_{22}'(0)$	$F_{23}'(0)$
-1.1198	-0.23329	-0.027649	-0.00092164	-0.0044312	-0.077764

The solution to (3.21) is clearly

$$F_0(\xi) = 1 - \frac{3}{\Gamma(1/3)}\int_0^{\xi} e^{-\eta^3}\, d\eta \qquad (3.27)$$

The remaining equations (3.22)-(3.26) are solved numerically and the results are shown graphically in Figure 10. The associated wall derivatives are given in Table 1. With the information provided in Figure 10 and Table 1, the temperature field and the wall heat flux can be easily determined. The wall heat flux is obtained by differentiating equation (3.17) as follows

$$q_w = -k\sqrt{\frac{3U_0}{2\nu r}}\,\frac{b}{R^{1/3}}T_1[\, F_0'(0) + F_1'(0)R + F_2'(0)R^2 + \ldots] \qquad (3.28)$$

Hence the heat transfer coefficient h is

$$h = -k\sqrt{\frac{3U_0}{2\nu r}}\,\frac{b}{R^{1/3}}[\, F_0'(0) + F_1'(0)R + F_2'(0)R^2 + \ldots] \qquad (3.29)$$

and the Nusselt number is

$$\begin{aligned} Nu &= \frac{hd}{k} \\ &= -bRe^{1/2}\frac{\sqrt{\frac{3d}{2r}}}{(1 - r^*/r)^{1/3}}[F_0'(0) + F_1'(0)(1 - r^*/r) + \\ &\quad + F_2'(0)(1 - r^*/r)^2 + \ldots\ ] \end{aligned} \qquad (3.30)$$

where b is given in (3.18) and Re is the Reynolds number defined by $U_0 d/\nu$. d and ν are the jet diameter and kinematic viscosity of the fluid, respectively. The constants $F_0'(0)$, $F_1'(0)$ and $F_2'(0)$ in the above equations are given by

$$F_0'(0) = -\frac{3}{\Gamma(1/3)} \tag{3.31a}$$

$$F_1'(0) = -0.23329 + 0.046658Pr^{-1} \tag{3.31b}$$

$$F_2'(0) = -0.077764 + 0.0015553Pr^{-1} - 0.0052878Pr^{-2} \tag{3.31c}$$

Obviously, the above solution is valid for $r > r^*$ only.

The calculation shows that for Prandtl number of the order of unity or larger, the solution (3.17) converges very fast and good accuracy is obtainable with terms of up to order 2. For the fluids with very small Prandtl number such as liquid metal, however, the solution converges only when R is small. In such a case, Euler's transformation [33] may be used for the evaluation of the sum. The Nusselt number profile is plotted in Figure 11 for Pr = 0.7, 7 and 20, respectively.

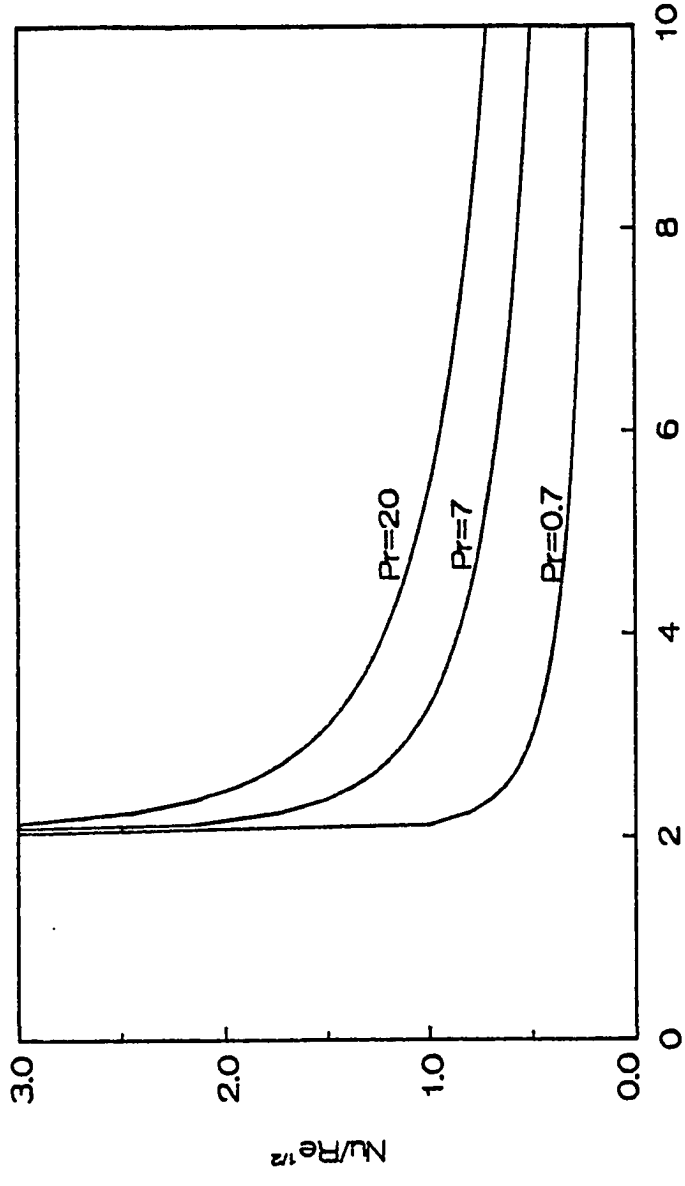

Fig. 11 Nusselt number profile for a step change in T_w at $r/r_o=2$

3.3.2 Solution for a Step Change in Wall Heat Flux

In this problem the prescribed wall heat flux is zero for $r \le r^*$ and q_1 for $r > r^*$ where r^* is located in the boundary layer region. Specifically, the boundary conditions are

$$T(r^*,z) = 0, \quad T(r,\infty) = 0, \quad -k\frac{\partial T(r>r^*,0)}{\partial z} = q_1 \tag{3.32}$$

A dimensionless temperature θ_{sq} is defined as follows

$$\theta_{sq} = \frac{b\sqrt{3U_0/2\nu r}\ k}{q_1 R^{1/3}}\ T \tag{3.33}$$

where the constant b is given by (3.18). The specific form (3.33) is motivated by the consideration that the transformed boundary condition on the wall is still a constant. The dimensionless form of the energy equation (3.3) and the boundary conditions (3.32) then become

$$\frac{\partial^2\theta_{sq}}{\partial\xi^2} + \left[\frac{2Pr}{9b^2}\frac{1-R}{R^{1/3}}\xi f' + \frac{Pr}{b}R^{1/3}f\right]\frac{\partial\theta_{sq}}{\partial\xi} - \frac{2Pr}{3b^2}R^{2/3}f'(1-R)\frac{\partial\theta_{sq}}{\partial R} -$$

$$- \frac{2Pr}{9b^2}R^{2/3}f'\left(\frac{1}{R}+\frac{1}{2}\right)\theta_{sq} = 0 \tag{3.34}$$

and

$$\frac{\partial\theta_{sq}}{\partial\xi} = -1 \quad \text{at} \quad \xi = 0 \tag{3.35a}$$

$$\theta_{sq} = 0 \quad \text{at} \quad \xi = \infty \tag{3.35b}$$

Note that the only difference between (3.15) and (3.34) is that (3.34) has one additional term, i.e. the last term. Proceeding as with equation (3.17), θ_{sq} can be written in the following form

$$\theta_{sq} = B_0(\xi) + B_1(\xi)R + B_2(\xi)R^2 + B_3(\xi)R^3 + \ldots \tag{3.36}$$

Following the same procedure as that in section 3.3.1 and introducing the following definitions

$$B_1 = e_1 B_{11} + B_{12} \tag{3.37a}$$

$$B_2 = e_2 B_{21} + e_1 B_{22} + B_{23} \tag{3.37b}$$

where e_1 and e_2 are given by (3.19), one obtains the following ordinary differential equations and the corresponding boundary conditions

$$B_0'' + 3\xi^2 B_0' - 3\xi B_0 = 0 \tag{3.38a}$$

$$B_0'(0) = -1, \quad B_0(\infty) = 0 \tag{3.38b}$$

$$B_{11}'' + 3\xi^2 B_{11}' - 12\xi B_{11} = \xi^4 B_0 - \xi^5 B_0' \tag{3.39a}$$

$$B_{11}'(0) = B_{11}(\infty) = 0 \tag{3.39b}$$

$$B_{12}'' + 3\xi^2 B_{12}' - 12\xi B_{12} = -\frac{15}{4}\xi^2 B_0' + \frac{3}{2}\xi B_0 \tag{3.40a}$$

$$B_{12}'(0) = B_{12}(\infty) = 0 \tag{3.40b}$$

$$B_{21}'' + 3\xi^2 B_{21}' - 21\xi B_{21} = 2.3864(4\xi^4 B_{11} - \xi^5 B_{11}') - \xi^8 B_0' + \xi^7 B_0 \tag{3.41a}$$

$$B_{21}'(0) = B_{21}(\infty) = 0 \tag{3.41b}$$

$$B_{22}'' + 3\xi^2 B_{22}' - 21\xi B_{22} = 4\xi^4 B_{12} - \xi^5 B_{12}' - \frac{15}{2}\xi B_{11} - \frac{15}{4}\xi^2 B_{11}' + \frac{1}{10}\xi^5 B_0' + \frac{1}{2}\xi^4 B_0 \tag{3.42a}$$

$$B_{22}'(0) = B_{22}(\infty) = 0 \tag{3.42b}$$

$$B_{23}'' + 3\xi^2 B_{23}' - 21\xi B_{23} = -\frac{15}{2}\xi B_{12} - \frac{15}{4}\xi^2 B_{12}' \tag{3.43a}$$

$$B_{23}'(0) = B_{23}(\infty) = 0 \tag{3.43b}$$

The solution of equation (3.38) can be obtained in closed form

$$B_0(\xi) = \frac{1}{\Gamma(2/3)}\left[e^{-\xi^3} + 3\xi\int_0^\xi \eta e^{-\eta^3} d\eta \right] - \xi \tag{3.44}$$

while equations (3.39)-(3.43) are solved numerically. Note that B_0, B_{11}, B_{12}, B_{21}, B_{22} and B_{23} in the above equations and F_0, F_{11}, F_{12}, F_{21}, F_{22} and F_{23} in section 3.3.1 are independent of Prandtl number, and , therefore, have to be calculated only once. The B_{ij} functions are shown graphically in Figure 12 and their values on the wall are given in Table 2. Finally, the wall temperature is given by

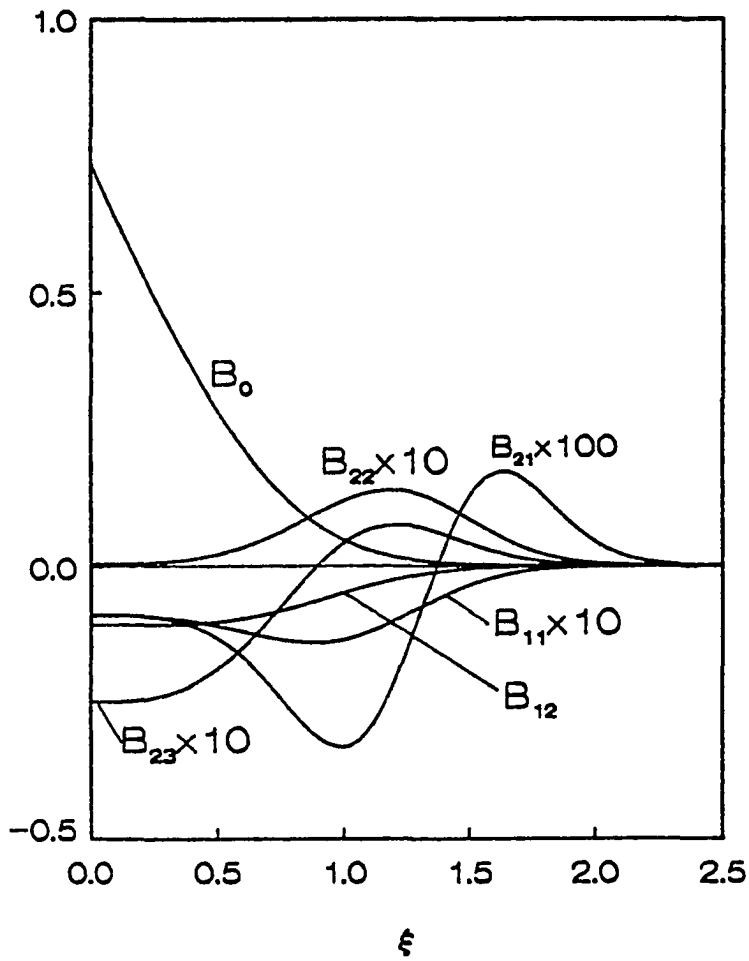

Fig. 12 B_{ij} functions for a step change in Q_w

Table 2. B_{ij} Values On The Wall

$B_0(0)$	$B_{11}(0)$	$B_{12}(0)$	$B_{21}(0)$	$B_{22}(0)$	$B_{23}(0)$
0.73849	-0.0091171	-0.10770	-0.00089019	0.00043415	-0.024726

$$T_w = \frac{q_1 R^{1/3}}{b\sqrt{\frac{3U_0}{2\nu r}}\, k}\left[B_0(0) + B_1(0)R + B_2(0)R^2 + \ldots \right] \tag{3.45}$$

The corresponding heat transfer coefficient h is

$$h = \frac{b\sqrt{\frac{3U_0}{2\nu r}}\, k}{R^{1/3}} \frac{1}{B_0(0) + B_1(0)R + B_2(0)R^2 + \ldots} \tag{3.46}$$

and the Nusselt number is

$$Nu = \frac{hd}{k}$$

$$= \frac{1}{(1 - r^*/r)^{1/3}} \frac{bRe^{1/2}\sqrt{\frac{3d}{2r}}}{B_0(0) + B_1(0)(1 - r^*/r) + B_2(0)(1 - r^*/r)^2 + \ldots} \tag{3.47}$$

where

$$B_0(0) = \frac{1}{\Gamma(2/3)} \tag{3.48a}$$

$$B_1(0) = -0.10770 + 0.015385\ Pr^{-1} \tag{3.48b}$$

$$B_2(0) = -0.024726 - 0.00073263\ Pr^{-1} - 0.0010623\ Pr^{-2} \tag{3.48c}$$

The Nusselt number profile is shown in Figure 13 for Pr = 0.7, 7 and 20 respectively. The comparison of Figure 13 with Figure 11 shows that the Nusselt number profiles for a step change in wall temperature and for a step change in wall heat flux are similar, but the latter is a little higher. As r approaches r^*, the Nusselt number is singular

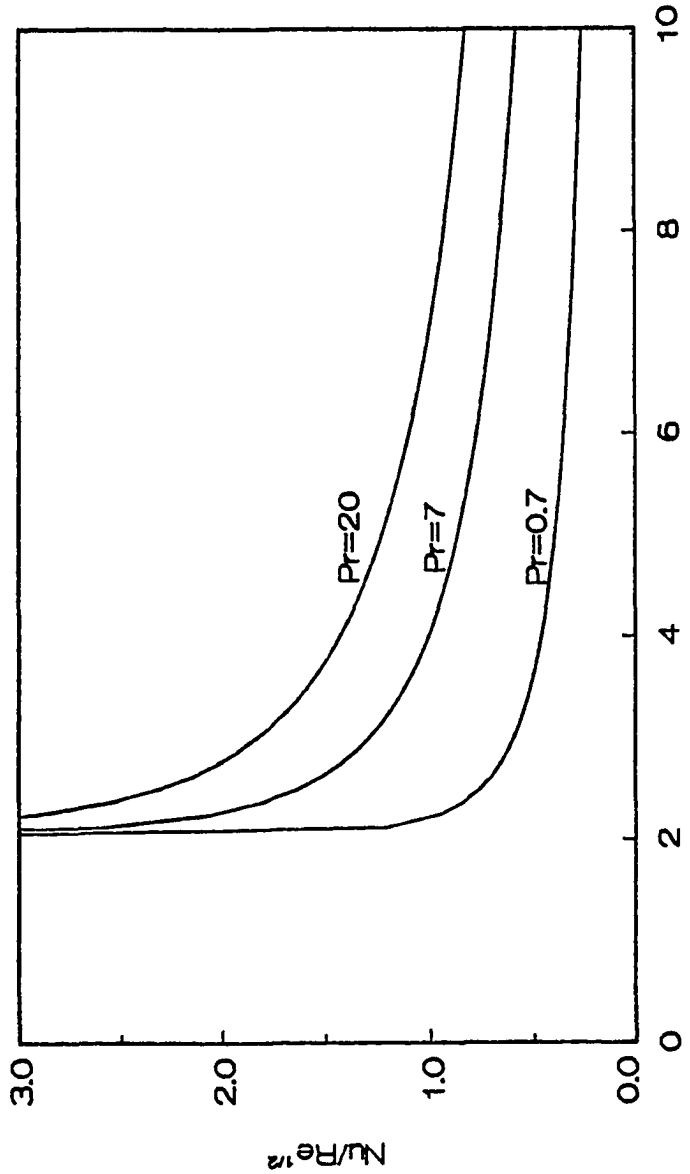

Fig. 13 Nusselt number profile for a step change in Q_w at $r/r_o=2$

because the wall temperature at $r = r^*$ is assumed to be equal to the temperature outside the thermal boundary layer as can be seen in the boundary conditions (3.12) and (3.32). As a matter of fact, the behavior of the Nusselt number profiles is similar to that of the Blasius flow over a flat plate with a constant wall temperature.

3.3.3 Solution for Continuous Change in Wall Temperature

We will now consider the case of a continuous wall temperature distribution $T_w(r)$ with $T_w(r) = 0$ for $r \leq r_1$, where r_1 may be taken to be $2r_0$ following the discussion of section 3.2. The temperature outside the boundary layer is assumed to be zero. In section 2.3.1, we have obtained the solution to the problem with a step change in wall temperature which can be written in explicit form as follows

$$\theta_{st}(r,z,r^*) = F_0\left[\frac{b\sqrt{3U_0/2\nu r}\,z}{(1 - r^*/r)^{1/3}}\right] + F_1\left[\frac{b\sqrt{3U_0/2\nu r}\,z}{(1 - r^*/r)^{1/3}}\right](1 - r^*/r) + \\ + F_2\left[\frac{b\sqrt{3U_0/2\nu r}\,z}{(1 - r^*/r)^{1/3}}\right](1 - r^*/r)^2 + \ldots \qquad (3.49)$$

For the problem with continuous wall temperature distribution $T_w(r)$, the solution can be obtained by the superposition method

$$T(r,z) = \int_{r_1}^{r} \theta_{st}(r,z,r^*)\frac{dT_w(r^*)}{dr}\,dr^* \qquad (3.50)$$

The wall heat flux is

$$q_w = - k\int_{r_1}^{r} \frac{\partial}{\partial z}\theta_{st}(r,0,r^*)\, \frac{d}{dr}T_w(r^*)\, dr^* \tag{3.51}$$

where

$$\frac{\partial}{\partial z}\theta_{st}(r,0,r^*) = \frac{b\sqrt{3U_0/2\nu r}}{(1 - r^*/r)^{1/3}}[F_0'(0) + F_1'(0)(1 - \frac{r^*}{r}) +$$

$$+ F_2'(0)(1 - \frac{r^*}{r})^2 + \ldots] \tag{3.52}$$

Consequently, the heat transfer coefficient is

$$h = - \frac{k}{T_w}\int_{r_1}^{r} \frac{\partial}{\partial z}\theta_{st}(r,0,r^*)\, \frac{dT_w(r^*)}{dr}\, dr^* \tag{3.53}$$

and the Nusselt number is

$$Nu = - \frac{bRe^{1/2}\sqrt{3d/2r}}{T_w(r)}\int_{r_1}^{r} \frac{1}{(1 - r^*/r)^{1/3}}[\, F_0'(0) + F_1'(0)(1 - r^*/r) +$$

$$+ F_2'(0)(1 - r^*/r)^2 + \ldots\,]\, \frac{dT_w(r^*)}{dr}\, dr^* \tag{3.54}$$

where $F_0'(0)$, $F_1'(0)$ and $F_2'(0)$ are given by (3.31). The Nusselt number profiles for different values of Prandtl number are shown in Figure 14 for $T_w = T_{w_0}[\, 0.02\, \frac{r^2 - r_1^2}{d^2} + 0.0024\, \frac{r^3 - r_1^3}{d^3} + 0.00032\, \frac{r^4 - r_1^4}{d^4}\,]$. The dimensionless wall temperature distribution T_w/T_{w_0} is also shown in the same Figure.

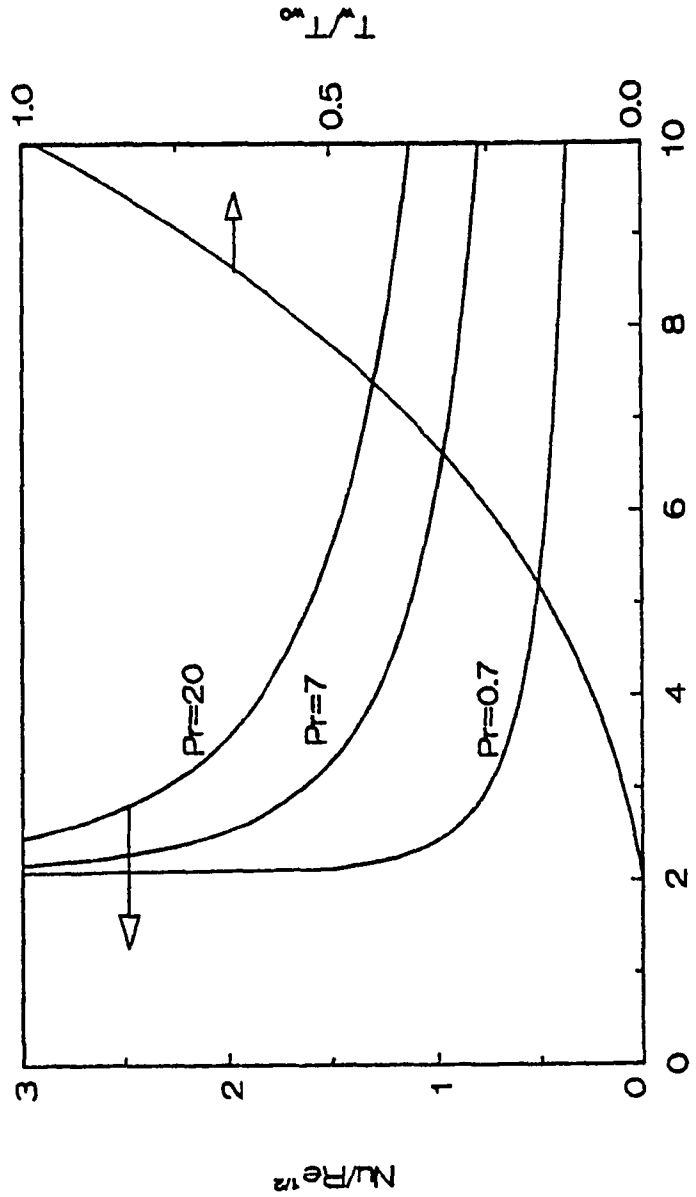

Fig. 14 Nusselt number profile for continuous T_w

3.3.4 Solution for Continuous Change in Wall Heat Flux

Similar to the case of section 3.3.3, the wall heat flux is assumed to have a continuous distribution $Q_w(r)$ with $Q_w(r) = 0$ for $r \leq r_1$. Consequently, the wall temperature is $T_w(r) = 0$ for $r \leq r_1$ if the temperature outside the thermal boundary layer is assumed to be zero for convenience. The temperature distribution for $r > r_1$ may be obtained from the corresponding solution for a step change in wall heat flux by the superposition method as follows

$$T(r,z) = \frac{1}{b\sqrt{3U_0/2\nu rk}} \int_{r_1}^{r} (1-r^*/r)^{1/3} \theta_{sq}(r,z,r^*) \frac{dQ_w(r^*)}{dr} dr^* \qquad (3.55)$$

where $\theta_{sq}(r,z,r^*)$ is defined by (3.36). The wall temperature for $r > r_1$ is

$$T_w = \frac{1}{b\sqrt{3U_0/2\nu rk}} \int_{r_1}^{r} (1 - r^*/r)^{1/3} \theta_{sq}(r,0,r^*) \frac{dQ_w(r^*)}{dr} dr^* \qquad (3.56)$$

where

$$\theta_{sq}(r,0,r^*) = B_0(0) + B_1(0)(1-\frac{r^*}{r}) + B_2(0)(1-\frac{r^*}{r})^2 + \ldots \qquad (3.57)$$

and $B_0(0)$, $B_1(0)$, $B_2(0)$ are given by (3.48). The heat transfer coefficient is given by

$$h = \frac{b\sqrt{3U_0/2\nu r}\, k\, Q_w(r)}{\int_{r_1}^{r}(1 - r^*/r)^{1/3}\theta_{sq}(r,0,r^*)\frac{dQ_w(r^*)}{dr}dr^*} \tag{3.58}$$

and the Nusselt number is

$$Nu = \frac{b\, Re^{1/2}\sqrt{3d/2r}\, Q_w(r)}{\int_{r_1}^{r}(1-\frac{r^*}{r})^{1/3}[B_0(0) + B_1(0)(1-\frac{r^*}{r}) + B_2(0)(1-\frac{r^*}{r})^2 + \ldots]\frac{dQ_w(r^*)}{dr}dr^*} \tag{3.59}$$

The Nusselt number profile is shown in Figure 15 for an increasing wall heat flux with r. Comparing Figures 14 and 15 with Figures 11 and 13, one can see that the Nusselt number for continuously increasing wall temperature or wall heat flux is higher than that for a step change in wall temperature or wall heat flux. The reason is that at the same location, the fluid is hotter for the case of a step change in wall temperature or wall heat flux than it is for the case of continuously increasing wall temperature or wall heat flux if the wall temperature or wall heat flux at that point is the same for both cases.

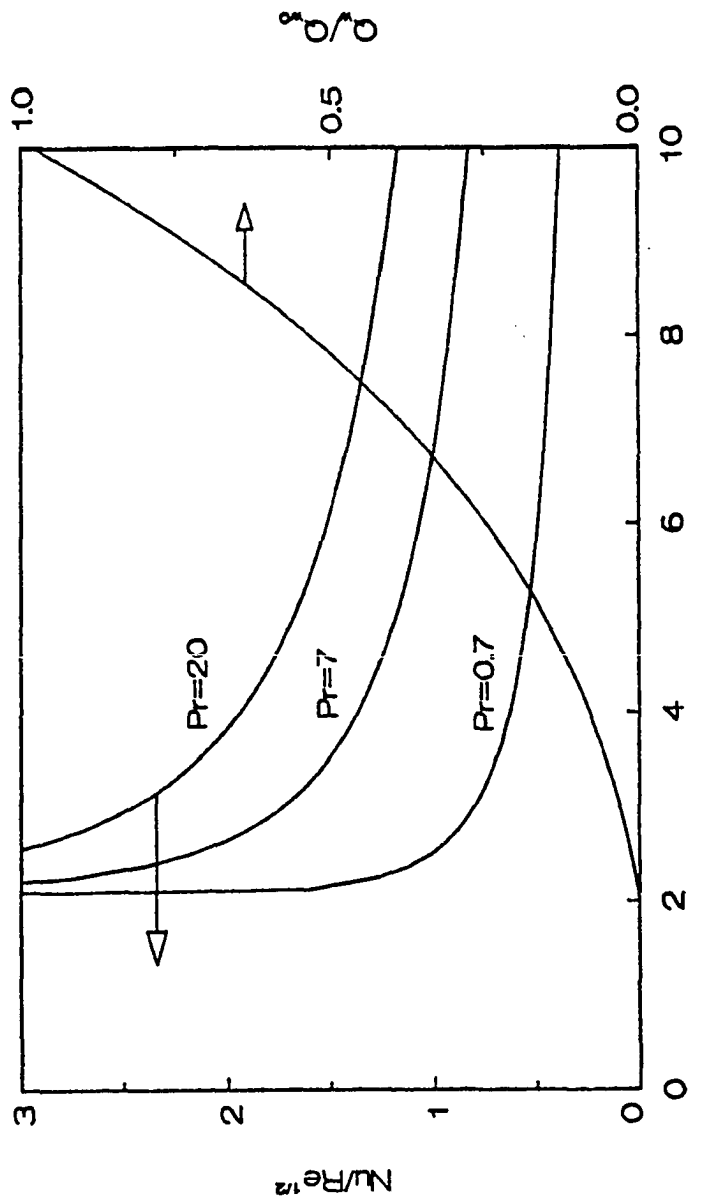

Fig. 15 Nusselt number profile for continuous Q_w

3.3.5 Solution to the Problem with $T_w = T_{w_2}$

Since the wall temperature is constant for $r > r_1$, it is possible to obtain a similarity solution approximately. The boundary conditions are

$$T = T_w(r_1) \qquad \text{at } z = 0 \tag{3.60a}$$

$$T = T_\infty \qquad \text{at } z = \infty \tag{3.60b}$$

We introduce the following dimensionless temperature

$$\theta_{ct} = \frac{T - T_\infty}{T_w(r_1) - T_\infty} \tag{3.61}$$

Then, the energy equation (3.3) and the boundary conditions (3.60) become

$$\frac{d^2\theta_{ct}}{d\eta^2} + Pr\ f \frac{d\theta_{ct}}{d\eta} = 0 \tag{3.62a}$$

$$\theta_{ct}(0) = 1, \qquad \theta_{ct}(\infty) = 0 \tag{3.62b}$$

Equation (3.62) can be integrated in closed form

$$\theta_{ct} = 1 - \frac{\int_0^\eta e^{-Pr\int_0^\eta f d\eta} d\eta}{\int_0^\infty e^{-Pr\int_0^\eta f d\eta} d\eta} \tag{3.63}$$

Hence the temperature distribution corresponding to wall temperature T_{w_2} is

$$T = T_\infty + [\, T_w(r_1) - T_\infty \,][\, 1 - \frac{\int_0^\eta e^{-Pr\int_0^\eta f d\eta} d\eta}{\int_0^\infty e^{-Pr\int_0^\eta f d\eta} d\eta} \,] \tag{3.64}$$

3.3.6 Solution to the Problem with $Q_w = Q_{w_2}$

The boundary conditions are

$$-k\frac{\partial T}{\partial z} = Q_w(r_1) \qquad \text{at} \quad z = 0 \tag{3.65a}$$

$$T = T_\infty \qquad \text{at} \quad z = \infty \tag{3.65b}$$

The dimensionless temperature θ_{cq}, is now introduced as follows

$$\theta_{cq} = \frac{T - T_\infty}{Q_w(r_1)} \sqrt{3U_0/2\nu r}\, k \tag{3.66}$$

The energy equation (3.3) and boundary conditions (3.65), therefore, can be written as

$$\frac{d^2\theta_{cq}}{d\eta^2} + Pr\, f\frac{d\theta_{cq}}{d\eta} - \frac{Pr}{3} f'\theta_{cq} = 0 \tag{3.67a}$$

$$\theta'_{cq}(0) = -1, \quad \theta_{cq}(\infty) = 0 \tag{3.67b}$$

which may be solved numerically. Once θ_{cq} is known, the temperature distribution corresponding Q_{w_2} is given by

$$T = T_\infty + \frac{Q_w(r_1)}{\sqrt{3U_0/2\nu r k}}\,\theta_{cq} \tag{3.68}$$

With the above solutions and those obtained in sections 3.3.3 and 3.3.4, we are able to obtain the solutions for arbitrary wall temperature and wall heat flux.

3.3.7 Solution for Arbitrary Wall Temperature

For the Prandtl number larger than unity, the thermal boundary layer thickness is always smaller than the total thickness of the fluid layer in the boundary layer region. Consequently, the temperature outside the thermal boundary layer is the same as the jet temperature. Following the previous discussion, if the jet temperature is T_∞ and the wall temperature is $T_w(r)$, the temperature distribution in the boundary layer region should be the sum of (3.50) and (3.64) for $r > r_1$. That is

$$T = T_\infty + [\, T_w(r_1) - T_\infty \,]\theta_{ct} + \int_{r_1}^{r} \theta_{st}(r,z,r^*)\frac{dT_w(r^*)}{dr}\,dr^* \tag{3.69}$$

The wall heat flux is

$$q_w = - k \sqrt{3U_0/2\nu r} \left\{ b\int_{r_1}^{r} \frac{1}{(1 - r^*/r)^{1/3}} \left[F_0'(0) + F_1'(0)(1 - r^*/r) + \right.\right.$$

$$\left.\left. + F_2'(0)(1 - r^*/r)^2 + \ldots \right] \frac{dT_w(r^*)}{dr} dr^* - \frac{T_w(r_1) - T_\infty}{\int_0^\infty e^{-Pr\int_0^\eta f d\eta} d\eta} \right\} \qquad (3.70)$$

Thus the corresponding heat transfer coefficient is

$$h = k \frac{\sqrt{3U_0/2\nu r}}{T_w(r) - T_\infty} \left(\frac{T_w(r_1) - T_\infty}{\int_0^\infty e^{-Pr\int_0^\eta f d\eta} d\eta} - b\int_{r_1}^{r} \frac{1}{(1 - r^*/r)^{1/3}} \left[F_0'(0) + \right.\right.$$

$$\left.\left. + F_1'(0)(1 - r^*/r) + F_2'(0)(1 - r^*/r)^2 + \ldots \right] \frac{dT_w(r^*)}{dr} dr^* \right) \qquad (3.71)$$

and the Nusselt number is

$$Nu = \frac{Re^{1/2} \sqrt{3d/2r}}{T_w(r) - T_\infty} \left(\frac{T_w(r_1) - T_\infty}{\int_0^\infty e^{-Pr\int_0^\eta f d\eta} d\eta} - b\int_{r_1}^{r} \frac{1}{(1 - r^*/r)^{1/3}} \left[F_0'(0) + \right.\right.$$

$$\left.\left. + F_1'(0)(1 - r^*/r) + F_2'(0)(1 - r^*/r)^2 + \ldots \right] \frac{dT_w(r^*)}{dr} dr^* \right) \qquad (3.72)$$

where $F_0'(0)$, $F_1'(0)$ and $F_2'(0)$ are given by (3.31). For the prandtl number smaller than unity, the thermal boundary layer reaches the free surface before the viscous boundary layer does. Consequently, the present solution is valid in a smaller region if $Pr < 1$.

3.3.8 Solution for Arbitrary Wall Heat Flux

The temperature distribution in the boundary layer region for the case of arbitrary wall heat flux $Q_w(r)$ and constant temperature T_∞ outside the boundary layer can be obtained by the superposition of (3.55) and (3.68) as follows

$$T = T_\infty + \frac{Q_w(r_1)}{\sqrt{3U_0/2\nu rk}}\,\theta_{cq} + \frac{1}{b\sqrt{3U_0/2\nu rk}}\int_{r_1}^{r}(1 - r^*/r)^{1/3}\theta_{sq}(r,z,r^*)\frac{dQ_w(r^*)}{dr}dr^* \qquad (3.73)$$

The wall temperature corresponding to the arbitrary wall heat flux Q_w is

$$T_w = T_\infty + \frac{Q_w(r_1)}{\sqrt{3U_0/2\nu rk}}\,\theta_{cq}(0) + \frac{1}{b\sqrt{3U_0/2\nu r\ k}}\int_{r_1}^{r}(1 - r^*/r)^{1/3}\theta_{sq}(r,0,r^*)\frac{dQ_w(r^*)}{dr}dr^* \qquad (3.74)$$

Consequently, the heat transfer coefficient is

$$h = k\sqrt{3U_0/2\nu r}\ Q_w(r)/\{Q_w(r_1)\theta_{cq}(0) + \frac{1}{b}\int_{r_1}^{r}(1 - r^*/r)^{1/3}[B_0(0) + B_1(0)(1-r^*/r) + B_2(0)(1-r^*/r)^2 + \ldots]\frac{dQ_w(r^*)}{dr}dr^*\} \qquad (3.75)$$

and the Nusselt number is obtained as

$$Nu = Re^{1/2}\sqrt{3d/2r}\,Q_w(r)/\{Q_w(r_1)\theta_{cq}(0) + \frac{1}{b}\int_{r_1}^{r}(1 - r^*/r)^{1/3}[B_0(0)+$$

$$+ B_1(0)(1-r^*/r) + B_2(0)(1-r^*/r)^2 + \ldots]\frac{dQ_w(r^*)}{dr}dr^*\} \qquad (3.76)$$

where $B_0(0)$, $B_1(0)$ and $B_2(0)$ are given by (3.48)

Equation (3.72) and equation (3.76) give the Nusselt number profiles in the boundary layer region for prescribed wall temperature and wall heat flux respectively. In chapter 2, the Nusselt number profile in the vicinity of the stagnation point has been obtained. The integral solution in the transition region between the stagnation region and the boundary layer region is also obtained in chapter 2. Hence, one can plot the Nusselt number profile throughout the stagnation region and the boundary layer region. Since the asymptotic solution in the stagnation region is valid only for small values of r and the integral solution can not be matched with the boundary layer region solution analytically, the solutions in different regions have to be matched graphically to obtain continuous Nusselt number distribution. The procedure can be described as follows: First, the Nusselt number profiles near the stagnation point and in the boundary layer region are plotted, then we plot the Nusselt number profile in the transition region between the stagnation region and the boundary layer region. Finally, each segment of curve is interpolated in such a way that the resulting curve is smooth everywhere. The results are

shown in Figures 16 and 17 for arbitrary wall temperature and wall heat flux respectively.

In Figures 16 and 17, the result of constant wall temperature and wall heat flux is compared with the result of increasing wall temperature and wall heat flux with r. The Figures indicate that the Nusselt number for increasing wall temperature or wall heat flux is higher than that for constant wall temperature or wall heat flux outside the stagnation region. It can be seen from Figures 16 and 17 that the Nusselt number near the stagnation point is essentially constant. At larger radial distance, however, the Nusselt number drops with r steeply. Very far away from the stagnation point, the Nusselt number decreases with r slowly.

The present result is compared with those obtained by Chaudhury [14] and Brdlik et al. [1] in Figure 18 for the case of constant wall temperature. The Figure shows good agreement between the present result and Chaudhury's integral solution. For Brdlik's result, however, the Nusselt number is considerably higher than the present result and Chaudhury's result. This is because the authors assumed that the velocity at the outer edge of the boundary layer was equal to $2U_0$, where U_0 is the jet velocity. The assumption seems unjustified since the velocity outside the boundary layer can not be higher than U_0. If the velocity outside the boundary layer is taken to be U_0 in Brdlik's solution, the result will be in good agreement with the present solution and Chaudhury's integral solution.

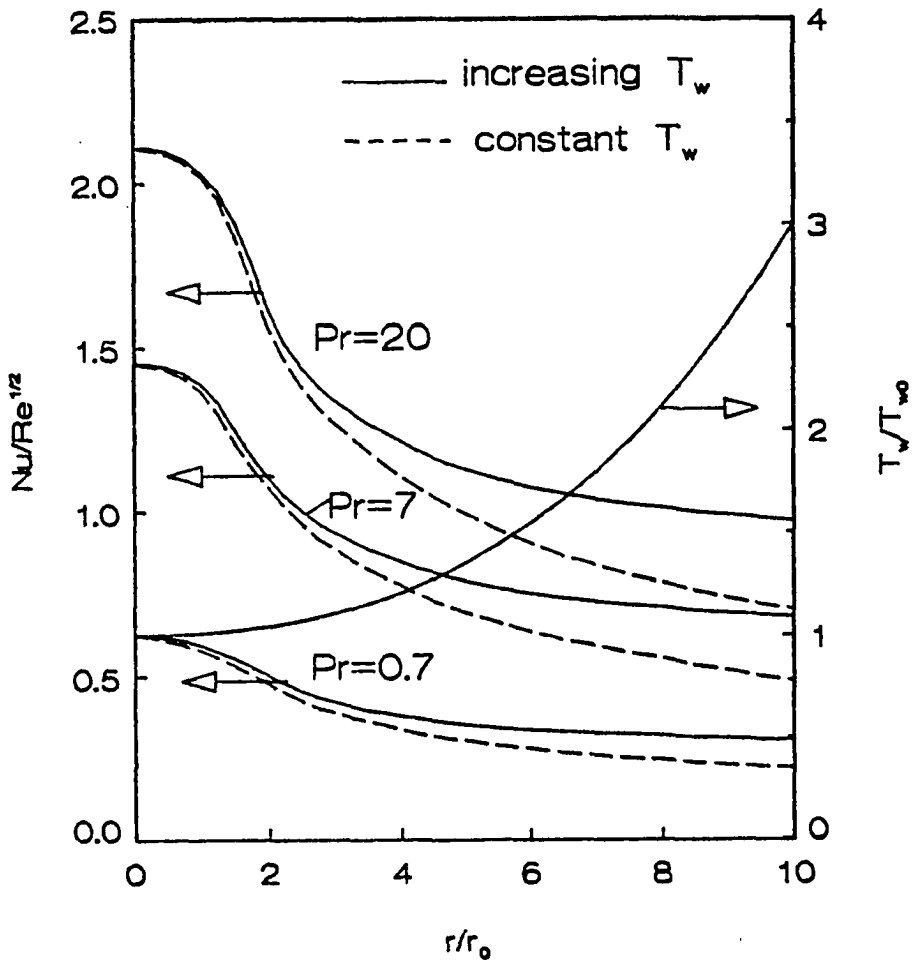

Fig. 16 Nusselt number profile for arbitrary T_w

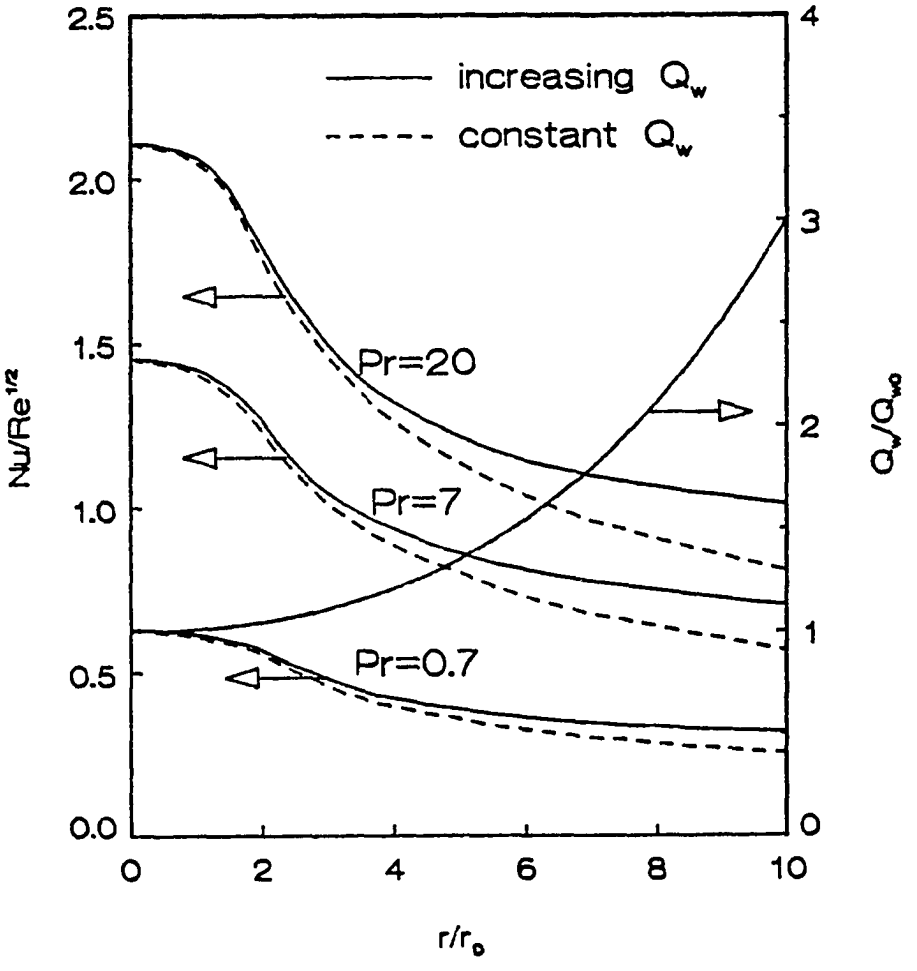

Fig. 17 Nusselt number profile for arbitrary Q_w

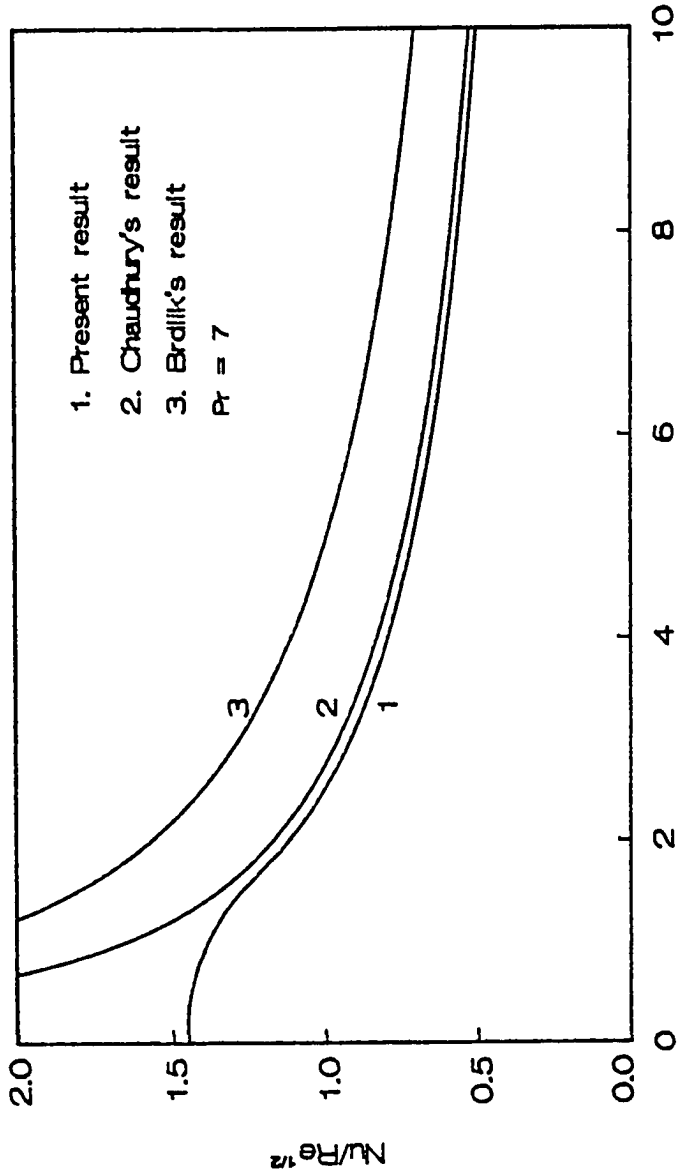

Fig. 18 Comparison with other results for constant T_w

3.4 Concluding remarks

In this chapter, the heat transfer in the boundary layer region of an axisymmetrical jet impinging normally on a flat plate with arbitrary wall temperature or wall heat flux has been investigated analytically. The solution converges very fast for Prandtl number of the order of unity or larger. For very small Prandtl number, however, the solution may be divergent when R is not very small. In such a case, Euler's transformation can be used to evaluate the sum. The solution is matched with that in the stagnation region obtained in chapter 2 so that the Nusselt number distribution throughout the stagnation region and the boundary layer region is obtained.

The solution presented in this chapter and that in chapter 2 may be useful in some applications. As we will see in the next chapter, they can be used to solve the conjugate problem in which an axisymmetrical jet impinges on the top surface of a solid plate with arbitrary temperature or heat flux distribution prescribed at the non-impingement surface.

Chapter 4

Conjugate Heat Transfer in Laminar Liquid Jet Impingement

4.1 Objectives

In engineering applications, most convective heat transfer problems are conjugate problems in which the conditions at the fluid-solid interface are unknown before the problems are solved. Therefore, the energy equations for the fluid and solid phases are coupled by the matching conditions at the interface of the two phases. Usually, to obtain an analytical solution, the general solutions to the energy equations for the both phases are obtained separately. The two solutions are then matched by requiring the continuity of the temperature and heat flux at the interface. This chapter will deal with the conjugate heat transfer between a laminar impinging liquid jet and a solid plate with arbitrary temperature or heat flux distribution prescribed at the non-impingement surface. In chapter 2 and chapter 3, the solutions for the fluid phase were obtained in terms of the interface temperature which is unknown for the present conjugate problem and will be determined by matching the solutions for the two phases. The general solution for the solid phase will be obtained by the method of separation of variables. The objectives of this chapter are: (1) to investigate the conjugate heat transfer characteristics associated with jet impingement; (2) to examine the effects of the ratio of the fluid conductivity to the solid conductivity, the aspect ratio of the thickness to the radius of the solid plate and the prescribed temperature or heat flux on the local Nusselt number distribution between the impinging jet and the solid plate.

4.2 Formulation

We now consider the conjugate heat transfer between a circular free impinging liquid jet and a solid plate which is laterally insulated as shown in Figure 1. The jet impinges on the top surface of the plate and an arbitrary temperature or heat flux is prescribed on the non-impingement surface. For the solid phase, the energy equation in cylindrical coordinates can be written as follows

$$\frac{\partial^2 T_s}{\partial r^2} + \frac{1}{r}\frac{\partial T_s}{\partial r} + \frac{\partial^2 T_s}{\partial z^2} = 0 \tag{4.1}$$

and the boundary conditions are

$$\frac{\partial T_s}{\partial r} = 0 \qquad \text{at} \quad r = 0 \tag{4.2a}$$

$$\frac{\partial T_s}{\partial r} = 0 \qquad \text{at} \quad r = R_0 \tag{4.2b}$$

$$T_s = T_b(r) \quad \text{or} \quad -k_s \frac{\partial T_s}{\partial z} = Q_b(r) \qquad \text{at} \quad z = -H \tag{4.2c}$$

$$T_s = T_f \quad \text{and} \quad k_s \frac{\partial T_s}{\partial z} = k_f \frac{\partial T_f}{\partial z} \qquad \text{at} \quad z = 0 \tag{4.2d}$$

where T_s and T_f are the temperature distribution in the solid phase and the fluid phase, k_s and k_f the conductivities of the plate and the fluid, T_b and Q_b the prescribed surface temperature and heat flux, respectively. R_0 is the radius of the plate and H is the thickness. To

nondimensionalize the energy equation, the following dimensionless variables and dimensionless parameters are introduced

$$\theta_s = \begin{cases} \dfrac{T_s - T_\infty}{T_{b0} - T_\infty} & \text{for prescribed temperature} \\ \dfrac{k_s(T_s - T_\infty)}{Q_{b0}H} & \text{for prescribed heat flux} \end{cases} \tag{4.3a}$$

$$\rho = \frac{r}{R_0} \tag{4.3b}$$

$$\zeta = \frac{z}{H} \tag{4.3c}$$

$$\epsilon = \frac{H}{R_0} \tag{4.3d}$$

where T_{b0} and Q_{b0} are prescribed temperature and heat flux at $r = 0$, R_0 and H are the radius and thickness of the plate, respectively. The energy equation (4.1) and the boundary conditions (4.2), therefore, can be written in the following form

$$\epsilon^2\left(\frac{\partial^2\theta_s}{\partial\rho^2} + \frac{1}{\rho}\frac{\partial\theta_s}{\partial\rho}\right) + \frac{\partial^2\theta_s}{\partial\zeta^2} = 0 \tag{4.4}$$

and

$$\frac{\partial\theta_s}{\partial\rho} = 0 \qquad \text{at} \quad \rho = 0 \tag{4.5a}$$

$$\frac{\partial\theta_s}{\partial\rho} = 0 \qquad \text{at} \quad \rho = 1 \tag{4.5b}$$

$$\theta_s = F_t(\rho) \quad \text{or} \quad \frac{\partial \theta_s}{\partial \zeta} = -F_q(\rho) \qquad \text{at} \quad \zeta = -1 \qquad (4.5c)$$

$$T_s = T_f \quad \text{and} \quad k_s \frac{\partial T_s}{\partial z} = k_f \frac{\partial T_f}{\partial z} \qquad \text{at} \quad z = 0 \qquad (4.5d)$$

where $F_t(\rho)$ and $F_q(\rho)$ are prescribed dimensionless temperature and heat flux given by

$$F_t(\rho) = \frac{T_b - T_\infty}{T_{b0} - T_\infty} \qquad (4.6a)$$

$$F_q(\rho) = \frac{Q_b}{Q_{b0}} \qquad (4.6b)$$

where T_b and Q_b are arbitrarily prescribed temperature and heat flux. Note that the matching condition (4.5d) is given in dimensional form since for the fluid phase, the dimensionless temperature is defined in different forms for different regions.

4.3 Solution and Matching Procedure

The solution to (4.4) which satisfies the boundary conditions (4.5a) and (4.5b) can be obtained by the method of separation of variables as follows

$$\theta_s = A_0\zeta + B_0 + \sum_{n=1}^{\infty}[A_n\cosh\epsilon\sigma_n(\zeta+1) + B_n\sinh\epsilon\sigma_n(\zeta+1)]J_0(\sigma_n\rho) \quad (4.7)$$

where σ_n are the roots of $J_1(\sigma_n) = 0$ and the coefficients A_n and B_n, $n = 0, 1, 2, \ldots$, can be determined by applying the boundary condition (4.5c) and the matching conditions (4.5d). Since the solution for the fluid phase is complicated, not all the coefficients can be written in explicit form. Hence an iteration procedure must be developed to determine some of the coefficients numerically. As was pointed out in [29] and [30], for conjugate problems the iteration procedure converges more rapidly if the thermal information is transferred through the interface by the heat transfer coefficient. The reason is that at any stage of iteration, the heat transfer coefficient is usually closer to the correct value than the interface temperature or heat flux. In the present problem, therefore, the iteration procedure begins with guessing the Nusselt number between the jet and the plate. Then the condition at the fluid-solid interface becomes

$$\frac{\partial\theta_s}{\partial\zeta} = -\epsilon ekNu(\rho)\theta_s \qquad \text{at} \quad \zeta = 0 \quad (4.8)$$

where $Nu(\rho)$ is the guessed Nusselt number and e and k are the dimensionless parameters defined as follows

$$e = \frac{R_0}{d} \tag{4.9a}$$

$$k = \frac{k_f}{k_s} \tag{4.9b}$$

The determination of the constant coefficients A_n and B_n is now described for two distinct cases. For prescribed heat flux at the non-impingement surface, the application of the boundary condition (4.5c) gives A_0 and B_n as follows

$$A_0 = -2\int_0^1 F_q(\rho)\rho d\rho \tag{4.10a}$$

$$B_n = -\frac{2}{\epsilon\sigma_n J_0^2(\sigma_n)}\int_0^1 F_q(\rho)J_0(\sigma_n\rho)\rho d\rho \tag{4.10b}$$

Applying condition (4.8), one can find that A_n is determined by the following equation

$$\sum_{n=1}^{\infty} A_n\int_0^1 S_1 J_0(\sigma_j\rho)\rho d\rho = \int_0^1 S_2 J_0(\sigma_j\rho)\rho d\rho \qquad j = 1, 2, 3, \ldots \tag{4.11}$$

where

$$S_1 = [\epsilon ekNu(\rho)\cosh\epsilon\sigma_n + \epsilon\sigma_n\sinh\epsilon\sigma_n]J_0(\sigma_n\rho) -$$

$$- 2\epsilon\sigma_n Nu(\rho)\sinh\epsilon\sigma_n\int_0^1 \frac{J_0(\sigma_n\rho)}{Nu(\rho)}\rho d\rho \tag{4.12}$$

and

$$S_2 = 2A_0Nu(\rho)\int_0^1 \frac{\rho}{Nu(\rho)}d\rho - A_0 - \sum_{n=1}^{\infty}B_n\{[\epsilon ekNu(\rho)\sinh\epsilon\sigma_n + \epsilon\sigma_n\cosh\epsilon\sigma_n]J_0(\sigma_n\rho) - 2\epsilon\sigma_nNu(\rho)\cosh\epsilon\sigma_n\int_0^1 \frac{J_0(\sigma_n\rho)}{Nu(\rho)}\rho d\rho\} \quad (4.13)$$

Finally, B_0 is given by

$$B_0 = -\frac{2A_0}{\epsilon ek}\int_0^1 \frac{\rho}{Nu(\rho)}d\rho - \frac{2}{ek}\sum_{n=1}^{\infty}\sigma_n(A_n\sinh\epsilon\sigma_n + B_n\cosh\epsilon\sigma_n)\int_0^1 \frac{J_0(\sigma_n\rho)}{Nu(\rho)}\rho d\rho \quad (4.14)$$

For prescribed temperature at the non-impingement surface, the application of (4.5c) leads to the following results

$$A_0 - B_0 = -2\int_0^1 F_t(\rho)\rho d\rho \quad (4.15a)$$

$$A_n = \frac{2}{J_0^2(\sigma_n)}\int_0^1 F_t(\rho)J_0(\sigma_n\rho)\rho d\rho \quad (4.15b)$$

After applying the condition (4.8), one obtains the following equations which determine B_n

$$\sum_{n=1}^{\infty}B_n\int_0^1 S_3J_0(\sigma_j\rho)\rho d\rho = \int_0^1 S_4J_0(\sigma_j\rho)\rho d\rho \qquad j = 1, 2, 3, \ldots \quad (4.16)$$

where

$$S_3 = \epsilon[\sigma_n\cosh\epsilon\sigma_n + ekNu(\rho)\sinh\epsilon\sigma_n]J_0(\sigma_n\rho) - 2\epsilon\sigma_n\cosh\epsilon\sigma_n\left[\frac{(1-2Nu(\rho)\int_0^1 \frac{\rho}{Nu(\rho)}d\rho}{\epsilon ek + 2\int_0^1 \frac{\rho}{Nu(\rho)}d\rho} + Nu(\rho)\right]\int_0^1 \frac{J_0(\sigma_n\rho)}{Nu(\rho)}\rho d\rho \quad (4.17)$$

and

$$S_4 = \frac{2[1-2Nu(\rho)\int_0^1 \frac{\rho}{Nu(\rho)}d\rho}{1+\frac{1}{\epsilon ek}\int_0^1 \frac{\rho}{Nu(\rho)}d\rho}\int_0^1 F_t(\rho)\rho d\rho -$$

$$- \sum_{n=1}^{\infty} A_n\{[\epsilon ekNu(\rho)\cosh\epsilon\sigma_n + \epsilon\sigma_n \sinh\epsilon\sigma_n]J_0(\sigma_n\rho) - \qquad (4.18)$$

$$- 2\epsilon\sigma_n[Nu(\rho) + \frac{1-2Nu(\rho)\int_0^1 \frac{\rho}{Nu(\rho)}d\rho}{\epsilon ek + 2\int_0^1 \frac{\rho}{Nu(\rho)}d\rho}]\sinh\epsilon\sigma_n \int_0^1 \frac{J_0(\sigma_n\rho)}{Nu(\xi)}\rho d\rho \}$$

Finally, A_0 is determined as follows

$$A_0 = -\frac{1}{1+\frac{2}{\epsilon ek}\int_0^1 \frac{\rho}{Nu(\rho)}d\rho}[\frac{2}{ek}\sum_{n=1}^{\infty}\sigma_n(A_n\sinh\epsilon\sigma_n +$$

$$+ B_n\cosh\epsilon\sigma_n)\int_0^1 \frac{J_0(\sigma_n\rho)}{Nu(\rho)}\rho d\rho + 2\int_0^1 F_t(\rho)\rho d\rho] \qquad (4.19)$$

If the infinite series in (4.11) and (4.16) are truncated after M terms, the two equations represent two systems of M linear algebraic equations for two sets of M unknowns, respectively. Once the equations (4.11) and (4.16) are solved, the coefficients A_n and B_n can be determined for arbitrarily prescribed temperature or heat flux at the non-impingement surface of the plate. Hence the temperature and heat flux at the fluid-solid interface can be calculated. The calculated interface temperature can then be used to compute the interface heat flux at the fluid phase by the equations obtained in the previous

chapters. Finally, the computed heat flux values are compared with those at the solid phase in the corresponding regions. If the agreement is not satisfactory, the initial guess of the Nusselt number is changed according to the following iterative scheme

$$Nu_{(n+1)} = Nu_{(n)} - \frac{1}{2}\frac{d}{k_f}\frac{q_{is} - q_{if}}{T_i - T_\infty} \tag{4.20}$$

where q_{is} and q_{if} denote the heat flux from the solid phase and fluid phase at the interface, $Nu_{(n+1)}$ and $Nu_{(n)}$ denote the (n+1)th guess and the nth guess, respectively. The above procedure is repeated until the required accuracy is achieved.

In the present calculation, the Nusselt number is initially guessed at 21 radial points on the interface. The assumed values are then represented by a finite Fourier cosine series such that a continuous Nusselt number profile is prescribed. The comparison of the interface heat flux for the fluid phase with that for the solid phase is carried out at the same discrete points on the interface.

The sensitivity of the solution to the number of the points, at which the Nusselt number is guessed and the comparison of the heat fluxes is carried out, is examined by calculating the Nusselt number for different numbers of the points. The calculation shows that the result is not sensitive to the number of the points. For 11 points and 21 points, for instance, the difference in the Nusselt number is less than 0.5%.

4.4 Results and Discussion

The main purpose of the present analysis is to investigate the distribution of the heat transfer coefficient between the impinging jet and the solid plate. In general, it is clear that the quantity $Nu/Re^{1/2}$ is a function of Prandtl number Pr, the conductivity ratio k and the aspect ratio ϵ. The prescribed temperature or heat flux profile may also influence the heat transfer coefficient distribution.

For the special case where the aspect ratio ϵ vanishes, the present conjugate problem becomes the convective problem of the previous chapters where the boundary conditions are prescribed at the impingement surface. For $\epsilon = 0.001$, the present result for $Nu/Re^{1/2}$ is compared with that of chapter 3 in Figure 19 for a prescribed increasing temperature shown in the same Figure. It is clear that the present result is essentially the same as the previous result for the same prescribed temperature distribution except in a small region near the edge of the plate. This is true for any value of the conductivity ratio k. The reason for the difference near the edge is that for the conjugate problem the radial derivative of the interface temperature vanishes at the edge of the plate since it is insulated, while the derivative of the prescribed temperature is not zero at the same location. The same behavior of Nusselt number near the insulated edge was also shown in [31] where the conjugate problem associated with laminar flow through a pipe was solved.

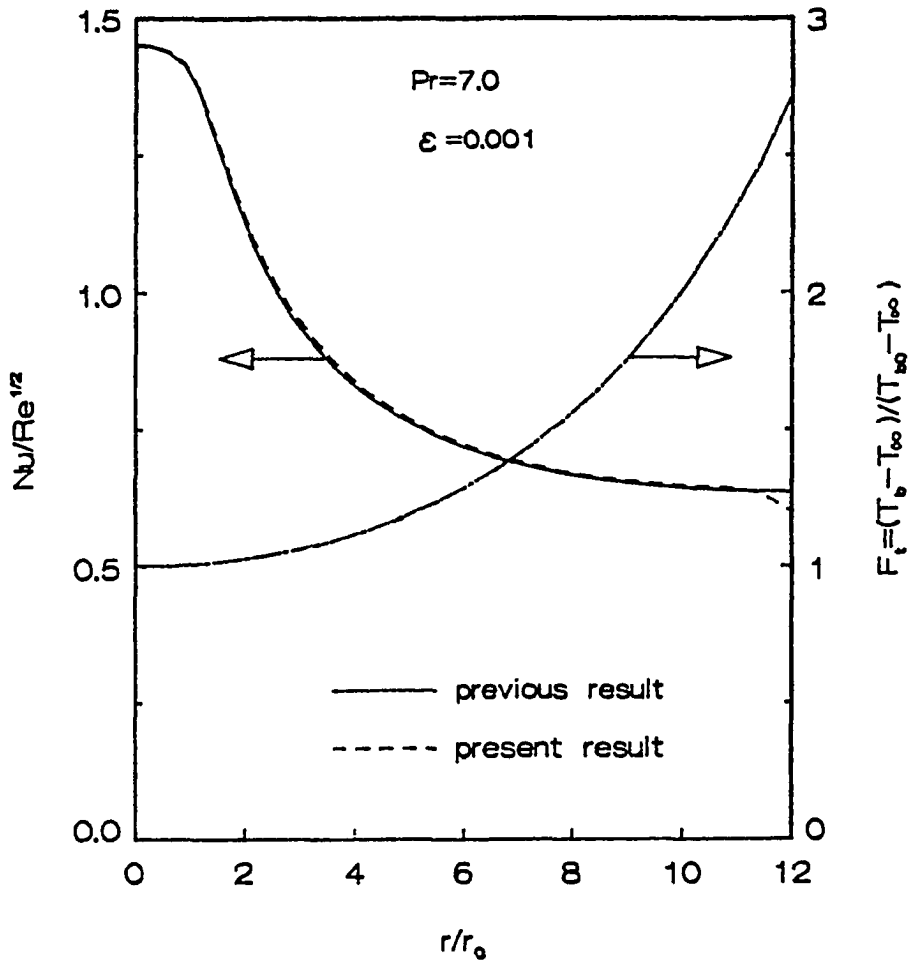

Fig. 19 Comparison with previous result

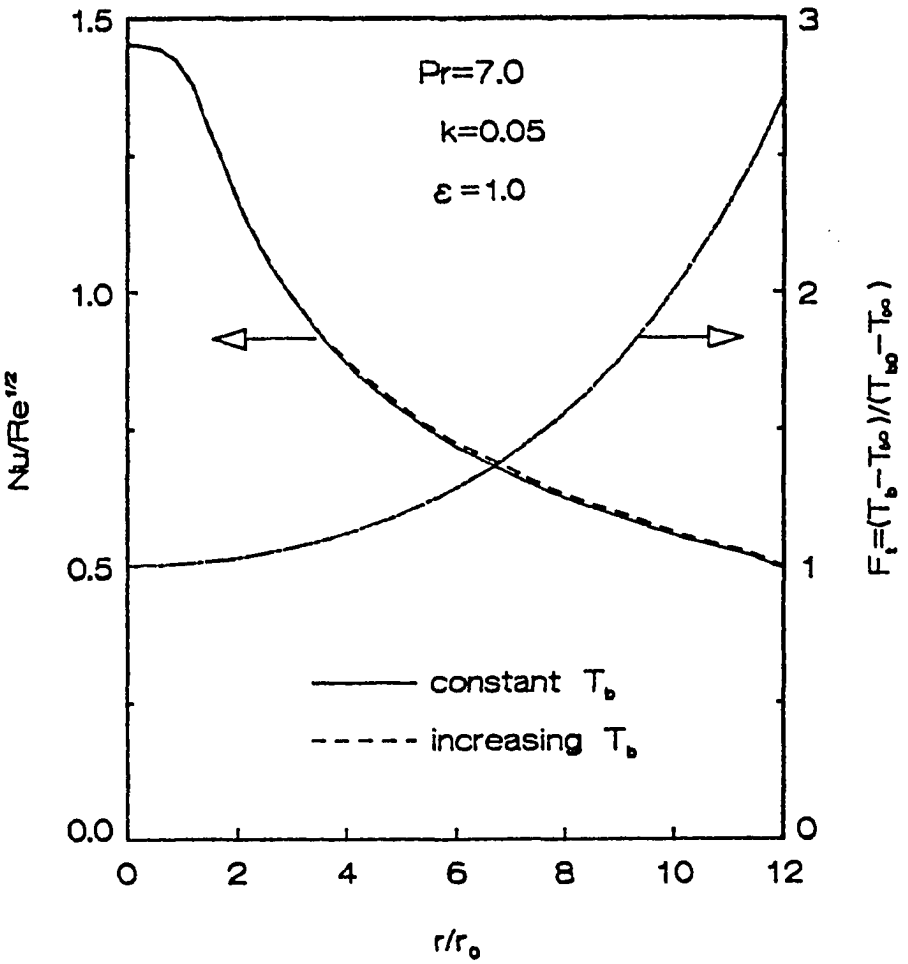

Fig. 20 Result for thick plate

Figure 20 shows the Nusselt number profile for $\epsilon = 1$, corresponding to the case of thick plate. For this case, the Nusselt number is almost the same for prescribed constant temperature and for prescribed increasing temperature. This is due to the fact that the prescribed temperature distribution loses its influence on the dimensionless interface temperature profile when the plate is sufficiently thick because of conductive effects. This is also true for the case of prescribed heat flux distribution. As we will see later, the prescribed temperature or heat flux may affect the Nusselt number profile considerably if the plate is not very thick.

When the solid conductivity is sufficiently high, the prescribed heat flux distribution has little effect on the Nusselt number profile even for moderate plate thicknesses. This case is shown in Figure 21 for $\epsilon = 0.3$ and $k = 0.005$ which corresponds to water jet impinging on a brass plate. It is seen that the Nusselt number for prescribed constant heat flux is very close to that for prescribed increasing heat flux. The reason is that the radial conduction in the solid phase is so severe that the dimensionless interface temperature profile is not affected by the prescribed heat flux distribution when k is small. If k is reduced to 0.0001, corresponding to air jet impinging on a copper plate, the difference in the Nusselt number will be less than 0.1%. On the other hand, the calculation shows that the prescribed temperature will affect the Nusselt number profile for the same values of ϵ and k. This is because the interface temperature profile always changes with the prescribed temperature profile for any value of k if the plate is not sufficiently thick.

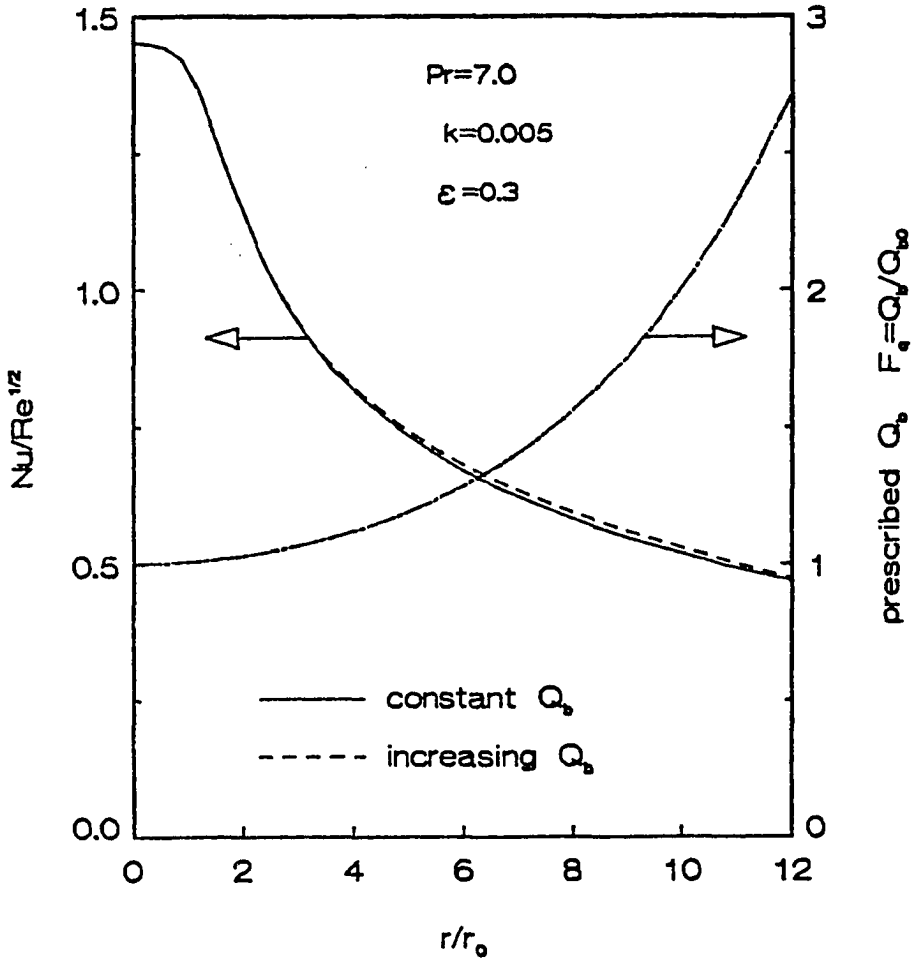

Fig. 21 Result for small k with prescribed heat flux

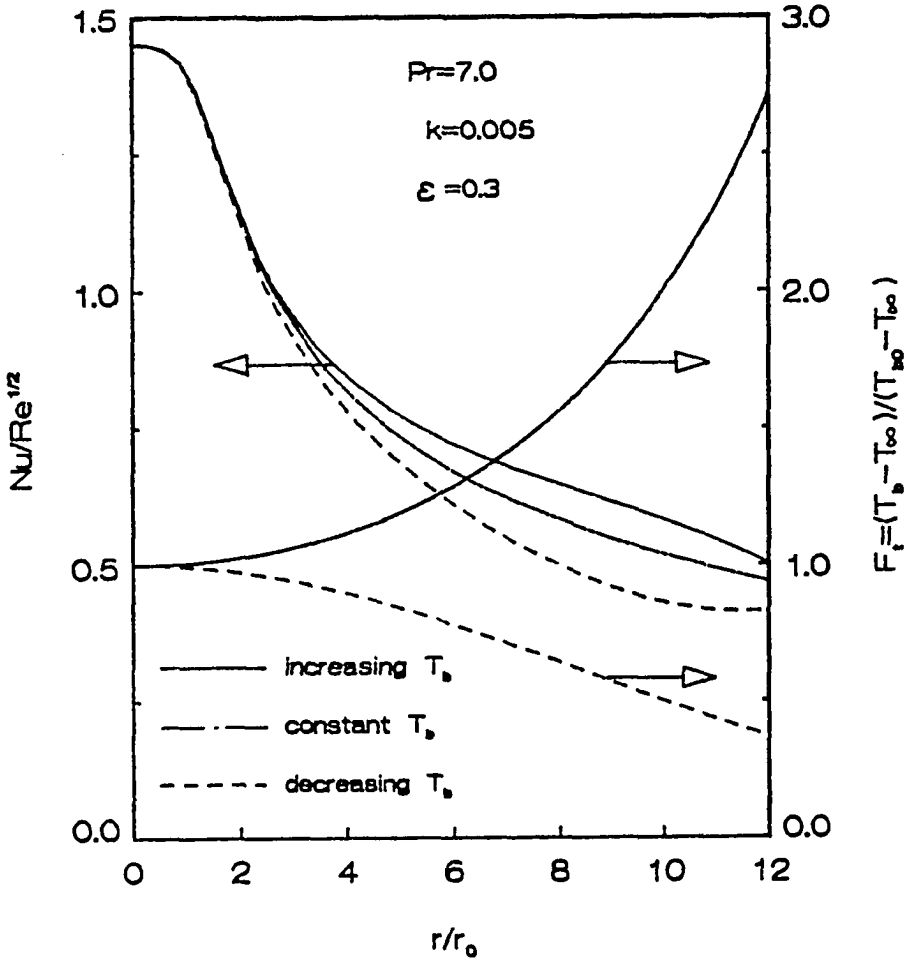

Fig. 22 Effect of prescribed temperature

The effect of the prescribed temprature profile on the Nusselt number distribution is shown in Figure 22 for a moderate plate thickness. The Figure indicates that the Nusselt number profile may be considerably affected by the prescribed temprature distribution. Increasing the prescribed temperature with r enhances the local Nusselt number while decreasing it reduces the local Nusselt number. The reason is that the interface temperature increases more steeply for prescribed increasing temperature than it does for prescribed constant temperature. Consequently, the local Nusselt number becomes higher for the prescribed increasing temperature since the steeper increase in the interface temperature results in higher local heat transfer coefficient outside the stagnation region according to the result of chapter 3. On the other hand, when the prescribed temperature decreases with r, the interface temperature increases more slowly than that for prescribed constant temperature. Consequently, the local Nusselt number becomes lower for the prescribed decreasing temperature. The prescribed heat flux distribution has similar effect on the local Nusselt number.

The effect of the aspect ratio ϵ on the local Nusselt number profile is shown in Figure 23 for a prescribed increasing temperature distribution. It is clear that the Nusselt number increases as ϵ is reduced. This is because small value of ϵ corresponds to thin plate and the effect of prescribed temperature on the interface temperature is larger when the plate is thinner.

In order to examine the effect of the conductivity ratio k on the Nusselt number profile, the Nusselt number is calculated for different values of k and the results are shown in Figure 24. It is evident that

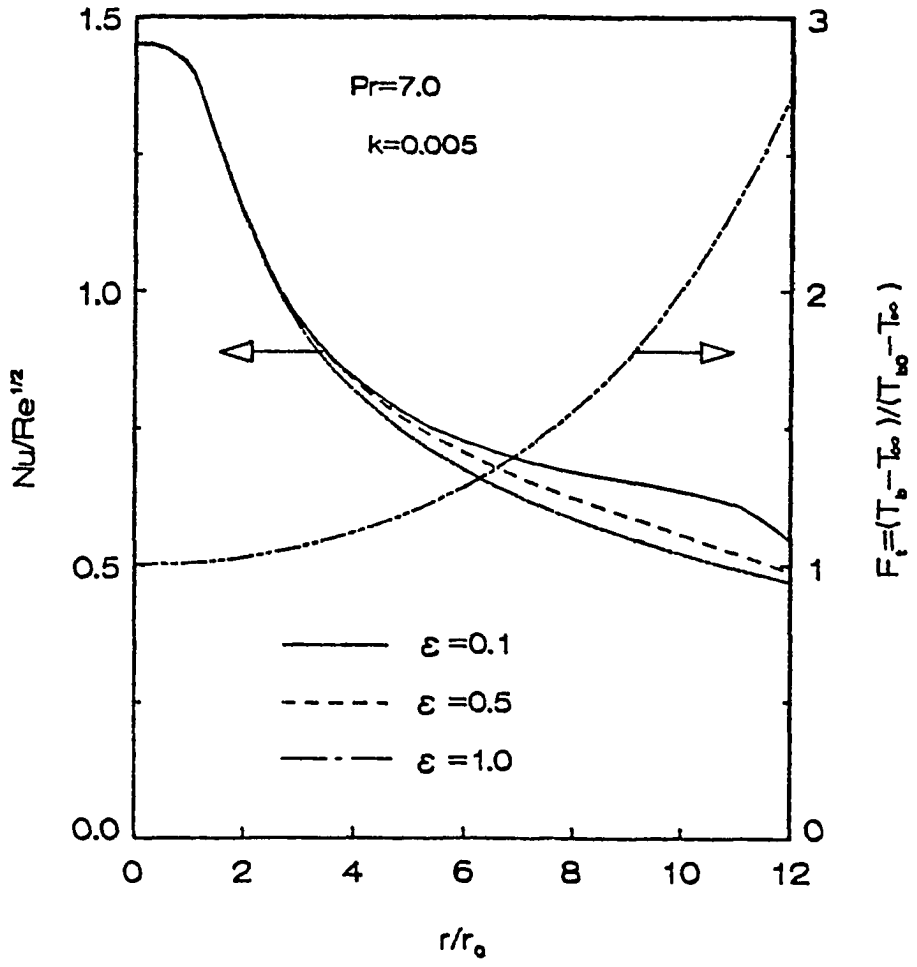

Fig. 23 The effect of aspect ratio

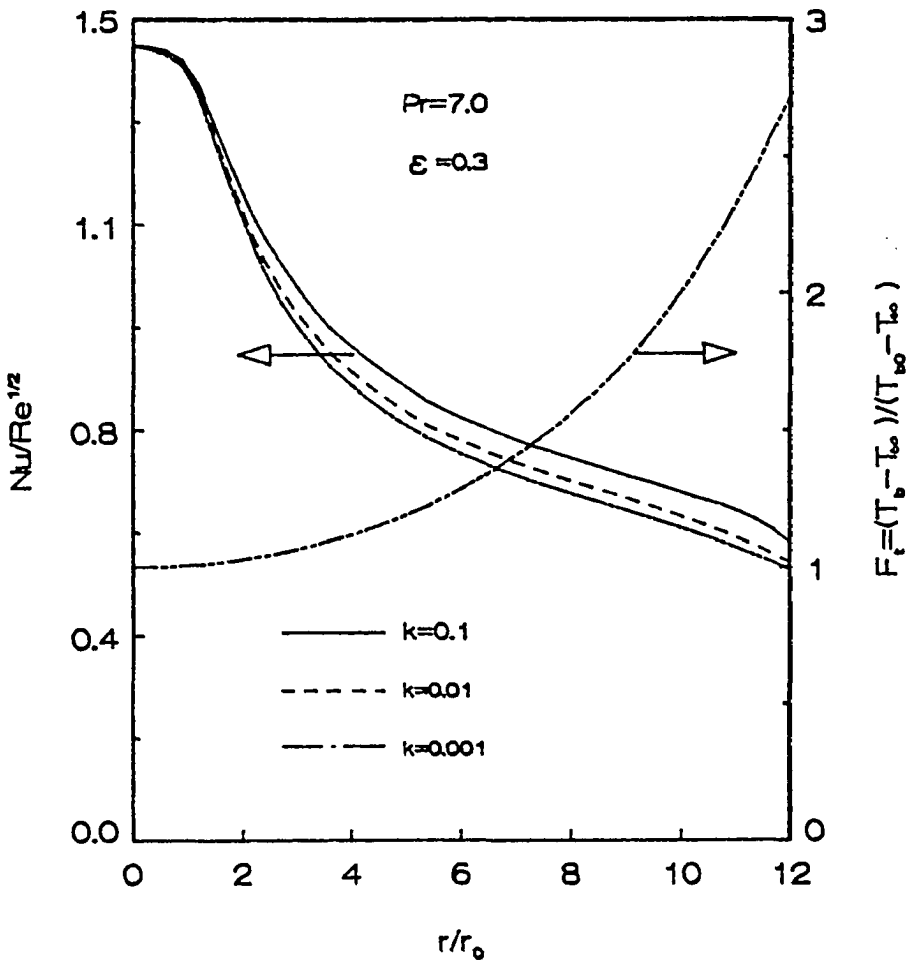

Fig. 24 The effect of conductivity ratio

the local Nusselt number increases with the value of k. This is because larger k represents smaller solid conductivity and hence the radial conduction in the solid phase is smaller so that the interface temperature increases with r more steeply. Consequently, the local Nusselt number becomes higher when k is larger.

4.5 Concluding Remarks

The conjugate problem associated with laminar free jet impingement has been solved analytically. The heat transfer coefficient between the jet and the solid plate is influenced by the Prandtl number of the fluid, the ratio of the fluid conductivity to the solid conductivity and the ratio of the thickness to the radius of the plate as well as the prescribed temperature or heat flux profile. For the special case of vanishing ϵ, the present result is in good agreement with the previous result of chapter 3 in which the temperature or heat flux is prescribed at the interface. When the solid conductivity is sufficiently high, the prescribed heat flux has little influence on the Nusselt number distribution because of the high radial conduction. It is found that for very thick plate, the effect of the prescribed temperature or heat flux profile on the local heat transfer coefficient is negligible. For thin plate, on the other hand, the prescribed temperature or heat flux profile has a considerable effect on the local heat transfer coefficient. Increasing the prescribed temperature or heat flux with r enhances the local Nusselt number while decreasing the prescribed temperature or heat flux with r reduces the local Nusselt number outside the stagnation region. The results also indicate that the local heat transfer coefficient becomes higher when k is larger.

Chapter 5

Conclusions and Applications

The conjugate heat transfer between a laminar impinging liquid jet and a solid plate has been investigated analytically. The local Nusselt number is found to depend upon the Prandtl number of the fluid, the ratio of the fluid conductivity to the solid conductivity and the ratio of the thickness to the radius of the plate as well as the prescribed temperature or heat flux distribution.

As the first step, the solution for the fluid phase is obtained in terms of the impingement surface temperature. The stagnation region solution shows considerable effect of the temprature or heat flux at the impingement surface on the stagnation point Nusselt number if the variation of the impingement surface temperature or heat flux is not small. The reason is that the radial velocity is so small that the radial convection is negligible in the vicinity of the stagnation point, hence the radial conduction plays a much more important role near the stagnation point than it does in other regions. Consequently, considerable error would result from using boundary layer energy equation in the presence of appreciable variation of impingement surface temperature or heat flux. For the boundary layer region, the solution is obtained by the superposition method. The asymptotic expansion converges very fast for Prandtl number of the order of unity or larger. For very small values of Prandtl number, however, the expansion may not converge unless R is also very small. In this case, Euler's transformation may be used to evaluate the sum.

The general solution for the solid phase is obtained by the method of separation of variables. The solution is matched with that for the fluid phase by requiring the continuity of the temperature and heat flux at the impingement surface. The local Nusselt number distribution is obtained for arbitrary temperature or heat flux prescribed on the non-impingement surface. Increasing the prescribed temperature or heat flux with r enhances the local Nusselt number while decreasing the prescribed temperature or heat flux with r reduces the local Nusselt number. The results show that the local heat transfer coefficient becomes higher when k is larger, other parameters being the same. The results also indicate that the effect of prescribed temperature or heat flux on the local Nusselt number becomes more pronounced as ϵ is decreased.

The results presented in this dissertation are useful in engineering applications. For instance, an array of impinging jets is used to obtain high heat transfer rate and maintain approximately uniform surface temperature in the cooling of microelectronic chips. From the results presented here, it is clear that the distance between jets should not exceed about 4 jet diameters in order to obtain approximately uniform surface temperature. Because the geometrical model of the present analysis is similar to the real case of a microelectronic chip cooled by a circular impinging liquid jet, the present results can be used to predict the surface temperature or heat flux distribution of the chip. The solution method developed here can be used to solve the more complicated conjugate problem associated with jet impingement in which there is heat generation in the solid phase. The similar problem with jet cooling at both sides of a solid plate can

also be solved by the same method. With jet impingement on the both sides, a solid plate can be cooled more efficiently.

As an example of the application of the present analysis, we now consider a microelectronic chip cooled by a laminar impinging FC-77 liquid jet or water jet with uniform heat flux Q_0 specified at the non-impingement surface, Figure 25. The chip is made of Silicon measuring 5 mm x 5 mm x 0.39 mm. In order to apply the results presented in the previous chapters, the chip is geometrically simplified as a circular disk of radius 3 mm with the same thickness. The simplification is reasonable everywhere except near the corner of the chip.

By applying the iteration scheme presented in chapter 4, the local Nusselt number distribution $Nu(\xi)$ can be obtained for the present geometry and parameters. The local heat transfer coefficient h(r) can then be calculated. The results for h(r) are presented in Figures 26 and 27 for FC-77 and water respectively. It is clear that for the same value of Reynolds number, the heat transfer coefficient for d = 0.5 mm is much higher than that for d = 1 mm. This is because smaller jet diameter corresponds to higher jet velocity if the Reynolds number and other parameters are the same. The Figures also indicate that the heat transfer coefficient for d = 1 mm is much more uniform than that for d = 0.5 mm. The comparison between Figure 26 and Figure 27 shows that the heat transfer coefficient for water is approximately 6 times higher than that for FC-77 due to the favorable thermal properties of water.

Figures 28 and 29 show the temperature profiles at the impingement surface for FC-77 and water respectively. The prescribed heat flux is 10^5 W/m^2 for all results shown in these two Figures. These results show

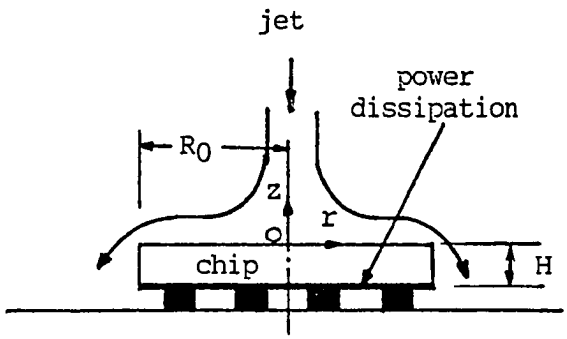

Fig. 25 Schematic diagram of a microelectronic chip

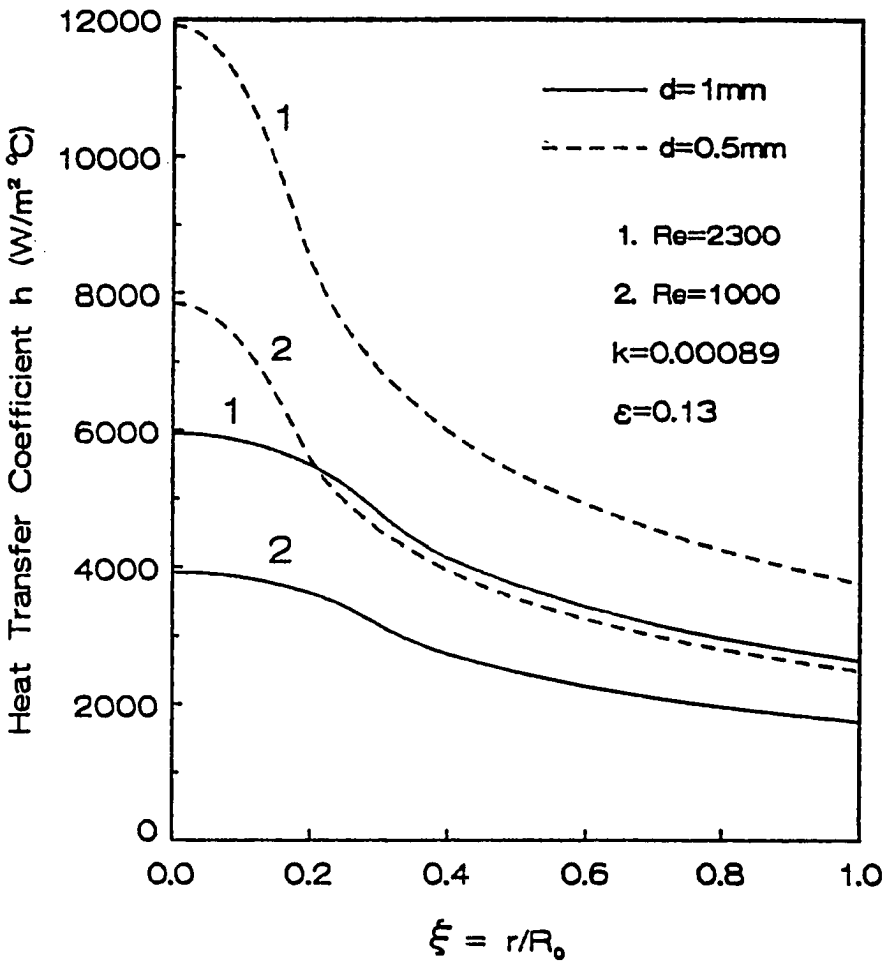

Fig. 26 Heat Transfer Coefficient for FC-77

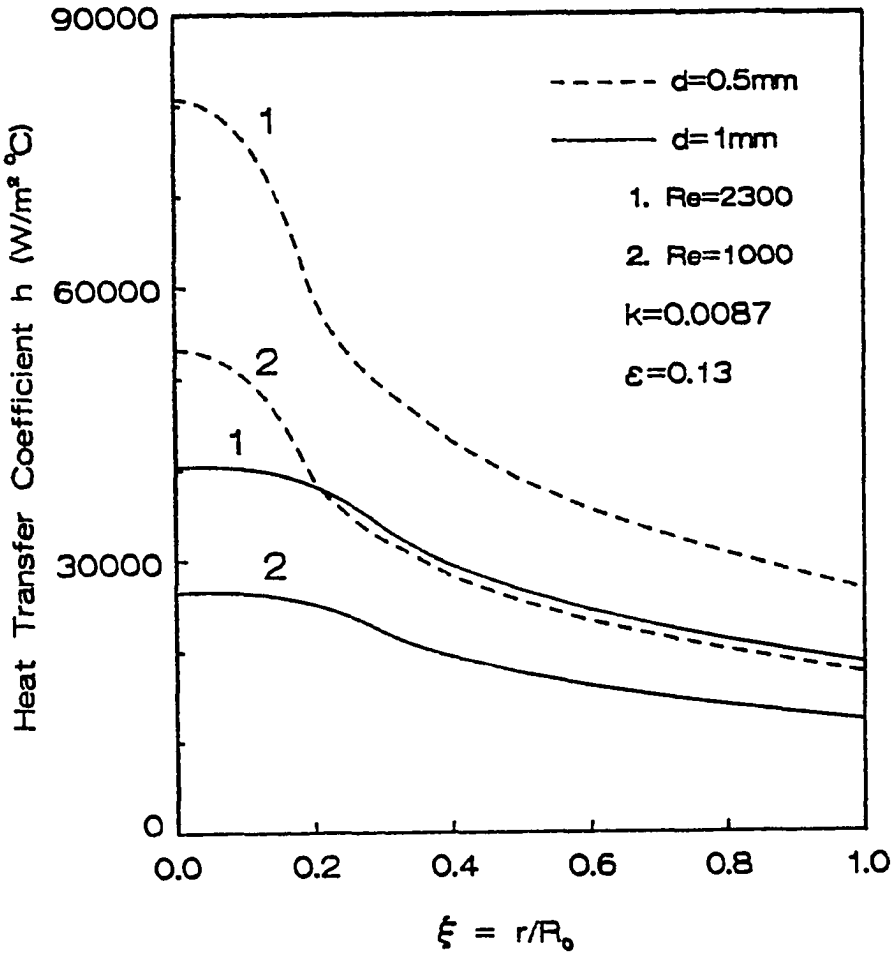

Fig. 27 Heat Transfer Coefficient for Water

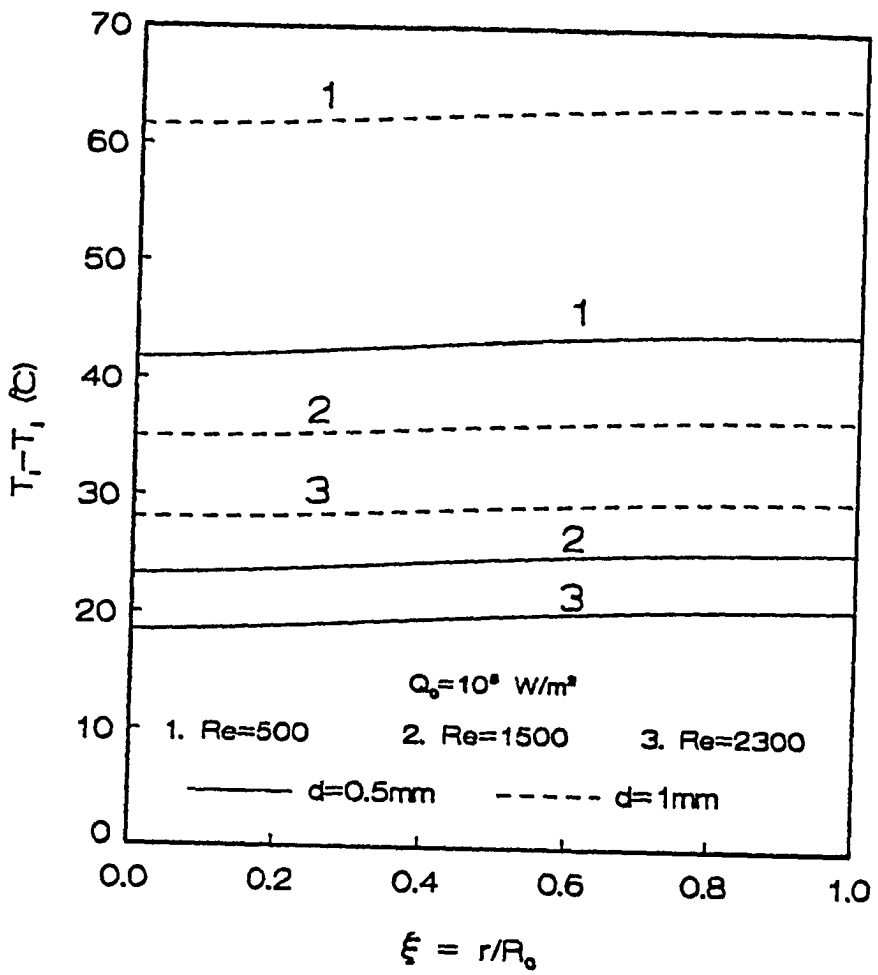

Fig. 28 Surface temperature for FC-77

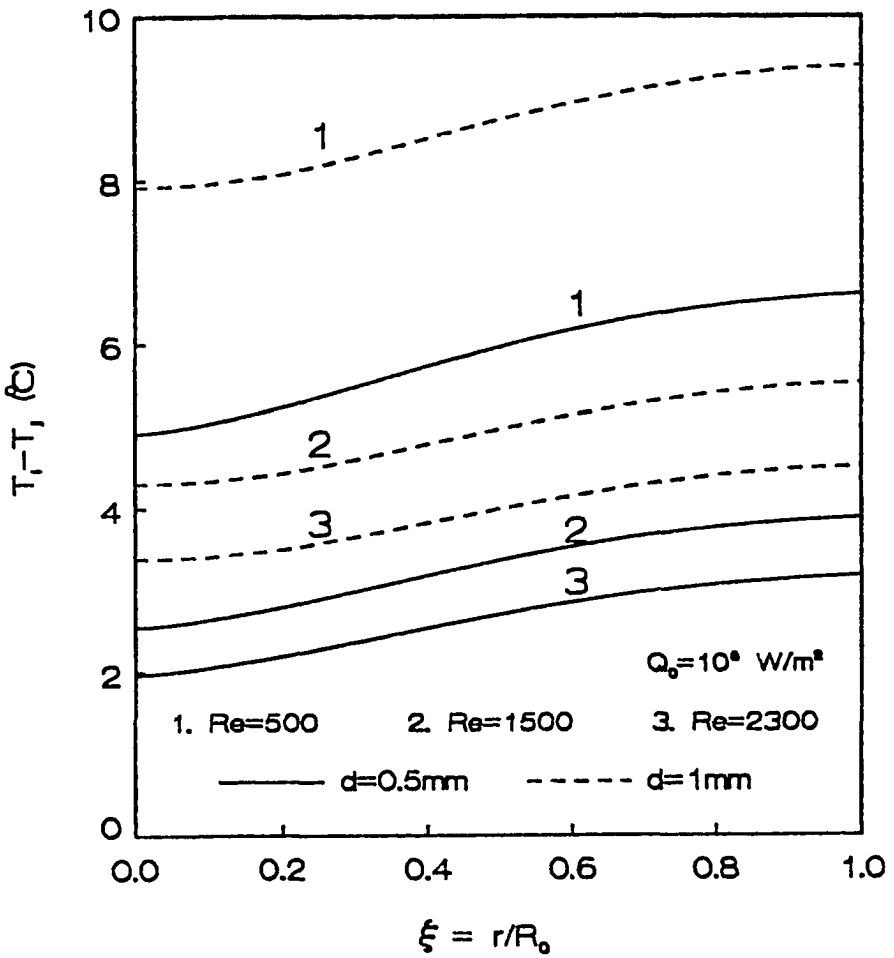

Fig. 29 Surface temperature for water

that the impingement surface temperature is reduced dramatically as the Reynolds number is increased. The reason is that higher Reynolds number corresponds to higher jet velocity, other parameters being the same. It can be seen that the impingement surface temperature for d = 0.5 mm is much lower than that for d = 1 mm if the Reynolds number is the same. This is due to the fact that smaller jet diameter results in higher heat transfer coefficient as shown in Figures 26 and 27. For all cases shown in Figure 28 and Figure 29, the temperature difference (T_{max} - T_{min}) which characterizes the impingement surface temperature non-uniformity ranges from 1.1°C to 2.4°C, where T_{max} is the maximum surface temperature and T_{min} is the minimum surface temperature. In general, the result for d = 0.5 mm shows higher values of (T_{max} - T_{min}) than that for d = 1 mm and the result for FC-77 gives higher values of (T_{max} - T_{min}) than that for water. Comparing Figure 28 with Figure 29, one can see that for the same Reynolds number and prescribed heat flux, water gives much lower impingement surface temperature than FC-77. This is because the heat transfer coefficient associated with water is much higher than that for FC-77 as shown in Figures 26 and 27. Since the surface temperature is directly proportional to the prescribed heat flux, the surface temperature distribution corresponding to other values of Q_0 can be obtained easily.

In practice, it is common to limit chip surface temperature to 85° C or lower. Hence (T_i - T_j) should be lower than about 65°C, where T_i is the impingement surface temperature and T_j is the jet temperature. The present results show that when the chip is cooled by a FC-77

liquid jet of diameter o.5 mm and Reynolds number 2300, the highest value of the temperature difference (T_i - T_j) can be maintained at 64.2 ^oC for the prescribed heat flux as high as $3.1x10^5$ W/m^2 at the non-impingement surface. If the jet diameter is increased to 1 mm with the Reynolds number being the same, the highest temperature difference (T_i - T_j) can be maintained at 64.2^oC for the prescribed heat flux as high as $2.15x10^5$ W/m^2. On the other hand, if the chip is cooled by a water jet with the same Reynolds number, the highest temperature difference (T_i - T_j) can be maintained at the same value for Q_o = $2.02x10^6$ W/m^2 when d = 0.5 mm and Q_o = $1.42x10^6$ W/m^2 when d = 1 mm. It is clear that impinging water jet can cool the microelectronic chip much more efficiently than FC-77 liquid jet.

The heat flux distribution at the impingement surface is shown in Figures 30 and 31 for FC-77 and water respectively. It can be seen that near the stagnation point, the heat flux for d = 0.5 mm is considerably higher than that for d = 1 mm. On the other hand, far away from the stagnation point, the heat flux for d = 1 mm is slightly higher than that for d = 0.5 mm. Consequently, the heat flux distribution for d = 1 mm is much more uniform than that for d = 0.5mm. Comparison between Figures 30 and 31 shows that the heat flux distribution at the impingement surface for water is more uniform than that for FC-77.

To examine the average thermal performance of the jet impingement cooling, we now consider the thermal resistance which is defined as follows

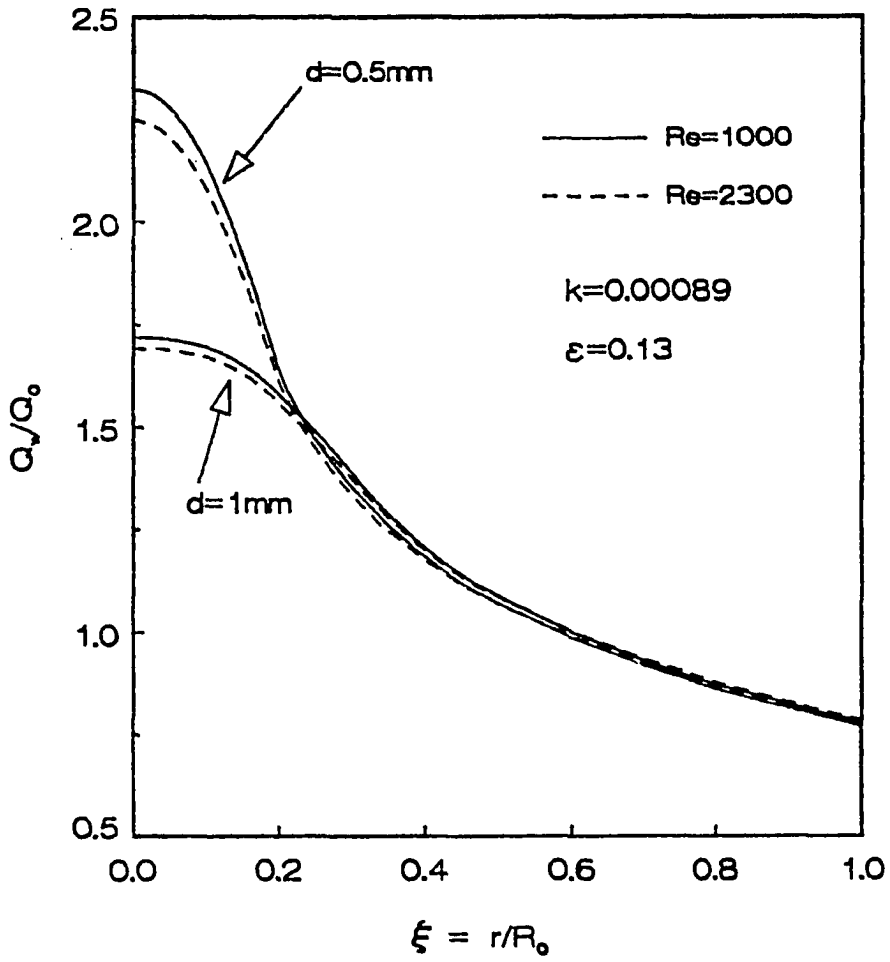

Fig. 30 Heat flux distribution for FC-77

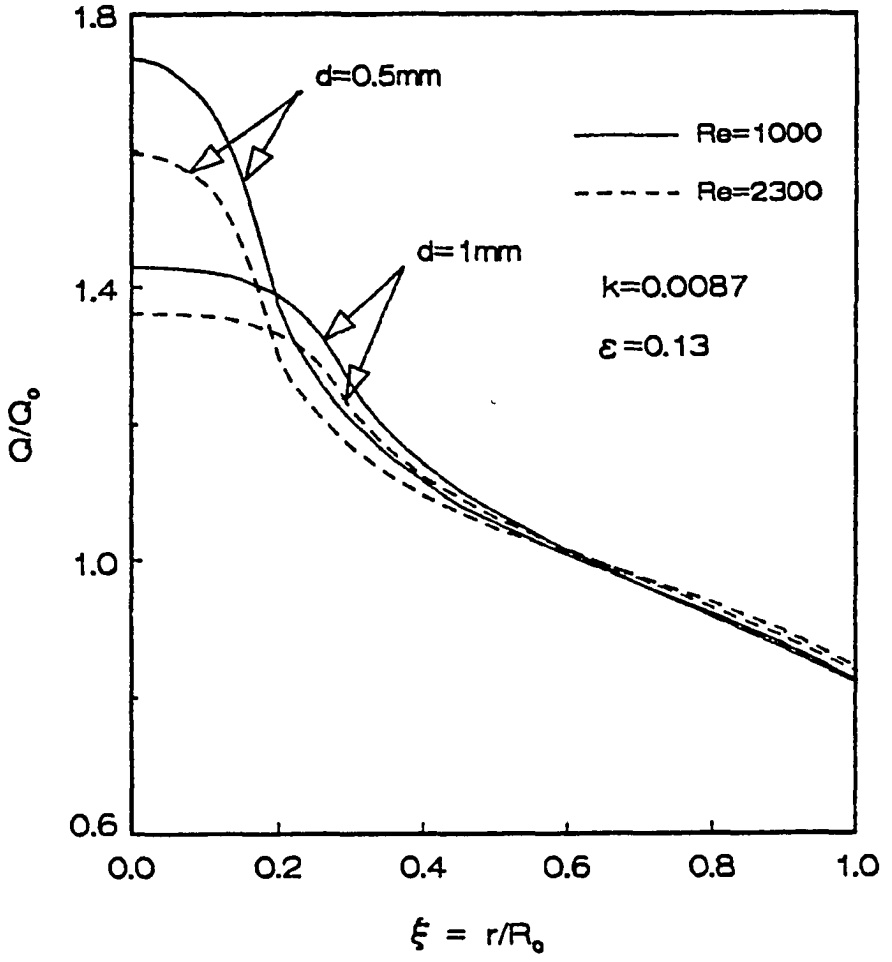

Fig. 31 Heat flux distribution for water

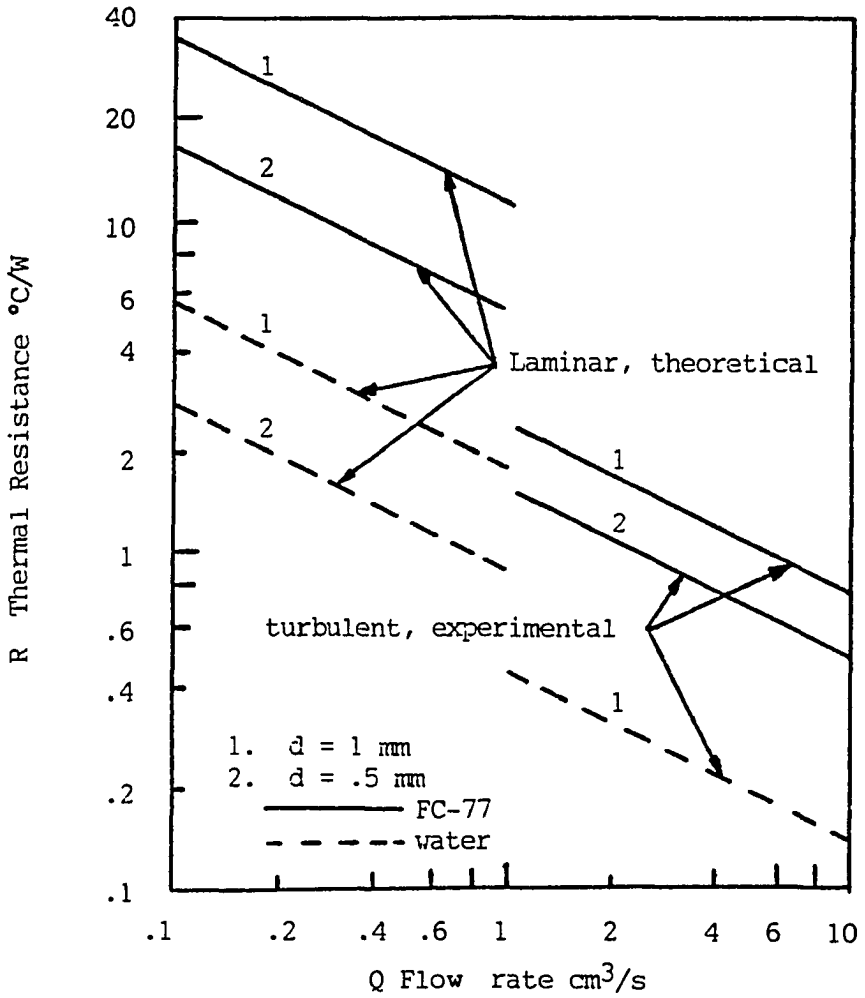

Fig. 32 Thermal resistance of jet impingement cooling

$$R = \frac{1}{\bar{h}A} \tag{5.1}$$

where $\bar{h}$ is the average heat transfer coefficient and A is the surface area of the disk. The result for R is shown in Figure 32 for different jet diameters and different fluids. The experimental result of [32] for turbulent jet impingement is also shown in the same Figure. It can be seen that smaller jet diameter results in smaller thermal resistance. The experimental result of [32] shows the same behavior. For the same Reynolds number and jet diameter, the thermal resistance for FC-77 is approximately 6 times higher than that for water. The Figure also indicates that the functional relation between the thermal resistance and the flow rate of the fluid is linear on the log-log graph and the lines for laminar jet are parallel to those for turbulent jet. Hence the present analytical result agrees qualitatively with the experimental result for turbulent jet of [32]. Note that the experimental result of [32] is based on a square brass chip measuring 12.7 mm x 12.7 mm x 1.9 mm. Consequently, it is not expected that the present result agrees with the experimental result quantitatively. In general, it is clear that a jet of diameter 0.5 mm gives better thermal performance than a jet of diameter 1 mm. This observation is also in agreement with the experimental result of [2].

It should be pointed out that real case may be better than that predicted by the present solution near the edge of the chip since the lateral surface of the chip is cooled by the fluid rather than insulated in the real case. Specifically, the highest impingement surface temperature which is located at the edge of the chip may be

lower than that calculated. Far away from the edge, the effect of the geometrical simplification in the present analytical model on the calculated result is negligible.

Bibliography

1. P. M. Brdlik and V. K. Savin, "Heat Transfer Between an Axisymmetric Jet and a Plate Normal to the Flow", J. Eng. Phys., Vol. 8, pp. 91-98, 1965.

2. L. M. Jiji and Z. Dagan, "Experimental Investigation of Single Phase Multi-Jet Impingement Cooling of an Array of Microelectronic Heat Sources", Proceedings of the International Symposium on Cooling Technology for Electronic Equipment, March 12-21, Honolulu pp. 265-283, 1987.

3. V. E. Nakoryakov, B. G. Pokusaev and E. N. Troyan, "Impingement of an Axisymmetric Liquid Jet on a Barrier", Int. J. Heat Mass transfer, Vol. 21, 1175-1184, 1978.

4. I. Tani and Y. Komutsu, "Impingement of a Round Jet on a Flat Surface", Proc. 11-th Int. Conf. Appli. Mech., pp. 672-676, 1964.

5. E. J. Watson, "The Radial Spread of a Liquid Jet Over a Horizontal Plane", J. Fluid Mech., Vol. 20, pp. 481-499, 1964.

6. R. G. Olsson and E. T. Turkdogan, "Radial Spread of a Liquid Stream on a Horizontal Plate", Nature, Vol. 211, pp. 813-816, 1966.

7. S. Goldstein, Editor, Modern Developments in Fluid Dynamics, Vol. 2, p. 631, Oxford University Press., London, 1952.

8. M. Sibulkin, "Heat Transfer near the Forward Stagnation Point of a Body of Revolution", J. Aeronaut. Sci., Vol. 19, pp. 570-571, 1952.

9. B. T. Chao and D. R. Jeng, "Unsteady Stagnation Point Heat Transfer", J. of Heat Transfer, Vol. 87, pp. 221-230, 1965.

10. Takao Sano, "Unsteady Boundary Layer in Impulsive Stagnation Flow", Int. J. Heat Mass Transfer, Vol. 20, pp. 1000-1001, 1977.

11. Takao Sano, "Unsteady Stagnation Point Heat Transfer with Blowing or Suction", J. of Heat Transfer, Vol. 103, pp. 448-452, 1981.

12. M. Kumari and G. Nath, "Unsteady Mixed Convection near the Stagnation Point in Three-Dimensional Flow", J. of Heat Transfer, Vol. 104, pp. 132-138, 1982.

13. B. M. Smolsky, L. A. Sergeyeva and V. L. Sergeyev, "Investigation of the Unsteady-State Heat Transfer in the Region of a Stagnation Point in Plane and Axisymmetric Flows", Int. J. Heat Mass Transfer, Vol. 28, pp. 7-16, 1985.

14. Z. H. Chaudhury, "Heat Transfer in a Radial Liquid Jet", J. Fluid Mech., Vol. 20, pp. 501-511, 1964.

15. N. R. Saad, W. J. M. Douglas and A. S. Mujumdar, "Prediction of Heat Transfer Under an Axisymmetric Laminar Impinging Jet", Ind. Eng. Chem. Fundam., Vol. 16, pp. 148-154, 1977.

16. A. W. Lipsett and R. R. Gilpin, "Laminar Jet Impingement Heat Transfer Including the Effects of Melting", Int. J. Heat Mass Transfer, Vol. 21, pp. 25-33, 1978.

17. Koshi Mitachi and Ryoji Ishiguro, "Heat Transfer of Wall Jets (1st Report: Theoretical Discussions of the Temperature Field)", Heat Transfer, Jap. Res., Vol. 3, No. 4, pp. 27-40, 1974.

18. C. D. Donaldson, R. S. Snedeker and D. P. Margolis, " A Study of Free Jet Impingement. Part 2. Free Jet Turbulent Structure and Impingement Heat Transfer", J. Fluid Mech., Vol. 45, pp. 476-513, 1970.

19. J. Kestin, P. F. Maeder and H. H. Sogin, Z. angew. Math. Phys. Vol. 12 , No. 115, 1961.

20. M. B. Glauert, "The Wall Jet", J. Fluid Mech., Vol. 1, pp. 625-643, 1956.

21. J. F. Tomich, "Heat and Momentum Transfer from Compressible Turbulent Jets of Hot Air Impinging Normally on a Surface", Ph.D. Thesis, Washington University, 1967.

22. M. Wolfshtein, "Some Solutions of the Plane Turbulent Jet", J. Basic Eng., Vol. 92, pp. 915-922, 1970.

23. B. G. Murray and T. D. Patten, " Heat Transfer Under an Array of Impinging Jets", Proc. 6th Intl. Heat Transfer Conf., Toronto, Canada, Part IV, pp. 7-11, Aug. 1978.

24. H. Martin, "Heat and Mass Transfer Between Impinging Jets and Solid Surfaces", Advances in Heat Transfer, Academic Press, Vol. 13, pp. 1-60, 1977.

25. B. N. Pamadi and I. A. Belov, "A Note on the Heat Transfer Characteristics of Circular Impinging Jet", Int. J. Heat Mass Transfer, Vol. 23, pp. 783-787, 1980.

26. R. Gardon and J. Cobonpue, "Heat Transfer between a Flat Plate and Jets of Air Impinging on It", Intl. Development in Heat Transfer, ASME, pp. 454-460, 1963.

27. H. Schlichting, Boundary Layer Theory, p. 100, McGraw-Hill, New York, 1968.

28. F. Homann, "The Effect of High Viscosity on the Flow around a Cylinder and around a Sphere", Tech. Memor., Nat. Adv. Comm. Aero., Wash., No. 1334, 1952.

29. E. M. Sparrow and M. Faghri, "Fluid-to-Fluid Conjugate Heat Transfer for a Vertical Pipe -- Internal Forced Convection and

External Natural Convection", J. of Heat Transfer, Vol. 102, pp. 402-407, 1980.

30. E. M. Sparrow and C. Prakash, "Interaction Between Internal Natural Convection in an Enclosure and External Natural Convection Boundary Layer Flow", Int. J. Heat Mass Transfer, Vol. 24, pp. 895-907, 1981.

31. G. S. Barozzi and G. Pagliarini, "A Method to Solve Conjugate Heat Transfer Problems: The Case of Fully Developed Laminar Flow in a Pipe", J. of Heat Transfer, Vol. 107, pp. 77-83, 1985.

32. L. M. Jiji, Z. Dagan, G. P. Zhang and X. S. Wang, "Feasibility of Multi-Jet Impingement Cooling of an Array of Microelectronic Heat Sources", Technical Report No. 7-75591, Dept. of Mechanical Engineering, The City College of New York, 1986.

33. Carl E. Pearson, Editor, Handbook of Applied Mathematics, Second Edition, pp. 694-695, Van Nostrand Reinhold Co., New York, 1983.

34. B. T. Chao and L. S. Cheema, "Forced Convection in Wedge Flow with Non-isothermal Surfaces", Int. J. Heat Mass Transfer, Vol. 14, 1363-1375, 1971.